ELLIPSOIDAL WAVELET REPRESENTATION OF THE GRAVITY FIELD

by

Michael Schmidt
and
Oliver Fabert

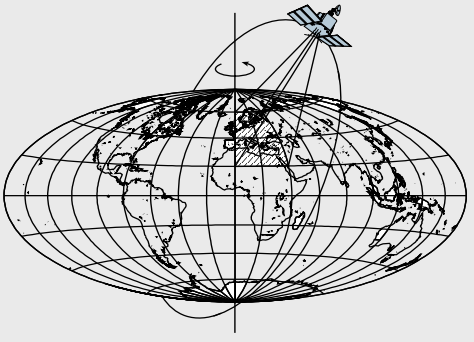

Report No. 487

Geodetic Science and Surveying

The Ohio State University
Columbus, Ohio 43210

January 2008

ELLIPSOIDAL WAVELET REPRESENTATION

OF THE GRAVITY FIELD

BY

MICHAEL SCHMIDT

OLIVER FABERT

Report No. 487

Geodetic Science

School of Earth Sciences

The Ohio State University

Columbus, Ohio 43210

January 2008

ABSTRACT

The determination and the representation of the gravity field of the Earth are some of the most important topics of physical geodesy. Traditionally in satellite gravity recovery problems the global gravity field of the Earth is modeled as a series expansion in terms of spherical harmonics. Since the Earth's gravity field shows heterogeneous structures over the globe, a multi-resolution representation is an appropriate candidate for an alternative spatial modeling. In the last years several approaches were pursued to generate a multi-resolution representation of the geopotential by means of spherical base functions.

Spherical harmonics are mostly used in global geodetic applications, because they are simple and the surface of Earth is nearly a sphere. However, an ellipsoid of rotation, i.e., a spheroid, means a better approximation of the Earth's shape. Consequently, ellipsoidal harmonics are more appropriate than spherical harmonics to model the gravity field of the Earth. However, the computation of the coefficients of a series expansion for the geopotential in terms of both, spherical or ellipsoidal harmonics, requires preferably homogeneous distributed global data sets.

Gravity field modeling in terms of spherical (radial) base functions has long been proposed as an alternative to the classical spherical harmonic expansion and is nowadays successfully used in regional or local applications. Applying scaling and wavelet functions as spherical base functions a multi-resolution representation can be established. Scaling and wavelet functions are characterized by the ability to localize both in the spatial and in the frequency domain. Thus, regional or even local structures of the gravity field can be modeled by means of an appropriate wavelet expansion. To be more specific, the application of the wavelet transform allows the decomposition of a given data set into a certain number of frequency-dependent detail signals. As mentioned before the spheroid means a better approximation of the Earth than a sphere. Consequently, we treat in this report the ellipsoidal wavelet theory to model the Earth's geopotential.

Modern satellite gravity missions such as the Gravity Recovery And Climate Experiment (GRACE) allow the determination of spatio-temporal, i.e., four-dimensional gravity fields. This issue is of great importance in the context of observing time-variable phenomena, especially for monitoring the climate change. Global spatio-temporal gravity fields are usually computed for fixed time intervals such as one month or ten days. In the last part of this report we outline regional spatio-temporal ellipsoidal modeling. To be more specific, we represent the time-dependent part of our ellipsoidal (spatial) wavelet model by series expansions in terms of one-dimensional B-spline functions. Thus, our concept allows to establish a four-dimensional multi-resolution representation of the gravity field by applying the tensor product technique.

ACKNOWLEDGEMENT

The research which led to this report was initiated during a visit to the Ohio State University (OSU) from February 2002 through January 2003, and partially supported by grants from the National Geospatial-Intelligence Agency's (NGA's) University Research Initiative (NURI), entitled 'Application of spherical wavelets to the solution of the terrestrial gravity field model' (NMA201-00-1-2006, 2000-2005, PIs: C. Shum), and from the National Science Foundation's Collaboration in Mathematics and Geosciences (CMG) Program, entitled 'Multi-resolution inversion of tectonically driven spatio-temporal gravity signals using wavelets and satellite data' (EAR-0327633, 2003-2007, PIs: C.K. Shum).

The authors benefited very much from discussions with many researchers at the OSU and thank C.K. Shum and the OSU for hospitality. Further thanks go to the German Geodetic Research Institute (DGFI) and the University of Munich (LMU), at which parts of the work were conducted. Finally we thank Erik W. Grafarend for many fruitful discussions, which were the actual starting point for this project.

Contents

Chapter 1

Introduction

The determination and the representation of the gravity field of the Earth are some of the most important topics of physical geodesy. Traditionally in satellite gravity recovery problems the global gravity field of the Earth is modeled as a series expansion in terms of spherical harmonics (Reigber et al., 2005). Since the Earth's gravity field shows heterogeneous structures over the globe, a *multi-resolution representation* is an appropriate candidate for an alternative spatial modeling. In the last years several approaches were pursued to generate a multi-resolution representation of the geopotential by means of spherical base functions; see e.g. Freeden (1999), Freeden et al. (1998), Freeden and Michel (2004), Kusche (2002), Prijatna and Haagmans (2001), Haagmans et al. (2002), Panet el al. (2005) or Schmidt et al. (2006, 2007a).

Spherical harmonics are mostly used in geodetic applications, because they are simple and the surface of Earth is nearly a sphere (Heiskanen and Moritz, 1967). However, an ellipsoid of rotation, i.e., a spheroid, means a better approximation of the Earth's shape. Consequently, ellipsoidal harmonics are more appropriate than spherical harmonics to model the gravity field of the Earth and the region of divergence of an ellipsoidal harmonic expansion is smaller than the corresponding one of a spherical harmonic expansion. However, the computation of the coefficients of a series expansion for the geopotential in terms of both, spherical or ellipsoidal harmonics, requires preferably homogeneous distributed global data sets. Since a wavelet function is characterized by its ability to localize both in the spatial and in the frequency domain, regional or even local structures can be modeled by means of an appropriate wavelet expansion. Applying the wavelet transform, a given data set can be decomposed into a certain number of frequency-dependent detail signals, i.e. a multi-resolution representation is performed.

In order to consider the Laplacian differential equation our approaches are based on an ellipsoidal wavelet theory. In chapter 2 we present the mathematical foundations. The basic formalism of *ellipsoidal signal representation* is introduced in section 2.1. Since spherical coordinates and spherical harmonics are still standard in modern gravity field modeling, we additionally introduce basic spher-

ical relations in section 2.2.

The *multi-resolution representation* is treated in detail in chapter 3. After introducing general ellipsoidal kernels in section 3.1 their properties are specialized in the following section 3.2 to ellipsoidal scaling functions and wavelets, which mean the basic components of the multi-resolution representation. As a special topic subsection 3.3 is dedicated to isotropic wavelets, which are generally definable only on spheres.

One of the main applications of the spherical wavelet theory lies in the *regularization* of inverse problems related to the sphere. In Earth's gravity field studies regularization is needed for the downward-continuation of the gravity data, e.g., from a satellite orbit to the Earth's surface. Thus, after introducing Sobolev spaces in section 4.1 we discuss regularization in the context of ellipsoidal wavelet theory in section 4.2.

In chapter 5 we treat the multi-resolution representation of *bandlimited signals* as a kind of specialisation. To be more specific we transfer the integal equation to series expansions, because in geodesy one is always interested in estimating the target coefficients by parameter estimation procedures, for instance, least-squares techniques. After presenting basic relations in section 5.1 we discuss the decomposition and the reconstruction of signals on the ellipsoid in detail in subsection 5.2. In the following section 5.3 we complete the chapter by a numerical example.

In chapter 6 we outline the *spatio-temporal ellipsoidal modeling* of the gravity field. This issue is of great importance in the context of observing time-variable phenomena, especially for monitoring the climate change by modern satellite missions like the Gravity Recovery And Climate Experiment (GRACE). We start with the definition of the spatio-temporal tensor product approach in section 6.1. The time-dependent part of our model is based on B-splines introduced in section 6.2. Finally we outline the four-dimensional (4-D) multi-resolution representation of spatio-temporal signals in section 6.3.

As mentioned before the ellipsoidal wavelet theory is more appropriate for modeling the Earth's geopotential than spherical base functions. However, all results based on the ellipsoidal theory and presented in this report can be easily transferred to the spherical case. This fact means another reason why we decided to derive our approaches in the ellipsoidal context.

Heiskanen and Moritz (1967) presented basic relations on ellipsoidal series expanisons of the gravity field. An extensive introduction to a spheroidal[1] harmonic model of the terrestrial gravity field was published by Thong and Grafarend (1989); the exact transformation formula between ellipsoidal and spherical harmonic expansions is given by Jekeli (1987).

[1] as mentioned before a spheroid means an ellipsoid of revolution

Chapter 2

Mathematical Foundations

The basic idea of the *multi-resolution representation* is to split a given input signal into a smoothed version and a certain number of band-pass signals by *successive low-pass filtering*. In the context of wavelet theory, this procedure consists of the *decomposition* of the signal into wavelet coefficients and the *(re)construction* of the (modified) signal by means of *detail signals*. The latter are the spectral components of the multi-resolution representation because they are related to certain frequency bands. In the sequel we want to transfer the concept of the multi-resolution representation from the well-known spherical theory into the ellipsoidal setting.

2.1 Basic Ellipsoidal Settings

First we introduce the gravitational potential $U(\boldsymbol{x})$, which is assumed to be harmonic in the exterior of the Earth, i.e., it fulfills the *Laplacian differential equation*. The geocentric position vector

$$\boldsymbol{x} = \Big[\, \sqrt{u^2+\epsilon^2}\cos\phi\cos\lambda,\ \sqrt{u^2+\epsilon^2}\cos\phi\sin\lambda,\ u\sin\phi \,\Big]^T = |\boldsymbol{x}|\,\boldsymbol{r} \tag{2.1}$$

of any arbitrary observation point $P = P(\boldsymbol{x})$ may be expressed by means of the *Jacobi ellipsoidal coordinates* (λ, ϕ, u) with λ = spheroidal longitude, ϕ = spheroidal latitude and u = spheroidal height; for details on the Jacobi ellipsoidal coordinates we refer to Thong and Grafarend (1989). Furthermore, in Eq. (2.1)

$$\epsilon = \sqrt{a^2 - b^2} \tag{2.2}$$

denotes the absolute eccentricity of the *reference ellipsoid*

$$\mathbb{E}^2_{a,b} = \{\, \boldsymbol{x} \,|\, 0 \le \lambda < 2\pi, -\pi/2 \le \phi \le \pi/2\,,\ u = b \,\} \tag{2.3}$$

of Somigliana-Pizetti type with semi-major axis a and semi-minor axis b. Finally, with $|\boldsymbol{x}| = \sqrt{u^2+\epsilon^2\cos^2\phi}$ the unit vector $\boldsymbol{r} = \boldsymbol{x}/|\boldsymbol{x}|$, introduced in Eq. (2.1), reads

$$\boldsymbol{r} = \left[\sqrt{\frac{u^2+\epsilon^2}{u^2+\epsilon^2\cos^2\phi}}\cos\phi\cos\lambda,\ \sqrt{\frac{u^2+\epsilon^2}{u^2+\epsilon^2\cos^2\phi}}\cos\phi\sin\lambda,\ \sqrt{\frac{u^2}{u^2+\epsilon^2\cos^2\phi}}\sin\phi \right]^T . \tag{2.4}$$

Expanding the three components of $\boldsymbol{r}$ into geometric series we obtain

$$\boldsymbol{r} = \begin{bmatrix} \left(1+\frac{1}{2}\,\sin^2\phi\,\frac{\epsilon^2}{u^2}+\mathcal{O}(\frac{\epsilon^4}{u^4})\right)\,\cos\phi\cos\lambda \\ \left(1+\frac{1}{2}\,\sin^2\phi\,\frac{\epsilon^2}{u^2}+\mathcal{O}(\frac{\epsilon^4}{u^4})\right)\,\cos\phi\sin\lambda \\ \left(1-\frac{1}{2}\,\cos^2\phi\,\frac{\epsilon^2}{u^2}+\mathcal{O}(\frac{\epsilon^4}{u^4})\right)\,\sin\phi \end{bmatrix} = \boldsymbol{\xi} + \delta\boldsymbol{r} \tag{2.5}$$

with the "spherical" unit vector

$$\boldsymbol{\xi} = [\,\cos\phi\cos\lambda,\ \cos\phi\sin\lambda,\ \sin\phi\,]^T \tag{2.6}$$

and the latitude-dependent ellipsoidal correction $\delta\boldsymbol{r} = \delta\boldsymbol{r}(\phi,u)$, which vanishes for $\epsilon = 0$. Besides the reference ellipsoid (2.3) we define the *unit sphere*

$$\mathbb{S}^2_1 = \{\,\boldsymbol{\xi}\,|\,0 \le \lambda < 2\pi, -\pi/2 \le \phi \le \pi/2\,\} =: \mathbb{S}^2\ . \tag{2.7}$$

In the sequel we additionally need the family of confocal ellipsoids

$$\mathbb{E}^2_{\sqrt{u^2+\epsilon^2},u} = \{\,\boldsymbol{x}\,|\,0 \le \lambda < 2\pi, -\pi/2 \le \phi \le \pi/2\,,\ u > 0\,\} \tag{2.8}$$

as well as the family of concentric spheres

$$\mathbb{S}^2_r = \{\,r\cdot\boldsymbol{\xi}\,|\,0 \le \lambda < 2\pi, -\pi/2 \le \phi \le \pi/2\,,\ r > 0\,\}\ . \tag{2.9}$$

of radius r. Recall, that in analogy to the definition (2.9) of spheres $\mathbb{S}^2_r$ as the collection of all points $P(r\cdot\boldsymbol{\xi})$ with the same radial coordinate r, the spheroidal coordinate u is chosen to define ellipsoids (2.8) as level sets. Since only ellipsoids of revolution are considered, the spheroidal longitude λ agrees with the spherical longitude. While the coordinate pair (λ,u) therefore has an obvious geometric background, the definition of the spheroidal latitude ϕ is more subtle. Actually it has no direct geometric interpretation, instead it is motivated by the attempt to have nice solutions of the Laplacian differential equation. Indeed, the spheroidal latitude ϕ is chosen so that solving the Laplacian differential equation via separation of variables again leads to the spherical harmonics. To be more specific, we split the gravitational potential $U(\lambda,\phi,u)$ into separable functions, i.e., $U(\lambda,\phi,u) = \Lambda(\lambda)\,\Phi(\phi)\,U(u)$, and obtain the solution of the *boundary value problem* for the outer space $\mathbb{E}^{2,\mathrm{ext}}_{a,b}$ of the reference ellipsoid $\mathbb{E}^2_{a,b}$ as *Fourier series*

$$U(\lambda,\phi,u) = \sum_{n=0}^{\infty}\sum_{m=-n}^{n} u_{nm}\,\frac{Q^\star_{nm}(\frac{u}{\epsilon})}{Q^\star_{nm}(\frac{b}{\epsilon})}\,e_{nm}(\lambda,\phi) \tag{2.10}$$

in terms of the *surface ellipsoidal harmonics*

$$e_{nm}(\lambda,\phi) = P^{\star}_{n|m|}(\sin\phi) \begin{Bmatrix} \cos m\lambda & \forall & m \geq n \\ \sin |m|\lambda & \forall & m < 0 \end{Bmatrix} = e_{nm}(\boldsymbol{\xi}) \ , \tag{2.11}$$

see e.g. Heiskanen and Moritz (1967). The functions $P^{\star}_{nm}(\,\cdot\,)$ and $Q^{\star}_{nm}(\,\cdot\,)$ are the normalized associated Legendre functions of the first and of the second kind, respectively; n means the degree and m the order. Defining the *outer ellipsoidal harmonics*

$$h^b_{nm}(\lambda,\phi,u) = \frac{Q^{\star}_{nm}(\frac{u}{\epsilon})}{Q^{\star}_{nm}(\frac{b}{\epsilon})}\, e_{nm}(\lambda,\phi) = h^b_{nm}(\boldsymbol{x}) \tag{2.12}$$

the Fourier series (2.10) can be rewritten as

$$U(\lambda,\phi,u) = \sum_{n=0}^{\infty} \sum_{m=-n}^{n} u_{nm}\, h^b_{nm}(\lambda,\phi,u) \ . \tag{2.13}$$

On the level ellipsoid, i.e., for $u = b$, the Eqs. (2.10) and (2.13) reduce to

$$U(\lambda,\phi,b) = \sum_{n=0}^{\infty} \sum_{m=-n}^{n} u_{nm}\, e_{nm}(\lambda,\phi) \tag{2.14}$$

with

$$h^b_{nm}(\lambda,\phi,b) = e_{nm}(\lambda,\phi) \ . \tag{2.15}$$

Hence, the representations (2.10) and (2.13) hold for all $\boldsymbol{x} \in \overline{\mathbb{E}}^{2,\mathrm{ext}}_{a,b}$, wherein

$$\overline{\mathbb{E}}^{2,\mathrm{ext}}_{a,b} = \mathbb{E}^{2,\mathrm{ext}}_{a,b} \cup \mathbb{E}^{2}_{a,b} \tag{2.16}$$

means the union of the outer space $\mathbb{E}^{2,\mathrm{ext}}_{a,b}$ and the reference ellipsoid $\mathbb{E}^{2}_{a,b}$. Obviously, the outer ellipsoidal harmonics (2.12) are the harmonic continuation of the surface ellipsoidal harmonics (2.11) into the outer space $\mathbb{E}^{2,\mathrm{ext}}_{a,b}$ of the reference ellipsoid $\mathbb{E}^{2}_{a,b}$. On $\mathbb{E}^{2}_{a,b}$ the surface ellipsoidal harmonics (2.11) fulfill the orthonormality condition with respect to the weighted scalar (inner) product

$$\left\langle\, e_{pq}(\lambda,\phi) \,|\, e_{nm}(\lambda,\phi) \,\right\rangle_w = \frac{1}{S_{a,b}} \int_{\mathbb{E}^2_{a,b}} dS_{a,b}(\phi)\, w(\phi)\, e_{pq}(\lambda,\phi)\, e_{nm}(\lambda,\phi) = \delta_{pm}\, \delta_{qn} \ . \tag{2.17}$$

Herein

$$\begin{aligned} S_{a,b} = \mathrm{area}(\mathbb{E}^2_{a,b}) &= 4\pi\, a^2 \left(\frac{1}{2} + \frac{1}{4} \frac{b^2}{a\epsilon} \ln \frac{a+\epsilon}{a-\epsilon} \right) \\ &= \frac{2\pi\, ab^2}{\epsilon} \left(\frac{a\epsilon}{b^2} + \mathrm{arcsinh}\left(\frac{\epsilon}{b}\right) \right) \end{aligned} \tag{2.18}$$

means the total area of the reference ellipsoid and

$$dS_{a,b}(\phi) = d\{\mathrm{area}(\mathbb{E}^2_{a,b})\} = a\,\sqrt{b^2 + \epsilon^2 \sin^2\phi}\,\cos\phi\,d\lambda\,d\phi \tag{2.19}$$

the corresponding ellipsoidal surface element. The weight function $w(\phi)$ is defined as

$$w(\phi) = \frac{a}{\sqrt{b^2 + \epsilon^2 \sin^2\phi}}\,\left(\frac{1}{2} + \frac{1}{4}\frac{b^2}{a\epsilon}\ln\frac{a+\epsilon}{a-\epsilon}\right)\;; \tag{2.20}$$

see e.g. Ardalan and Grafarend (2001). The procedure presented before can be interpreted as follows: due to the weight function (2.20) we remove the ellipsoidal part of both the ellipsoidal surface element (2.19) and the total area (2.18). What remains is the orthonormality condition for the (spherical) harmonics $e_{nm}(\lambda,\phi)$ given on the unit sphere $\mathbb{S}^2$. Hence, we summarize that in the sense of the weighted scalar product (2.17) the set of surface ellipsoidal harmonics (2.11) constitutes a complete orthonormal basis of the space $L_2(\mathbb{E}^2_{a,b})$ of square-integrable functions on the reference ellipsoid (2.3).

The *series coefficients* u_{nm} of the Fourier series (2.13) are computed by the *ellipsoidal Fourier transform*

$$\begin{aligned} u_{nm} &= \left\langle\, f(\lambda_q,\phi_q,b)\,|\,e_{nm}(\lambda_q,\phi_q)\,\right\rangle_w \\ &= \frac{1}{S_{a,b}}\int_{\mathbb{E}^2_{a,b}} dS_{a,b}(\phi_q)\,w(\phi_q)\,f(\lambda_q,\phi_q,b)\,e_{nm}(\lambda_q,\phi_q) \end{aligned} \tag{2.21}$$

from given boundary values

$$f(\lambda_q,\phi_q,b) = f(\boldsymbol{x}_q) = U(\boldsymbol{x}_q) \qquad \forall \quad \boldsymbol{x}_q \in \mathbb{E}^2_{a,b}\,. \tag{2.22}$$

Inserting Eq. (2.21) into Eq. (2.13) yields under the consideration of the Eqs. (2.15) and (2.22)

$$\begin{aligned} U(\lambda,\phi,u) &= \frac{1}{S_{a,b}}\int_{\mathbb{E}^2_{a,b}} dS_{a,b}(\phi_q)\,w(\phi_q)\,\times \\ &\qquad \times\left(\sum_{n=0}^{\infty}\sum_{m=-n}^{n} h^b_{nm}(\lambda_q,\phi_q,b)\,h^b_{nm}(\lambda,\phi,u)\right) f(\lambda_q,\phi_q,b) \\ &= \frac{1}{S_{a,b}}\int_{\mathbb{E}^2_{a,b}} dS_{a,b}(\phi_q)\,w(\phi_q)\;K^e_{\mathrm{AP}}(\lambda_q,\phi_q,b,\lambda,\phi,u)\;f(\lambda_q,\phi_q,b) \\ &= \frac{1}{S_{a,b}}\int_{\mathbb{E}^2_{a,b}} dS_{a,b}(\phi_q)\,w(\phi_q)\;K^e_{\mathrm{AP}}(\boldsymbol{x},\boldsymbol{x}_q)\;U(\boldsymbol{x}_q) \\ &= \left\langle\, K^e_{\mathrm{AP}}(\boldsymbol{x},\boldsymbol{x}_q)\,|\,U(\boldsymbol{x}_q)\,\right\rangle_w \end{aligned} \tag{2.23}$$

with $\boldsymbol{x} \in \overline{\mathbb{E}}^{2,\mathrm{ext}}_{a,b}$ and $\boldsymbol{x}_q \in \mathbb{E}^2_{a,b}$. In this inner product we find the *ellipsoidal Abel-Poisson kernel*

$$K^e_{\mathrm{AP}}(\boldsymbol{x}, \boldsymbol{x}_q) = \sum_{n=0}^{\infty} \sum_{m=-n}^{n} h^b_{nm}(\boldsymbol{x})\, h^b_{nm}(\boldsymbol{x}_q)$$

$$= \sum_{n=0}^{\infty} \sum_{m=-n}^{n} \frac{Q^\star_{nm}(\frac{u}{\epsilon})}{Q^\star_{nm}(\frac{b}{\epsilon})}\, e_{nm}(\boldsymbol{\xi})\, e_{nm}(\boldsymbol{\xi}_q)\ . \tag{2.24}$$

At the surface of the reference ellipsoid, i.e. for $u = b$, the ellipsoidal Abel-Poisson kernel reduces to

$$K^e_{\mathrm{AP}}(\boldsymbol{x}, \boldsymbol{x}_q) = \sum_{n=0}^{\infty} \sum_{m=-n}^{n} e_{nm}(\boldsymbol{\xi})\, e_{nm}(\boldsymbol{\xi}_q)\ . \tag{2.25}$$

Inserting the *addition theorem*

$$\sum_{m=-n}^{n} e_{nm}(\boldsymbol{\xi})\, e_{nm}(\boldsymbol{\xi}_q) = (2n+1)\ P_n(\boldsymbol{\xi}^T \boldsymbol{\xi}_q) \tag{2.26}$$

into Eq. (2.25) yields the *Legendre series*

$$K^e_{\mathrm{AP}}(\boldsymbol{x}, \boldsymbol{x}_q) = \sum_{n=0}^{\infty} (2n+1)\ P_n(\boldsymbol{\xi}^T \boldsymbol{\xi}_q) \tag{2.27}$$

of the *delta function* $\delta(\,\cdot\,)$, i.e. $K^e_{\mathrm{AP}}(\boldsymbol{x}, \boldsymbol{x}_q) = \delta(\boldsymbol{\xi} - \boldsymbol{\xi}_q)$.

For numerical applications we deal now with the quotient $Q^\star_{nm}(\frac{u}{\epsilon})/Q^\star_{nm}(\frac{b_0}{\epsilon})$. In the sequel we assume that the reference ellipsoid (2.3) is defined by the values $a =: a_0$ and $b =: b_0$ for the semi-major and the semi-minor axis, respectively; thus, the eccentricity (2.2) is given as $\epsilon = \sqrt{a_0^2 - b_0^2}$. According to Martinec and Grafarend (1997) we may write

$$\frac{Q^\star_{nm}(\frac{u}{\epsilon})}{Q^\star_{nm}(\frac{b_0}{\epsilon})} = \frac{e^{n+1} \sum_{k=0}^{\infty} a_{nmk} e^{2k}}{e_0^{n+1} \sum_{k=0}^{\infty} a_{nmk} e_0^{2k}} \tag{2.28}$$

with

$$e = \frac{\epsilon}{\sqrt{u^2 + \epsilon^2}} = \frac{\epsilon}{\sqrt{u^2 + a_0^2 + b_0^2}} = \frac{\epsilon}{a}\ , \tag{2.29}$$

$$e_0 = \frac{\epsilon}{\sqrt{b_0^2 + \epsilon^2}} = \frac{\epsilon}{a_0}\ . \tag{2.30}$$

The coefficients a_{nmk} can, for instance, be computed by the recurrence relation

$$a_{nmk} = \frac{(n+2k-1)^2 - m^2}{2k\,(2n+2k+1)}\ a_{nm,k-1} \qquad \text{for} \quad k \geq 1 \tag{2.31}$$

starting with $a_{nm0} = 1$. Thus, it follows from Eq. (2.28) considering the right-hand sides of the Eqs. (2.29) and (2.30)

$$\frac{Q^{\star}_{nm}(\frac{u}{\epsilon})}{Q^{\star}_{nm}(\frac{b_0}{\epsilon})} = \Big(\frac{a_0}{a}\Big)^{n+1} \frac{1 + \sum\limits_{k=1}^{\infty} a_{nmk} e^{2k}}{1 + \sum\limits_{k=1}^{\infty} a_{nmk} e_0^{2k}} \; . \tag{2.32}$$

Expanding the denominator into a geometric series yields

$$\begin{aligned}
\frac{Q^{\star}_{nm}(\frac{u}{\epsilon})}{Q^{\star}_{nm}(\frac{b_0}{\epsilon})} &= \Big(\frac{a_0}{a}\Big)^{n+1} \left(1 + \sum_{k=1}^{\infty} a_{nmk} e^{2k}\right) \left(1 - \sum_{k=1}^{\infty} a_{nmk} e_0^{2k} + \ldots\right) \\
&= \Big(\frac{a_0}{a}\Big)^{n+1} \left(1 + a_{nm1} e^2 + \ldots\right) \left(1 - a_{nm1} e_0^2 + \ldots\right) \\
&= \Big(\frac{a_0}{a}\Big)^{n+1} \left(1 + a_{nm1} (e^2 - e_0^2) + \ldots\right) \\
&= \Big(\frac{a_0}{a}\Big)^{n+1} + \Big(\frac{a_0}{a}\Big)^{n+1} \; a_{nm1} \; (a^{-2} - a_0^{-2}) \; \epsilon^2 + \ldots \; .
\end{aligned} \tag{2.33}$$

According to Eq. (2.31) the coefficients a_{nm1} are given as $a_{nm1} = ((n+1)^2 - m^2)/(4n+6)$. In case that the reference ellipsoid $\mathbb{E}^2_{a_0,b_0}$ corresponds to the reference sphere $\mathbb{S}^2_R$ with radius $R = a_0 = b_0$ Eq. (2.33) reduces with $\epsilon = 0$ to

$$\frac{Q^{\star}_{nm}(\frac{u}{\epsilon})}{Q^{\star}_{nm}(\frac{b_0}{\epsilon})} = \left(\frac{R}{r}\right)^{n+1} \tag{2.34}$$

with $a = u = r$.

Due to the relation (2.34) between the ellipsoidal and the spherical theory we at first study in the next section some spherical features in more detail.

2.2 Basic Spherical Settings

In the spherical theory we choose according to Eq. (2.34) the sphere

$$\mathbb{S}^2_R = \{\, R \cdot \boldsymbol{r} \,|\, 0 \leq \lambda < 2\pi, -\pi/2 \leq \beta \leq \pi/2 \,,\; R > 0 \,\} \; . \tag{2.35}$$

as defined in Eq. (2.9) with $r = R$ as the reference sphere; in order to avoid a mix-up between the ellipsoidal and the spherical scenarios we substitute the greek letter β for ϕ and $\boldsymbol{r}$ for the unit vector $\boldsymbol{\xi}$. Hence, the coordinate triple (λ, β, r) consists of $\lambda =$ spherical longitude, $\beta =$ spherical latitude and $r =$ radius. Note, that the spherical longitude is equivalent to the ellipsoidal longitude introduced

in Eq. (2.1). Usually in Eq. (2.35) R is defined as a mean Earth radius. However, $\mathbb{S}^2_R$ can also be identified with the *Brillouin sphere* or the *Bjerhammer sphere*; see e.g. Torge (2001). In spherical coordinates the position vector $\boldsymbol{x}$ of an arbitrary point $P = P(\boldsymbol{x})$ reads

$$\boldsymbol{x} = r \cdot \left[\, \cos\beta \cos\lambda, \, \cos\beta \sin\lambda, \, \sin\beta \, \right]^T = r \cdot \boldsymbol{r} \tag{2.36}$$

with $|\boldsymbol{x}| = r$. Analogous to Eq. (2.10) and considering the result (2.34) we obtain the solution

$$U(\lambda, \beta, r) = \sum_{n=0}^{\infty} \sum_{m=-n}^{n} u^s_{nm} \, \left(\frac{R}{r} \right)^{n+1} e_{nm}(\lambda, \beta) = U(\boldsymbol{x}) \tag{2.37}$$

of the Laplacian differential equation for the gravitational potential $U(\boldsymbol{x})$ in a point $P(\boldsymbol{x})$ with $\boldsymbol{x} \in \overline{\mathbb{S}}^{2,\mathrm{ext}}_R = \mathbb{S}^{2,\mathrm{ext}}_R \cup \mathbb{S}^2_R$, wherein $\mathbb{S}^{2,\mathrm{ext}}_R$ means the exterior of the sphere $\mathbb{S}^2_R$, cf. Eq. (2.16). The *surface spherical harmonics*

$$e_{nm}(\lambda, \beta) = P^{\star}_{n|m|}(\sin\beta) \, \left\{ \begin{array}{lll} \cos m\lambda & \forall & m \geq n \\ \sin |m|\lambda & \forall & m < 0 \end{array} \right\} = e_{nm}(\boldsymbol{r}) \; , \tag{2.38}$$

(see e.g. Heiskanen and Moritz (1967, p. 21)) fulfill the orthonormality condition

$$\left\langle \, e_{pq}(\lambda, \beta) \, | \, e_{nm}(\lambda, \beta) \, \right\rangle = \frac{1}{S_R} \int_{\mathbb{S}^2_R} dS_R(\beta) \, e_{pq}(\lambda, \beta) \, e_{nm}(\lambda, \beta) = \delta_{pm} \, \delta_{qn} \tag{2.39}$$

with respect to the sphere $\mathbb{S}^2_R$. Herein

$$S_R = \mathrm{area}(\mathbb{S}^2_R) = 4\pi \, R^2 \tag{2.40}$$

means the total area of the sphere and

$$dS_R(\beta) = d\{\mathrm{area}(\mathbb{S}^2_R)\} = R^2 \, \cos\beta \, d\lambda \, d\beta \tag{2.41}$$

the corresponding spherical surface element; cf. Eqs. (2.18) and (2.19) as well as the comments following Eq. (2.20). From Eq. (2.39) we conclude that the set of surface spherical harmonics (2.38) constitutes a complete orthonormal basis of the space $L_2(\mathbb{S}^2_R)$ of square-integrable functions on the reference sphere (2.35).

Defining the *outer spherical harmonics*

$$h^R_{nm}(\lambda, \beta, r) = \left(\frac{R}{r} \right)^{n+1} e_{nm}(\lambda, \beta) = h^R_{nm}(\boldsymbol{x}) \tag{2.42}$$

the Fourier series (2.37) can be rewritten as

$$U(\lambda, \beta, r) = \sum_{n=0}^{\infty} \sum_{m=-n}^{n} u^s_{nm} \, h^R_{nm}(\lambda, \beta, r) \; . \tag{2.43}$$

On the reference sphere $\mathbb{S}_R^2$, i.e., for $r = R$, the Eqs. (2.37) and (2.43) reduce to

$$U(\lambda, \beta, R) = \sum_{n=0}^{\infty} \sum_{m=-n}^{n} u_{nm}^s \, e_{nm}(\lambda, \beta) \tag{2.44}$$

with $h_{nm}^R(\lambda, \beta, R) = e_{nm}(\lambda, \beta)$. The *series coefficients* u_{nm}^s are computable via the *spherical Fourier transform*

$$\begin{aligned} u_{nm}^s &= \left\langle \, f(\lambda_q, \beta_q, R) \, | \, e_{nm}(\lambda_q, \beta_q) \, \right\rangle \\ &= \frac{1}{S_R} \int_{\mathbb{S}_R^2} dS_R(\beta_q) \, f(\lambda_q, \beta_q, R) \, e_{nm}(\lambda_q, \beta_q) \end{aligned} \tag{2.45}$$

from given boundary values

$$f(\lambda_q, \beta_q, R) = f(\boldsymbol{x}_q) = U(\boldsymbol{x}_q) \qquad \forall \quad \boldsymbol{x}_q = R \cdot \boldsymbol{r}_q \in \mathbb{S}_R^2 \, . \tag{2.46}$$

Inserting Eq. (2.45) into Eq. (2.43) yields under the consideration of the Eqs. (2.42) and (2.46)

$$\begin{aligned} U(\lambda, \beta, r) &= \frac{1}{S_R} \int_{\mathbb{S}_R^2} dS_R(\beta_q) \, \left(\sum_{n=0}^{\infty} \sum_{m=-n}^{n} h_{nm}^R(\lambda_q, \beta_q, R) \, h_{nm}^R(\lambda, \beta, r) \right) \, f(\lambda_q, \beta_q, R) \\ &= \frac{1}{S_R} \int_{\mathbb{S}_R^2} dS_R(\beta_q) \, K_{\mathrm{AP}}^s(\lambda_q, \beta_q, R, \lambda, \beta, r) \, f(\lambda_q, \beta_q, R) \\ &= \frac{1}{S_R} \int_{\mathbb{S}_R^2} dS_R(\beta_q) \, K_{\mathrm{AP}}^s(\boldsymbol{x}, \boldsymbol{x}_q) \, U(\boldsymbol{x}_q) \\ &= \left\langle \, K_{\mathrm{AP}}^s(\boldsymbol{x}, \boldsymbol{x}_q) \, | \, U(\boldsymbol{x}_q) \, \right\rangle \end{aligned} \tag{2.47}$$

with $\boldsymbol{x} = r \cdot \boldsymbol{r} \in \overline{\mathbb{S}}_R^{2,\mathrm{ext}}$ and $\boldsymbol{x}_q = R \cdot \boldsymbol{r}_q \in \mathbb{S}_R^2$. The *spherical Abel-Poisson kernel*

$$\begin{aligned} K_{\mathrm{AP}}^s(\boldsymbol{x}, \boldsymbol{x}_q) &= \sum_{n=0}^{\infty} \sum_{m=-n}^{n} h_{nm}^R(\boldsymbol{x}) \, h_{nm}^b(\boldsymbol{x}_q) \\ &= \sum_{n=0}^{\infty} \sum_{m=-n}^{n} \left(\frac{R}{r} \right)^{n+1} e_{nm}(\boldsymbol{r}) \, e_{nm}(\boldsymbol{r}_q) \end{aligned} \tag{2.48}$$

reduces on the sphere $\mathbb{S}_R^2$, i.e. for $r = R$, to

$$K_{\mathrm{AP}}^s(\boldsymbol{x}, \boldsymbol{x}_q) = \sum_{n=0}^{\infty} \sum_{m=-n}^{n} e_{nm}(\boldsymbol{r}) \, e_{nm}(\boldsymbol{r}_q) \, . \tag{2.49}$$

Inserting the addition theorem

$$\sum_{m=-n}^{n} e_{nm}(\boldsymbol{r}) \, e_{nm}(\boldsymbol{r}_q) = (2n+1) \, P_n(\boldsymbol{r}^T \boldsymbol{r}_q) \tag{2.50}$$

yields the Legendre series

$$K^s_{\mathrm{AP}}(\boldsymbol{x},\boldsymbol{x}_q) = \sum_{n=0}^{\infty} (2n+1)\; P_n(\boldsymbol{r}^T\boldsymbol{r}_q)\;. \tag{2.51}$$

In the spherical theory the argument $\boldsymbol{r}^T\boldsymbol{r}_q$ of the Legendre polynomial $P_n(\,\cdot\,)$ in Eq. (2.51) defines the spherical distance $\alpha = \arccos(\boldsymbol{r}^T\boldsymbol{r}_q)$ between two points $P(\boldsymbol{r})$ and $P(\boldsymbol{r}_q)$ on the unit sphere $\mathbb{S}^2$. Thus, if we keep $\boldsymbol{x} = R\cdot\boldsymbol{r}$ fixed and vary $\boldsymbol{x}_q = R\cdot\boldsymbol{r}_q$ the spherical Abel-Poisson kernel is *rotational symmetric*, i.e. isotropic. However, for the level ellipsoid $\mathbb{E}^2_{a,b}$, i.e. for Eq. (2.27), this statement holds only, if the position vector $\boldsymbol{x}$, Eq. (2.1), points either to the north or to the south pole. The deviation from the rotational symmetry depends on the ellipsoidal correction $\delta\boldsymbol{r}$ defined in Eq. (2.5). But due to the formal identity of the Eqs. (2.27) and (2.51) we conclude that wavelet theory for functions on the ellipsoid mostly agrees with the wavelet theory for functions on the sphere. Another excellent feature, already mentioned, is the fact that according to the Eqs. (2.39) and (2.17) the surface harmonics $e_{nm}(\,\cdot\,)$ constitute orthonormal bases of the Hilbert spaces $L_2(\mathbb{S}^2_R)$ and $L_2(\mathbb{E}^2_{a,b})$.

Next, we introduce the general *spherical kernel*

$$\begin{aligned} K^s(\boldsymbol{x},\boldsymbol{x}_q) &= \sum_{n=0}^{\infty}\sum_{m=-n}^{n} k_n\, h^R_{nm}(\boldsymbol{x})\, h^R_{nm}(\boldsymbol{x}_q) \\ &= \sum_{n=0}^{\infty}\sum_{m=-n}^{n} \left(\frac{R^2}{r\,r_q}\right)^{n+1} k_n\, e_{nm}(\boldsymbol{r})\, e_{nm}(\boldsymbol{r}_q). \end{aligned} \tag{2.52}$$

with $\boldsymbol{x},\boldsymbol{x}_q \in \overline{\mathbb{S}}^{2,\mathrm{ext}}_R$. Since the *Legendre coefficients* k_n depend exclusively on the degree n, the addition theorem (2.50) can be applied. Thus, the kernel (2.52) is rotational symmetric and can be expanded as the Legendre series

$$K^s(\boldsymbol{x},\boldsymbol{x}_q) = \sum_{n=0}^{\infty} (2n+1)\; \left(\frac{R^2}{r\,r_q}\right)^{n+1} k_n\, P_n(\boldsymbol{r}^T\boldsymbol{r}_q)\;. \tag{2.53}$$

Note, that in the Abel-Poisson case (2.48) all Legendre coefficients k_n are equal to one.

Eq. (2.47) can be rewritten as *spherical convolution*

$$U(\boldsymbol{x}) = \left(\; K^s_{\mathrm{AP}} \star U \;\right)(\boldsymbol{x}) \tag{2.54}$$

generally defined as

$$\begin{aligned} \mathcal{K}^s f(\boldsymbol{x}) := \left(\; K^s \star f \;\right)(\boldsymbol{x}) &= \left\langle\; K^s(\boldsymbol{x},\boldsymbol{x}_q) \,|\, f(\boldsymbol{x}_q) \;\right\rangle \\ &= \frac{1}{S_R}\int_{\mathbb{S}^2_R} dS_R(\beta_q)\; K^s(\boldsymbol{x},\boldsymbol{x}_q)\; f(\boldsymbol{x}_q) \end{aligned} \tag{2.55}$$

for a function $f \in L_2(\mathbb{S}_R^2)$ and a kernel $K^s(\boldsymbol{x}, \boldsymbol{x}_q)$ according to (2.52) with $\boldsymbol{x} \in \overline{\mathbb{S}}_R^{2,\mathrm{ext}}$ and $\boldsymbol{x}_q \in \mathbb{S}_R^2$. For studying this convolution in the spectral domain we need the

Lemma (Funk-Hecke formula): *Let $f \in L_2(\mathbb{S}_R^2)$, i.e.,*

$$f(\boldsymbol{x}_q) = \sum_{n=0}^{\infty} \sum_{m=-n}^{n} f_{nm}^s \, e_{nm}(\boldsymbol{r}_q) \tag{2.56}$$

with $\boldsymbol{x}_q \in \mathbb{S}_R^2$, and K^s a spherical kernel, i.e.,

$$\begin{aligned} K^s(\boldsymbol{x}, \boldsymbol{x}_q) &= \sum_{n=0}^{\infty} \sum_{m=-n}^{n} k_n \, h_{nm}^R(\boldsymbol{x}) \, h_{nm}^R(\boldsymbol{x}_q) \\ &= \sum_{n=0}^{\infty} \sum_{m=-n}^{n} \left(\frac{R}{r}\right)^{n+1} k_n \, e_{nm}(\boldsymbol{r}) \, e_{nm}(\boldsymbol{r}_q) \end{aligned} \tag{2.57}$$

with $\boldsymbol{x} \in \overline{\mathbb{S}}_R^{2,\mathrm{ext}}$ and $\boldsymbol{x}_q \in \mathbb{S}_R^2$. Then the spherical convolution

$$\mathcal{K}^s f(\boldsymbol{x}) = \left(K^s \star f \right)(\boldsymbol{x}) = \frac{1}{S_R} \int_{\mathbb{S}_R^2} dS_R(\beta_q) \; K^s(\boldsymbol{x}, \boldsymbol{x}_q) \; f(\boldsymbol{x}_q) \tag{2.58}$$

is given from the products of the spherical Fourier coefficients f_{nm}^s and k_n of f and K^s, i.e.

$$\mathcal{K}^s f(\boldsymbol{x}) = \left(K^s \star f \right)(\boldsymbol{x}) = \sum_{n=0}^{\infty} \sum_{m=-n}^{n} k_n \; f_{nm}^s \; h_{nm}^R(\boldsymbol{x}) \; . \tag{2.59}$$

This statement can be proven by introducing Eqs. (2.56) and (2.57) into Eq. (2.58) and considering the orthonormality condition (2.39).

The comparison of the result (2.59) with the representation (2.43) shows, that the spherical Fourier coefficients $(K^s f)_{nm}^s$ of the spherical convolution $\mathcal{K}^s f(\boldsymbol{x})$ are defined as

$$(\mathcal{K}^s f)_{nm}^s = k_n \; f_{nm}^s \; . \tag{2.60}$$

For $\boldsymbol{x}, \boldsymbol{x}_q \in \mathbb{S}_R^2$, i.e., $r = r_q = R$ the kernel (2.57) reads

$$K^s(\boldsymbol{x}, \boldsymbol{x}_q) = \sum_{n=0}^{\infty} \sum_{m=-n}^{n} k_n \, e_{nm}(\boldsymbol{r}) \, e_{nm}(\boldsymbol{r}_q) \; . \tag{2.61}$$

Considering the orthonormality condition (2.39) we obtain

$$K^s(\boldsymbol{x}, \boldsymbol{x}_q) = \sum_{n=0}^{\infty} (2n+1) \, k_n \, P_n(\boldsymbol{r}^T \boldsymbol{r}_q) =: K^s(\boldsymbol{r}^T \boldsymbol{r}_q) \; , \tag{2.62}$$

cf. the Abel-Poisson kernel (2.51). Since $\alpha = \arccos(\boldsymbol{r}^T\boldsymbol{r}_q)$ the argument $\boldsymbol{r}^T\boldsymbol{r}_q = \cos\alpha =: t$ is restricted to $-1 \leq t \leq 1$. Thus, the kernel $K^s(\boldsymbol{r}^T\boldsymbol{r}_q) = K^s(t)$ is a member of the space $L_2([-1,1])$ spanned by the Legendre polynomials $P_n(\,\cdot\,)$. Equation (2.62) is known as the *inverse Legendre transform*. Consequently, the *Legendre transform* is defined as

$$k_n = \int_{-1}^{1} K^s(t)\; P_n(t)\; dt\;. \tag{2.63}$$

From the results presented before we conclude, that according to Eq. (2.58) $\mathcal{K}^s$ means an *integral operator* with the rotational symmetric kernel $K^s(\boldsymbol{r}^T\boldsymbol{r}_q) =: K^s(t)$ defined in Eq. (2.62). Nearly all operators in gravimetry with the sphere as reference surface are from the above type. Examples include the spherical Abel-Poisson as already studied, the radial derivatives on the sphere, the spherical Stokes operator or the operators computing spherical single-/double-layer potentials.

Next, we study the *spherical scalar product*

$$\left\langle\; f(\boldsymbol{x}) \,|\, g(\boldsymbol{x}) \;\right\rangle = \frac{1}{S_R} \int_{\mathbb{S}_R^2} dS_R(\beta)\, f(\boldsymbol{x})\, g(\boldsymbol{x}) \tag{2.64}$$

of two functions $f, g \in L_2(\mathbb{S}_R^2)$ with $\boldsymbol{x} \in \mathbb{S}_R^2$ in more detail. Expanding both functions into spherical Fourier series, i.e.,

$$f(\boldsymbol{x}) = \sum_{n=0}^{\infty} \sum_{m=-n}^{n} f_{nm}^s\; e_{nm}(\boldsymbol{r})\;, \tag{2.65}$$

$$g(\boldsymbol{x}) = \sum_{n=0}^{\infty} \sum_{m=-n}^{n} g_{nm}^s\; e_{nm}(\boldsymbol{r}) \tag{2.66}$$

according to Eq. (2.44) yields under the consideration of the orthonormality condition (2.39)

$$\begin{aligned}
\left\langle\; f(\boldsymbol{x}) \,|\, g(\boldsymbol{x}) \;\right\rangle &= \frac{1}{S_R} \int_{\mathbb{S}_R^2} dS_R(\beta) \left(\sum_{n=0}^{\infty} \sum_{m=-n}^{n} f_{nm}^s\; e_{nm}(\boldsymbol{r}) \right) \left(\sum_{p=0}^{\infty} \sum_{q=-p}^{p} g_{pq}^s\; e_{pq}(\boldsymbol{r}) \right) \\
&= \left(\sum_{n=0}^{\infty} \sum_{m=-n}^{n} \sum_{p=0}^{\infty} \sum_{q=-p}^{p} f_{nm}^s\; g_{pq}^s \right) \frac{1}{S_R} \int_{\mathbb{S}_R^2} dS_R(\beta)\, e_{nm}(\boldsymbol{r})\; e_{pq}(\boldsymbol{r}) \\
&= \sum_{n=0}^{\infty} \sum_{m=-n}^{n} f_{nm}^s\; g_{nm}^s\;.
\end{aligned} \tag{2.67}$$

Thus, the scalar product $\left\langle\; f(\boldsymbol{x}) \,|\, g(\boldsymbol{x}) \;\right\rangle$, defined in the spatial domain on the sphere, corresponds in the spectral domain to the sum of the products of the spherical Fourier coefficients f_{nm}^s and g_{nm}^s. This relation is known as *Parseval's identity*. The $L_2(\mathbb{S}_R^2)$-norm $\|f\|_{L_2(\mathbb{S}_R^2)}$ of the function $f(\boldsymbol{x})$ is defined as

$$\|f\|_{L_2(\mathbb{S}_R^2)} = \sqrt{\left\langle\; f(\boldsymbol{x}) \,|\, f(\boldsymbol{x}) \;\right\rangle}\;. \tag{2.68}$$

Applying Parseval's identity (2.67) we finally obtain

$$\|f\|_{L_2(\mathbb{S}_R^2)} = \sqrt{\sum_{n=0}^{\infty} \sum_{m=-n}^{n} (f_{nm}^s)^2} \; . \tag{2.69}$$

Note, that the norm can also be interpreted as the energy content or the global root-mean-square (rms) value of the function $f(\boldsymbol{x})$.

From Eq. (2.61) we conclude that besides the complete set of spherical harmonics $e_{nm}(\boldsymbol{r})$ the functions $K^s(\boldsymbol{r}^T\boldsymbol{r}_q)$ as defined in Eq. (2.62) span the space $L_2(\mathbb{S}_R^2)$. For this reason, they are called *spherical base functions*. Hence, the function (2.65) can be modeled as

$$f(\boldsymbol{x}) = \frac{1}{S_R} \int_{\mathbb{S}_R^2} dS_R(\beta_q) \; K^s(\boldsymbol{r}^T\boldsymbol{r}_q) \; c^s(\boldsymbol{x}_q) = \left(\; K^s \; \star \; c^s \; \right)(\boldsymbol{x}) \tag{2.70}$$

with an unknown function $c^s(\boldsymbol{x}_q)$ and $\boldsymbol{x}_q \in \mathbb{S}_R^2$.

Chapter 3

Multi-Resolution Representation on the Ellipsoid

As already mentioned the fundamental idea of a multi-resolution representation is to split a given input signal into a smoother version and a number of detail signals by successive low-pass filtering; this procedure, which provides a sequence of signal approximations at different resolutions, is also known as multi-resolution analysis (Mertins, 1999). The detail signals are the spectral components or modules of the multi-resolution representation because they are related to specific frequency bands.

3.1 Ellipsoidal Kernels

We already mentioned that we can study functions on the ellipsoid as functions on the sphere via introducing an appropriate weighted inner product, cf. the orthonormality condition (2.17). However, we also have seen from the discussion in the context of Eq. (2.51), that the exclusive restriction to rotational symmetric kernels on the ellipsoid is no longer natural and appropriate. In the following we present the natural multi-resolution representation based on the ellipsoidal harmonics. For this we start with introducing the *generalized ellipsoidal kernel*

$$\begin{aligned} K^e(\boldsymbol{x}, \boldsymbol{x}_q) &= \sum_{n=0}^{\infty} \sum_{m=-n}^{n} k_{nm}\, h^b_{nm}(\boldsymbol{x})\, h^b_{nm}(\boldsymbol{x}_q) \\ &= \sum_{n=0}^{\infty} \sum_{m=-n}^{n} \frac{Q^\star_{nm}(\frac{u}{\epsilon})}{Q^\star_{nm}(\frac{b}{\epsilon})} \frac{Q^\star_{nm}(\frac{u_q}{\epsilon})}{Q^\star_{nm}(\frac{b}{\epsilon})}\, k_{nm}\, e_{nm}(\boldsymbol{\xi})\, e_{nm}(\boldsymbol{\xi}_q) \end{aligned} \tag{3.1}$$

with $\boldsymbol{x}, \boldsymbol{x}_q \in \overline{\mathbb{E}}^{2,\mathrm{ext}}_{a,b}$, cf. Eq. (2.52). On the reference ellipsoid, i.e., for the special case $\boldsymbol{x}, \boldsymbol{x}_q \in \mathbb{E}^2_{a,b}$, Eq. (3.1) reads

$$K^e(\boldsymbol{x}, \boldsymbol{x}_q) = \sum_{n=0}^{\infty} \sum_{m=-n}^{n} k_{nm}\, e_{nm}(\boldsymbol{\xi})\, e_{nm}(\boldsymbol{\xi}_q)\ . \tag{3.2}$$

Next, we define the *ellipsoidal convolution*

$$\begin{aligned} \mathcal{K}^e f(\boldsymbol{x}) = \big(\ K^e \star f\ \big)_w(\boldsymbol{x}) &= \big\langle\ K^e(\boldsymbol{x}, \boldsymbol{x}_q)\,|\, f(\boldsymbol{x}_q)\ \big\rangle_w \\ &= \frac{1}{S_{a,b}} \int_{\mathbb{E}^2_{a,b}} dS_{a,b}(\phi_q)\ w(\phi_q)\ K^e(\boldsymbol{x}, \boldsymbol{x}_q)\ f(\boldsymbol{x}_q) \end{aligned} \tag{3.3}$$

for a function $f \in L_2(\mathbb{E}^2_{a,b})$ and a kernel $K^e(\boldsymbol{x}, \boldsymbol{x}_q)$ according to (3.1) with $\boldsymbol{x} \in \overline{\mathbb{E}}^{2,\mathrm{ext}}_{a,b}$ and $\boldsymbol{x}_q \in \mathbb{E}^2_{a,b}$, cf. Eq. (2.23). For studying the relation (3.3) in the spectral domain we need the

Lemma (generalized Funk-Hecke formula): *Let $f \in L_2(\mathbb{E}^2_{a,b})$, i.e.,*

$$f(\boldsymbol{x}_q) = \sum_{n=0}^{\infty} \sum_{m=-n}^{n} f_{nm}\ e_{nm}(\boldsymbol{\xi}_q) \tag{3.4}$$

with $\boldsymbol{x}_q \in \mathbb{E}^2_{a,b}$, and K^e a generalized ellipsoidal kernel, i.e.,

$$\begin{aligned} K^e(\boldsymbol{x}, \boldsymbol{x}_q) &= \sum_{n=0}^{\infty} \sum_{m=-n}^{n} k_{nm}\, h^b_{nm}(\boldsymbol{x})\, h^b_{nm}(\boldsymbol{x}_q) \\ &= \sum_{n=0}^{\infty} \sum_{m=-n}^{n} \frac{Q^\star_{nm}(\frac{u}{\epsilon})}{Q^\star_{nm}(\frac{b}{\epsilon})}\, k_{nm}\, e_{nm}(\boldsymbol{\xi})\, e_{nm}(\boldsymbol{\xi}_q) \end{aligned} \tag{3.5}$$

with $\boldsymbol{x} \in \overline{\mathbb{E}}^{2,\mathrm{ext}}_{a,b}$ and $\boldsymbol{x}_q \in \mathbb{E}^2_{a,b}$. Then the ellipsoidal convolution

$$\mathcal{K}^e f(\boldsymbol{x}) = \big(\ K^e \star f\ \big)_w(\boldsymbol{x}) = \frac{1}{S_{a,b}} \int_{\mathbb{E}^2_{a,b}} dS_{a,b}(\phi_q)\ w(\phi_q)\ K^e(\boldsymbol{x}, \boldsymbol{x}_q)\ f(\boldsymbol{x}_q) \tag{3.6}$$

is given from the products of the ellipsoidal Fourier coefficients f_{nm} and k_{nm} of f and K^e, i.e.

$$\mathcal{K}^e f(\boldsymbol{x}) = \big(\ K^e \star f\ \big)_w(\boldsymbol{x}) = \sum_{n=0}^{\infty} \sum_{m=-n}^{n} k_{nm}\ f_{nm}\ h^b_{nm}(\boldsymbol{x})\ . \tag{3.7}$$

This statement can be proven by introducing the Eqs. (3.4) and (3.5) into Eq. (3.6) and considering the orthonormality condition (2.17).

The comparison of the result (3.7) with the representation (2.13) shows, that the ellipsoidal Fourier coefficients $(K^e f)_{nm}$ of the ellipsoidal convolution $\mathcal{K}^e f(\boldsymbol{x})$ are defined as

$$(\mathcal{K}^e f)_{nm} = k_{nm}\ f_{nm}\ . \tag{3.8}$$

Analog to the spherical theory the ellipsoidal scalar product, already introduced in Eq. (2.17), of two functions $f, g \in L_2(\mathbb{E}^2_{a,b})$ with $\boldsymbol{x} \in \mathbb{E}^2_{a,b}$, i.e.,

$$f(\boldsymbol{x}) = \sum_{n=0}^{\infty} \sum_{m=-n}^{n} f_{nm}\, e_{nm}(\boldsymbol{\xi}) \;, \tag{3.9}$$

$$g(\boldsymbol{x}) = \sum_{n=0}^{\infty} \sum_{m=-n}^{n} g_{nm}\, e_{nm}(\boldsymbol{\xi}) \tag{3.10}$$

is defined as

$$\left\langle\, f(\boldsymbol{x}) \,|\, g(\boldsymbol{x}) \,\right\rangle_w = \frac{1}{S_{a,b}} \int_{\mathbb{E}^2_{a,b}} dS_{a,b}(\phi)\, w(\phi)\, f(\boldsymbol{x})\, g(\boldsymbol{x}) \;. \tag{3.11}$$

Inserting the representations (3.9) and (3.10) into Eq. (3.11) and considering the orthonormality condition (2.17) yields

$$\begin{aligned}
&\left\langle\, f(\boldsymbol{x}) \,|\, g(\boldsymbol{x}) \,\right\rangle_w \\
&\quad = \frac{1}{S_{a,b}} \int_{\mathbb{E}^2_{a,b}} dS_{a,b}(\phi)\, w(\phi) \left(\sum_{n=0}^{\infty} \sum_{m=-n}^{n} f_{nm}\, e_{nm}(\boldsymbol{\xi}) \right) \left(\sum_{p=0}^{\infty} \sum_{q=-p}^{p} g_{pq}\, e_{pq}(\boldsymbol{\xi}) \right) \\
&\quad = \left(\sum_{n=0}^{\infty} \sum_{m=-n}^{n} \sum_{p=0}^{\infty} \sum_{q=-p}^{p} f_{nm}\, g_{pq} \right) \frac{1}{S_{a,b}} \int_{\mathbb{E}^2_{a,b}} dS_{a,b}(\phi)\, w(\phi)\, e_{nm}(\boldsymbol{\xi})\, e_{pq}(\boldsymbol{\xi}) \\
&\quad = \sum_{n=0}^{\infty} \sum_{m=-n}^{n} f_{nm}\, g_{nm} \;.
\end{aligned} \tag{3.12}$$

Thus, the scalar product $\left\langle\, f(\boldsymbol{x}) \,|\, g(\boldsymbol{x}) \,\right\rangle_w$, defined in the spatial domain on the reference ellipsoid, corresponds in the spectral domain to the sum of the products of the ellipsoidal Fourier coefficients f_{nm} and g_{nm}. We denote this relation as the *ellipsoidal Parseval identity*. The $L_2(\mathbb{E}^2_{a,b})$-norm $\|f\|_{L_2(\mathbb{E}^2_{a,b})}$ of the function $f(\boldsymbol{x})$ is defined as

$$\|f\|_{L_2(\mathbb{E}^2_{a,b})} = \sqrt{\left\langle\, f(\boldsymbol{x}) \,|\, f(\boldsymbol{x}) \,\right\rangle_w} \;. \tag{3.13}$$

Applying the ellipsoidal Parseval identity (3.12) we finally obtain

$$\|f\|_{L_2(\mathbb{E}^2_{a,b})} = \sqrt{\sum_{n=0}^{\infty} \sum_{m=-n}^{n} (f_{nm})^2} \;. \tag{3.14}$$

Besides the ellipsoidal harmonics $e_{nm}(\boldsymbol{\xi})$ the functions $K^e(\boldsymbol{x}, \boldsymbol{x}_q)$ for $\boldsymbol{x}, \boldsymbol{x}_q \in \mathbb{E}^2_{a,b}$ as defined in Eq. (3.5) span the space $L_2(\mathbb{E}^2_{a,b})$. For this reason, they are called *ellipsoidal base functions*. Thus, the

Eq. (3.2) means a transformation between different sets of base functions. Analog to Eq. (2.70) a function $f(\boldsymbol{x})$ with $\boldsymbol{x} \in \overline{\mathbb{E}}_{a,b}^{2,\mathrm{ext}}$ can be modeled as

$$f(\boldsymbol{x}) = \frac{1}{S_{a,b}} \int_{\mathbb{E}_{a,b}^2} dS_{a,b}(\phi_q)\; w(\phi_q)\; K^e(\boldsymbol{x}, \boldsymbol{x}_q)\; c(\boldsymbol{x}_q) = \big(\; K^e \;\star\; c \;\big)_w(\boldsymbol{x}) \tag{3.15}$$

with the unknown function $c(\boldsymbol{x}_q)$ and $\boldsymbol{x}_q \in \mathbb{E}_{a,b}^2$. We will deal with such kind of series expansions in chapter 4.

3.2 Ellipsoidal Scaling Functions and Wavelets

In order to derive an ellipsoidal multi-resolution representation we identify the kernel $K^e(\boldsymbol{x}, \boldsymbol{x}_q)$, as defined in Eq. (3.1), with the *generalized ellipsoidal scaling function*

$$\begin{aligned}\Phi_j(\boldsymbol{x}, \boldsymbol{x}_q) &= \sum_{n=0}^{\infty} \sum_{m=-n}^{n} \phi_{j;nm}\, h_{nm}^b(\boldsymbol{x})\, h_{nm}^b(\boldsymbol{x}_q) \\ &= \sum_{n=0}^{\infty} \sum_{m=-n}^{n} \frac{Q_{nm}^\star(\frac{u}{\epsilon})}{Q_{nm}^\star(\frac{b}{\epsilon})} \frac{Q_{nm}^\star(\frac{u_q}{\epsilon})}{Q_{nm}^\star(\frac{b}{\epsilon})}\, \phi_{j;nm}\, e_{nm}(\boldsymbol{\xi})\, e_{nm}(\boldsymbol{\xi}_q)\end{aligned} \tag{3.16}$$

of *resolution level (scale)* $j \in \mathbb{N}_0$. In other words we define scaling functions and wavelets via the series coefficients $\phi_{j;nm}$. In the sequel we also want to deal with *bandlimited ellipsoidal scaling function*. Such a function is defined by finite sums, i.e., Eq. (3.16) reduces to

$$\Phi_j(\boldsymbol{x}, \boldsymbol{x}_q) = \sum_{n=0}^{n_j'} \sum_{m=-n}^{n} \phi_{j;nm}\; h_{nm}^b(\boldsymbol{x})\, h_{nm}^b(\boldsymbol{x}_q)\;, \tag{3.17}$$

$$= \boldsymbol{h}(\boldsymbol{x})^T \boldsymbol{B}_j\, \boldsymbol{h}(\boldsymbol{x}_q)\;. \tag{3.18}$$

With $\overline{n}_j = (2n_j' + 1)^2$ the $\overline{n}_j \times 1$ vectors $\boldsymbol{h}(\boldsymbol{x})$ and $\boldsymbol{h}(\boldsymbol{x}_q)$ are defined as

$$\boldsymbol{h}(\boldsymbol{x}) = \big[\; (h_{00}^b(\boldsymbol{x}),\; h_{1,-1}^b(\boldsymbol{x}),\; \ldots,\; h_{n_j',n_j'}^b(\boldsymbol{x})\;\big]^T\;, \tag{3.19}$$

for $\boldsymbol{h}(\boldsymbol{x}_q)$ replace $\boldsymbol{x}$ by $\boldsymbol{x}_q$. Furthermore, $\boldsymbol{B}_j$ means an $\overline{n}_j \times \overline{n}_j$ diagonal matrix given as

$$\boldsymbol{B}_j = \mathrm{diag}(\phi_{j;00}, \phi_{j;1,-1}, \phi_{j;10}, \phi_{j;11}, \ldots, \phi_{j;n_j',n_j'})\;. \tag{3.20}$$

In the following we introduce additional restrictions on the Legendre coefficients $\phi_{j;nm}$.

3.2.1 Ellipsoidal Multi-Resolution Representation of the Second Kind

In the ellipsoidal multi-resolution representation of the second kind we choose coefficients $\phi_{j;nm}$ for $j \in \mathbb{N}_0$ with $n \in \mathbb{N}_0$ and $-n \leq m \leq n$ such that

$$(\phi_{j;00})^2 = 1 \ , \quad 0 \leq (\phi_{j;nm})^2 \leq 1 \ , \quad (\phi_{j+1;nm})^2 \geq (\phi_{j;nm})^2 \ , \quad \lim_{j \to \infty} (\phi_{j;nm})^2 = 1 \ ; \tag{3.21}$$

for the spherical analogon in case of rotational symmetric base functions see Freeden et al. (1998a), Freeden (1999); cf. section 3.3. Since the squares of the Legendre coefficients $\phi_{j;nm}$ are used within the conditions (3.21), we call this approach multi-resolution representation of the *second* kind. We notice from the conditions (3.21), that the scaling functions for $j = 0, 1, \ldots$ establish a set of consecutive *low-pass filters* with

$$\lim_{j \to \infty} \Phi_j(\boldsymbol{x}, \boldsymbol{x}_q) = \delta(\boldsymbol{\xi} - \boldsymbol{\xi}_q) \tag{3.22}$$

according to Eq. (2.27). The fundamental idea of the multi-resolution representation of the second kind is the decomposition of a signal $f_{j+1}(\boldsymbol{x})$ of level $j+1$ with $\boldsymbol{x} \in \mathbb{E}^2_{a,b}$, defined as a double convolution of the input signal $f \in L_2(\mathbb{E}^2_{a,b})$ with the level$-(j+1)$ scaling function $\Phi_{j+1}(\boldsymbol{x}, \boldsymbol{x}_q)$, i.e.

$$f_{j+1}(\boldsymbol{x}) = \left(\ \Phi_{j+1} \ \star \ \Phi_{j+1} \ \star \ f \ \right)_w(\boldsymbol{x}) =: \mathcal{P}_{j+1} f(\boldsymbol{x}) \ , \tag{3.23}$$

into the low-pass filtered level$-j$ signal

$$f_j(\boldsymbol{x}) = \left(\ \Phi_j \ \star \ \Phi_j \ \star \ f \ \right)_w(\boldsymbol{x}) =: \mathcal{P}_j f(\boldsymbol{x}) \tag{3.24}$$

and the level$-j$ detail signal

$$g_j(\boldsymbol{x}) = \left(\ \widetilde{\Psi}_j \ \star \ \Psi_j \ \star \ f \ \right)_w(\boldsymbol{x}) =: \mathcal{R}_j f(\boldsymbol{x}) \tag{3.25}$$

absorbing all the fine structures of $f_{j+1}(\boldsymbol{x})$ missing in $f_j(\boldsymbol{x})$ with $\boldsymbol{x} \in \mathbb{E}^2_{a,b}$. In other words the signal $f_j(\boldsymbol{x})$ means the level$-j$ approximation of the level$-(j+1)$ signal $f_{j+1}(\boldsymbol{x})$ or the input signal $f(\boldsymbol{x})$, respectively. In this approach, the decomposition

$$f_{j+1}(\boldsymbol{x}) = f_j(\boldsymbol{x}) + g_j(\boldsymbol{x}) \ . \tag{3.26}$$

is performed via the *ellipsoidal wavelet function* $\Psi_j(\boldsymbol{x}, \boldsymbol{x}_q)$ of level j and its dual $\widetilde{\Psi}_j(\boldsymbol{x}, \boldsymbol{x}_q)$ defined as

$$\Psi_j(\boldsymbol{x}, \boldsymbol{x}_q) = \sum_{n=0}^{\infty} \sum_{m=-n}^{n} \ \psi_{j;nm} \ e_{nm}(\boldsymbol{\xi}) \, e_{nm}(\boldsymbol{\xi}_q) \ , \tag{3.27}$$

$$\widetilde{\Psi}_j(\boldsymbol{x}, \boldsymbol{x}_q) = \sum_{n=0}^{\infty} \sum_{m=-n}^{n} \ \widetilde{\psi}_{j;nm} \ e_{nm}(\boldsymbol{\xi}) \, e_{nm}(\boldsymbol{\xi}_q) \ . \tag{3.28}$$

Applying Eq. (3.7) to the Eqs. (3.23), (3.24) and (3.25) yields

$$f_{j+1}(\boldsymbol{x}) = \sum_{n=0}^{\infty} \sum_{m=-n}^{n} (\phi_{j+1;nm})^2 \, f_{nm} \, e_{nm}(\boldsymbol{\xi}) \; , \tag{3.29}$$

$$f_{j}(\boldsymbol{x}) = \sum_{n=0}^{\infty} \sum_{m=-n}^{n} (\phi_{j;nm})^2 \, f_{nm} \, e_{nm}(\boldsymbol{\xi}) \; , \tag{3.30}$$

$$g_{j}(\boldsymbol{x}) = \sum_{n=0}^{\infty} \sum_{m=-n}^{n} \psi_{j;nm} \, \widetilde{\psi}_{j;nm} \, f_{nm} \, e_{nm}(\boldsymbol{\xi}) \; . \tag{3.31}$$

Considering these results in Eq. (3.26) the (ellipsoidal) *two-scale relation*

$$\psi_{j;nm} \, \widetilde{\psi}_{j;nm} = (\phi_{j+1;nm})^2 - (\phi_{j;nm})^2 \tag{3.32}$$

between the coefficients of the wavelet functions and the scaling functions is derived. Since the scaling functions $\Phi_{j+1}(\boldsymbol{x}, \boldsymbol{x}_q)$ and $\Phi_{j}(\boldsymbol{x}, \boldsymbol{x}_q)$ act as low-pass filters, the spherical wavelet function (3.27) and its dual (3.28) can be interpreted as *band-pass filters*. The successive application of Eq. (3.26) yields the ellipsoidal multi-resolution representation

$$f(\boldsymbol{x}) = f_{j'}(\boldsymbol{x}) + \sum_{j=j'}^{\infty} g_j(\boldsymbol{x}) \qquad \text{with} \qquad j' \in \mathbb{N}_0 \tag{3.33}$$

of the input signal $f \in L_2(\mathbb{E}^2_{a,b})$ as an alternative to the series expansion (3.9) in terms of ellipsoidal harmonics (2.11). By substituting the Eqs. (3.30) and (3.31) into the right-hand side of Eq. (3.33) and comparing the result with Eq. (3.9) we obtain the condition

$$(\phi_{j';nm})^2 + \sum_{j=j'}^{\infty} \psi_{j;nm} \, \widetilde{\psi}_{j;nm} = 1 \tag{3.34}$$

for the series coefficients of the ellipsoidal scaling and wavelet functions. If we restrict the series coefficients $\psi_{j;nm}$ and $\widetilde{\psi}_{j;nm}$ to

$$\psi_{j;nm} = \widetilde{\psi}_{j;nm} \quad \forall \quad n \in \mathbb{N}_0 \; , \quad -n \leq m \leq n \tag{3.35}$$

it follows

$$\Psi_j(\boldsymbol{x}, \boldsymbol{x}_q) = \widetilde{\Psi}_j(\boldsymbol{x}, \boldsymbol{x}_q) = \sum_{n=0}^{\infty} \sum_{m=-n}^{n} \psi_{j;nm} \, e_{nm}(\boldsymbol{\xi}) \, e_{nm}(\boldsymbol{\xi}_q) \tag{3.36}$$

for the spherical wavelet function (3.27) and its dual (3.28), respectively. Furthermore, the condition (3.34) reduces to

$$(\phi_{j';nm})^2 + \sum_{j=j'}^{\infty} (\psi_{j;nm})^2 = 1 \; . \tag{3.37}$$

According to Eq. (3.32) the coefficients $\psi_{j;nm}$ of the ellipsoidal wavelet function are calculable from

$$\psi_{j;nm} = \sqrt{(\phi_{j+1;nm})^2 - (\phi_{j;nm})^2} \; . \tag{3.38}$$

Equation (3.25) allows the introduction of the *ellipsoidal wavelet coefficients*

$$c_j(\boldsymbol{x}) = \big(\; \Psi_j \star f \; \big)_w(\boldsymbol{x}) =: \Psi_j f(\boldsymbol{x}) \; . \tag{3.39}$$

Finally we summarize that the *ellipsoidal multi-resolution representation of the second kind* reads

$$\begin{aligned} f(\boldsymbol{x}) &= \underbrace{\big(\; \Phi_{j'} \star \Phi_{j'} \star f \; \big)_w(\boldsymbol{x})}_{f_{j'}(\boldsymbol{x})} + \sum_{j=j'}^{\infty} \underbrace{\big(\; \Psi_j \star c_j \; \big)_w(\boldsymbol{x})}_{g_j(\boldsymbol{x})} \qquad \text{with} \qquad j' \in \mathbb{N}_0 \; . \\ &= \qquad\qquad + \end{aligned} \tag{3.40}$$

3.2.2 Ellipsoidal Multi-Resolution Representation of the First Kind

In case of the ellipsoidal multi-resolution representation of the first kind we replace the conditions (3.21) for the coefficients $\phi_{j;nm}$ of the level$-j$ scaling function (3.16) by the conditions

$$\phi_{j;00} = 1 \; , \quad 0 \leq \phi_{j;nm} \leq 1 \; , \quad \phi_{j+1;nm} \geq \phi_{j;nm} \; , \quad \lim_{j \to \infty} \phi_{j;nm} = 1 \; . \tag{3.41}$$

Note, that these conditions affect that the diagonal matrix $\boldsymbol{B}_j$ defined in Eq. (3.20) for the bandlimited case is at least positive semi-definite. In this approach we avoid the computation of ellipsoidal wavelet coefficients (3.39) and, consequently, the multi-resolution representation (3.40) reduces to the *ellipsoidal multi-resolution representation of the first kind*, i.e.,

$$\begin{aligned} f(\boldsymbol{x}) &= \underbrace{\big(\; \Phi_{j'} \star f \; \big)_w(\boldsymbol{x})}_{f_{j'}(\boldsymbol{x})} + \sum_{j=j'}^{\infty} \underbrace{\big(\; \Psi_j \star f \; \big)_w(\boldsymbol{x})}_{g_j(\boldsymbol{x})} \qquad \text{with} \qquad j' \in \mathbb{N}_0 \; . \\ &= \qquad\qquad + \end{aligned} \tag{3.42}$$

Thus, the smoother level$-j$ signal $f_j(\boldsymbol{x})$ and the level$-j$ detail signal $g_j(\boldsymbol{x})$ are defined as

$$f_j(\boldsymbol{x}) = \big(\; \Phi_j \star f \; \big)_w(\boldsymbol{x}) \; , \tag{3.43}$$

$$g_j(\boldsymbol{x}) = \big(\; \Psi_j \star f \; \big)_w(\boldsymbol{x}) \; . \tag{3.44}$$

In the frequency domain both signals can be rewritten analogously to the Eqs. (3.30) and (3.31) as

$$f_j(\boldsymbol{x}) = \sum_{n=0}^{\infty} \sum_{m=-n}^{n} \phi_{j;nm} \, f_{nm} \, e_{nm}(\boldsymbol{\xi}) \;\; , \tag{3.45}$$

$$g_j(\boldsymbol{x}) = \sum_{n=0}^{\infty} \sum_{m=-n}^{n} \psi_{j;nm} \, f_{nm} \, e_{nm}(\boldsymbol{\xi}) \; . \tag{3.46}$$

Consequently, the two-scale relation (3.32) reads now

$$\psi_{j;nm} = \phi_{j+1;nm} - \phi_{j;nm} \ . \tag{3.47}$$

In the same manner as for the multi-resolution representation of the second kind we obtain the condition

$$\phi_{j';nm} + \sum_{j=j'}^{\infty} \psi_{j;nm} = 1 \tag{3.48}$$

for the coefficients of the scaling and wavelet functions by introducing the representations (3.45) and (3.46) into (3.42).

For numerical investigations we rewrite the Eqs. (3.40) and (3.42) as

$$\begin{aligned} f(\boldsymbol{x}) &= \underbrace{f_{j'}(\boldsymbol{x}) + \sum_{j=j'}^{J} g_j(\boldsymbol{x})}_{} + \underbrace{\sum_{j=J+1}^{\infty} g_j(\boldsymbol{x})}_{} \ . \\ &= \qquad f_{J+1}(\boldsymbol{x}) \qquad + \quad s(\boldsymbol{x}) \end{aligned} \tag{3.49}$$

The influence of neglecting the non-stochastic high-frequency signal $s(\boldsymbol{x})$ (*omission error*) on the multi-resolution representation is known as *aliasing error*; see e.g., Kusche (2002).

Due to the definitions (3.21) and (3.41) of the ellipsoidal scaling and wavelet functions the mean values of the detail signal $g_j(\boldsymbol{x}) = g_j(\lambda, \phi, b)$, vanish over the ellipsoid $\mathbb{E}^2_{a,b}$, i.e., it follows

$$\frac{1}{S_{a,b}} \int_{\mathbb{E}^2_{a,b}} dS_{a,b}(\phi)\, w(\phi)\, g_j(\lambda, \phi, b) = 0 \tag{3.50}$$

for all $j \in \{j', \ldots, J\}$. Note, that the same statement holds for the ellipsoidal wavelet coefficients (3.39).

3.2.3 Order-Independent Coefficients

With Eq. (3.16) we introduced the generalized ellipsoidal scaling function $\Phi_j(\boldsymbol{x}, \boldsymbol{x}_q)$. However, in the case of order-independent coefficients, i.e., the coefficients $\phi_{j;nm}$ are restricted to the conditions

$$\phi_{j;nm} = \phi_{j,n} \quad \forall \quad n \in \mathbb{N}_0 \ , \quad -n \le m \le n \ , \tag{3.51}$$

the ellipsoidal scaling function (3.16) reduces for $\boldsymbol{x}, \boldsymbol{x}_q \in \mathbb{E}^2_{a,b}$ to

$$\begin{aligned} \Phi_j(\boldsymbol{x}, \boldsymbol{x}_q) &= \sum_{n=0}^{\infty} \sum_{m=-n}^{n} \phi_{j;n}\, e_{nm}(\boldsymbol{\xi})\, e_{nm}(\boldsymbol{\xi}_q) \ , \\ &= \sum_{n=0}^{\infty} (2n+1)\ \phi_{j;n}\, P_n(\boldsymbol{\xi}^T \boldsymbol{\xi}_q) \ . \end{aligned} \tag{3.52}$$

As we already discussed in the context of Eq. (2.51), functions of the type (3.52) are not rotational symmetric (except at the poles) on the reference ellipsoid $\mathbb{E}^2_{a,b}$. However, since they would be isotropic on a sphere, we denote kernel functions of the type (3.52) in the sequel as *rotational symmetric* or *isotropic*. If we substitute the unit vectors $\boldsymbol{r}$ and $\boldsymbol{r}_q$ for the unit vectors $\boldsymbol{\xi}$ and $\boldsymbol{\xi}_q$, i.e., we neglect the deviations $\delta\boldsymbol{r}$ and $\delta\boldsymbol{r}_q$ as defined in Eq. (2.5), we would obtain from Eq. (3.52) the definition equation of the spherical level$-j$ scaling function; for an intensive study of the spherical wavelet theory we refer here to Freeden et al. (1998a), Freeden (1999) and Freeden and Michel (2004). Recall that the deviation $\delta\boldsymbol{r}$ vanishes for $\epsilon = 0$, i.e., the ellipsoid mutates to a sphere.

Under the condition (3.51) we obtain from Eq. (3.38) the relation

$$\psi_{j;n} = \sqrt{(\phi_{j+1;n})^2 - (\phi_{j;n})^2} \tag{3.53}$$

for the Legendre coefficients $\psi_{j;n} = \widetilde{\psi}_{j;n}$ of the rotational symmetric ellipsoidal wavelet function

$$\begin{aligned}\Psi_j(\boldsymbol{x},\boldsymbol{x}_q) &= \sum_{n=0}^{\infty}\sum_{m=-n}^{n} \psi_{j;n}\, e_{nm}(\boldsymbol{\xi})\, e_{nm}(\boldsymbol{\xi}_q)\ ,\\ &= \sum_{n=0}^{\infty}(2n+1)\ \psi_{j;n}\ P_n(\boldsymbol{\xi}^T\boldsymbol{\xi}_q)\ .\end{aligned} \tag{3.54}$$

In case of bandlimited scaling functions as defined in Eq. (3.17) the Eqs. (3.52) and (3.54) reduce to

$$\begin{aligned}\Phi_j(\boldsymbol{x},\boldsymbol{x}_q) &= \sum_{n=0}^{n'_j}\sum_{m=-n}^{n} \phi_{j;n}\, e_{nm}(\boldsymbol{\xi})\, e_{nm}(\boldsymbol{\xi}_q)\ ,\\ &= \sum_{n=0}^{n'_j}(2n+1)\ \phi_{j;n}\ P_n(\boldsymbol{\xi}^T\boldsymbol{\xi}_q)\ ,\end{aligned} \tag{3.55}$$

$$\begin{aligned}\Psi_j(\boldsymbol{x},\boldsymbol{x}_q) &= \sum_{n=0}^{n'_{j+1}}\sum_{m=-n}^{n} \psi_{j;n}\, e_{nm}(\boldsymbol{\xi})\, e_{nm}(\boldsymbol{\xi}_q)\ ,\\ &= \sum_{n=0}^{n'_{j+1}}(2n+1)\ \psi_{j;n}\ P_n(\boldsymbol{\xi}^T\boldsymbol{\xi}_q)\ ;\end{aligned} \tag{3.56}$$

the different values n'_j and n'_{j+1} for the upper summation index are due to the relation (3.53).

As a first example of such an ellipsoidal function (3.55) we introduce the *Shannon scaling function* defined by the Legendre coefficients

$$\phi_{j;n} = \left\{\begin{array}{lll} 1 & \text{for} & n = 0,\ldots,2^j-1 \\ 0 & \text{for} & n \geq 2^j \end{array}\right\} =: \phi^{\mathrm{Sh}}_{j;n} \tag{3.57}$$

of resolution level $j \in \mathbb{N}_0$ with $n'_j = 2^j - 1$. In Fig. 4.1 the *Shannon wavelet function* $\Psi_j(\boldsymbol{x}, \boldsymbol{x}_q) =: \Psi_j^{\mathrm{Sh}}(\boldsymbol{x}, \boldsymbol{x}_q)$ for various level values j is shown. The corresponding level$-j$ Legendre coefficients are calculated by inserting (3.57) into Eq. (3.38), i.e.,

$$\psi_{j;n} = \left\{ \begin{array}{lll} 0 & \text{for} & n = 0, \ldots, 2^j - 1 \\ 1 & \text{for} & n = 2^j, \ldots, 2^{j+1} - 1 \\ 0 & \text{for} & n \geq 2^{j+1} \end{array} \right\} =: \psi_{j;n}^{\mathrm{Sh}} \; . \tag{3.58}$$

As can be seen from the two panels a) and b) of Fig. 3.1 the Shannon wavelet functions show global oscillations. These undesired effects can be mainly suppressed by using the *Blackman wavelet function* $\Psi_j(\boldsymbol{x}, \boldsymbol{x}_q) =: \Psi_j^{\mathrm{Bl}}(\boldsymbol{x}, \boldsymbol{x}_q)$ shown in Fig. 3.2. To be more specific, the *Blackman scaling function* is defined by the Legendre coefficients

$$\phi_{j;n} = \left\{ \begin{array}{lll} 1 & \text{for} & n = 0, \ldots, 2^{j-1} - 1 \\ A_j(n) & \text{for} & n = 2^{j-1}, \ldots, 2^j - 1 \\ 0 & \text{for} & n \geq 2^j \end{array} \right\} =: \phi_{j;n}^{\mathrm{Bl}} \; . \tag{3.59}$$

The Blackman scaling function is based on the Blackman window

$$A_j(n) = 0.42 - 0.50 \, \cos\left(\frac{2\pi n}{2^j}\right) + 0.08 \, \cos\left(\frac{4\pi n}{2^j}\right) \; , \tag{3.60}$$

which is often used in classical signal analysis; see e.g. Mertins (1999). Inserting (3.59) into Eq. (3.53) yields the Legendre coefficients

$$\psi_{j;n} = \left\{ \begin{array}{lll} 0 & \text{for} & n = 0, \ldots, 2^{j-1} - 1 \\ \sqrt{1 - (A_j(n))^2} & \text{for} & n = 2^{j-1}, \ldots, 2^j - 1 \\ \sqrt{(A_{j+1}(n))^2} & \text{for} & n = 2^j, \ldots, 2^{j+1} - 1 \\ 0 & \text{for} & n \geq 2^{j+1} \end{array} \right\} =: \psi_{j;n}^{\mathrm{Bl}} \tag{3.61}$$

of the Blackman wavelet function $\Psi_j^{\mathrm{Bl}}(\boldsymbol{x}, \boldsymbol{x}_q)$.

We want to emphasize particularly, that both the Shannon and the Blackman wavelet functions are *strictly bandlimited*, i.e. only the Legendre coefficients within a finite frequency band B_j are different from zero. In the case of the Blackman wavelet, for instance, it follows from Eq. (3.61)

$$B_j := \{ \, n \, | \, 2^{j-1} \leq n < 2^{j+1} \, \} \; . \tag{3.62}$$

It can be taken from Fig. 4.2c, that for level $j = 7$ the frequency band reads $B_7 = \{ \, n \, | \, 64 \leq n \leq 255 \}$.

For more details concerning these and other scaling and wavelet functions we refer to the textbooks of Freeden (1999) and Freeden et al. (1998) as well as to Schmidt et al. (2007a).

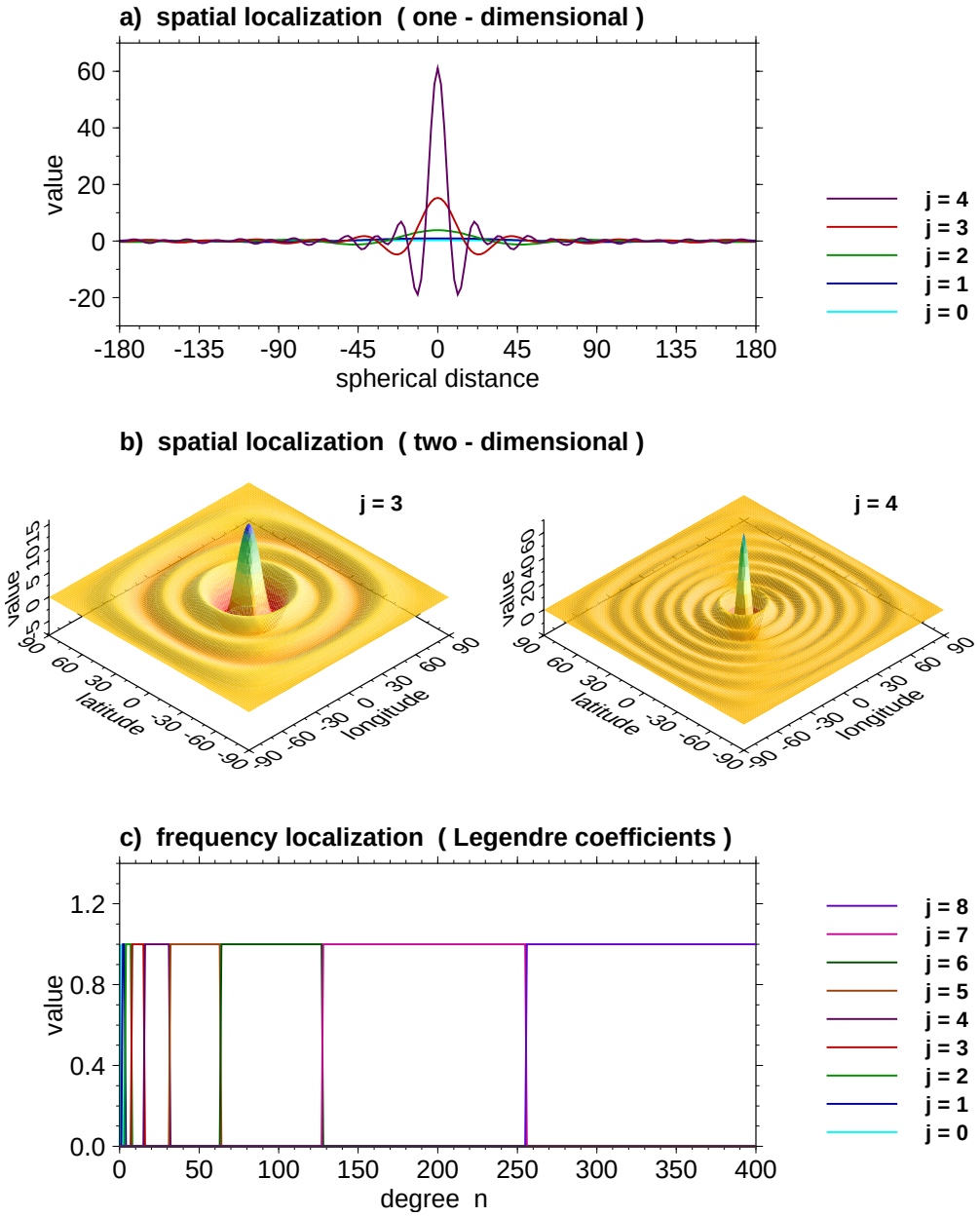

Figure 3.1: Shannon wavelet functions for different resolution levels j ; a) one-dimensional representation in dependence on the argument $\alpha = \arccos(\boldsymbol{\xi}^T \boldsymbol{\xi}_q)$, b) two-dimensional representation on the reference ellipsoid $\mathbb{E}^2_{a,b}$ with $b = 6356751.92\text{m}$ and $\epsilon = 521853.58\text{m}$, c) frequency representation: since the wavelet functions are non-overlapping, they are orthogonal to each other.

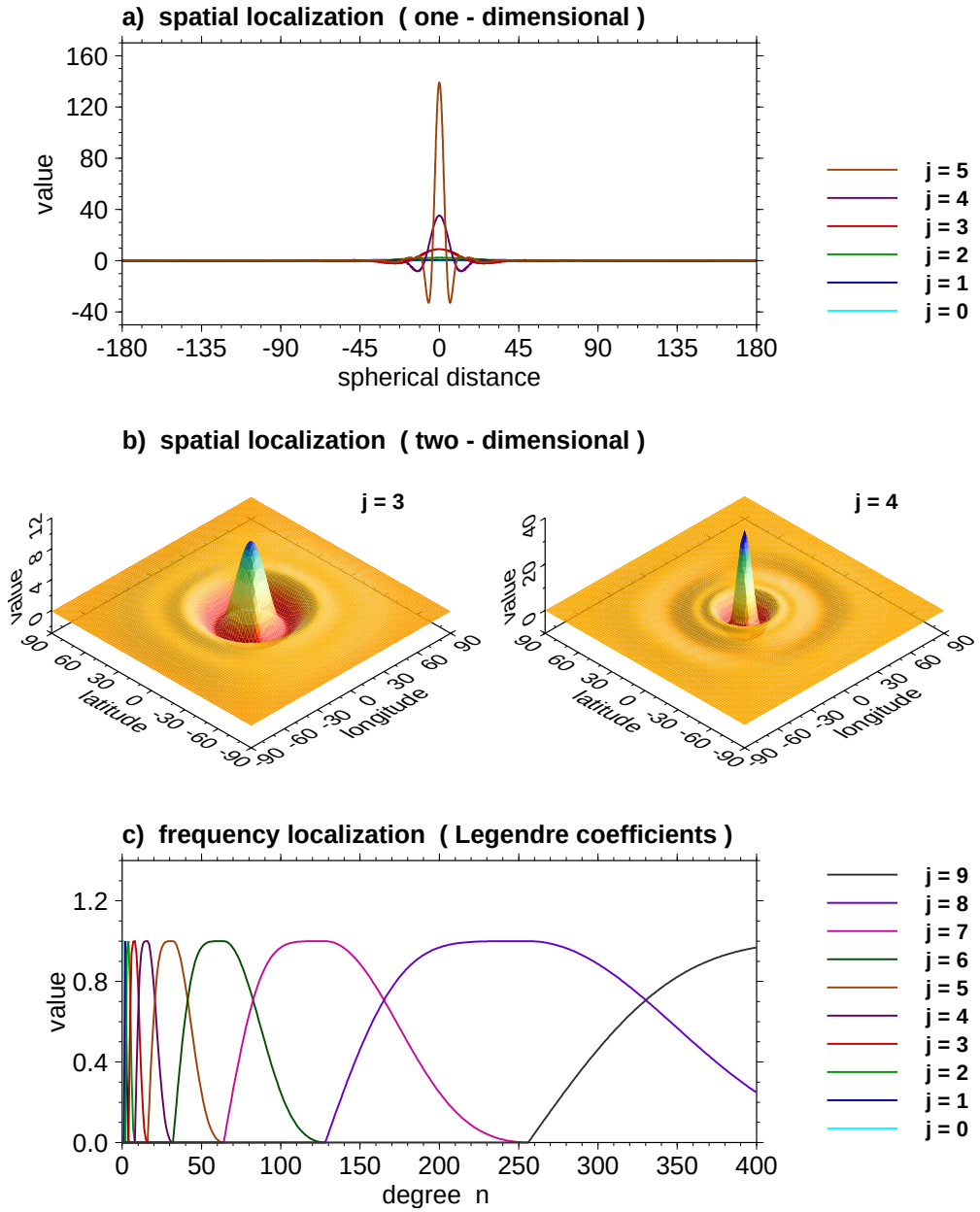

Figure 3.2: Blackman wavelet functions for different resolution levels j ; a) one-dimensional representation in dependence on the argument $\alpha = \arccos(\boldsymbol{\xi}^T \boldsymbol{\xi}_q)$, b) two-dimensional representation on the reference ellipsoid $\mathbb{E}^2_{a,b}$ with $b = 6356751.92$m and $\epsilon = 521853.58$m, c) frequency representation.

Different detail signals $g_{j_1}(\boldsymbol{x})$ and $g_{j_2}(\boldsymbol{x})$, i.e. $j_1 \neq j_2$, computed by level$-j_1$ and level$-j_2$ Shannon wavelets $\Psi^{\mathrm{Sh}}_{j_1}(\boldsymbol{x}, \boldsymbol{x}_q)$ and $\Psi^{\mathrm{Sh}}_{j_2}(\boldsymbol{x}, \boldsymbol{x}_q)$, respectively, are *orthogonal* to each other, since it follows

$$
\begin{aligned}
&\left\langle\, g_{j_1}(\boldsymbol{x}) \,|\, g_{j_2}(\boldsymbol{x}) \,\right\rangle_w = \\
&\quad = \frac{1}{S_{a,b}} \int_{\mathbb{E}^2_{a,b}} dS_{a,b}(\phi)\, w(\phi) \sum_{n=0}^{\infty} \sum_{l=0}^{\infty} (\psi^{\mathrm{Sh}}_{j_1;n})^2\, (\psi^{\mathrm{Sh}}_{j_2;l})^2 \,\times \\
&\qquad\qquad \times \sum_{m=-n}^{n} \sum_{k=-l}^{l} f_{nm}\, f_{lk}\, e_{nm}(\boldsymbol{\xi})\, e_{lk}(\boldsymbol{\xi}) \\
&\quad = \sum_{n=0}^{\infty} \sum_{l=0}^{\infty} (\psi^{\mathrm{Sh}}_{j_1;n})^2\, (\psi^{\mathrm{Sh}}_{j_2;l})^2 \sum_{m=-n}^{n} \sum_{k=-l}^{l} f_{nm}\, f_{lk} \,\times \\
&\qquad\qquad \times \frac{1}{S_{a,b}} \int_{\mathbb{E}^2_{a,b}} dS_{a,b}(\phi)\, w(\phi)\, e_{nm}(\boldsymbol{\xi})\, e_{lk}(\boldsymbol{\xi}) \\
&\quad = \sum_{n=0}^{\infty} (\psi^{\mathrm{Sh}}_{j_1;n})^2\, (\psi^{\mathrm{Sh}}_{j_2;n})^2 \sum_{m=-n}^{n} f^2_{nm} = 0\,. \qquad (3.63)
\end{aligned}
$$

by applying the Eqs. (3.31), (3.35), (3.51), (3.61) and considering the orthonormality condition (2.17).

3.3 Isotropic Wavelets

We outlined in the previous subsection that the spherical wavelet theory is obtained from the ellipsoidal wavelet theory by restricting to Legendre coefficients $\phi_{j;nm}$ and $\psi_{j;nm}$, which are independent of the order $m = -n, ..., n$. The motivation for this was given by the conclusion that for $\epsilon = 0$, i.e., when the ellipsoidal is a sphere, the resulting scaling and wavelet functions Φ_j and Ψ_j become rotational symmetric or isotropic, that is, the values of

$$
\begin{aligned}
\Phi_j(\boldsymbol{x}, \boldsymbol{x}_q) &= \sum_{n=0}^{\infty} \sum_{m=-n}^{n} \phi_{j;n}\, e_{nm}(\boldsymbol{\xi})\, e_{nm}(\boldsymbol{\xi}_q)\,, \\
&= \sum_{n=0}^{\infty} (2n+1)\, \phi_{j;n}\, P_n(\boldsymbol{\xi}^T \boldsymbol{\xi}_q)\,. \qquad (3.64)
\end{aligned}
$$

and $\Psi_j(\boldsymbol{x}, \boldsymbol{x}_q)$ depend only on the geometric distance α given by $\cos\alpha = \boldsymbol{\xi}^T \boldsymbol{\xi}_q$. Since this no longer holds for an arbitrary ellipsoid with $\epsilon \neq 0$, i.e., the quantity α does not correspond to the geometric distance between $\boldsymbol{\xi}$ and $\boldsymbol{\xi}_q$, it is no longer natural to restrict ourselves to scaling and wavelet functions with order-independent coefficients.

On the other hand, as seen before restricting to coefficients depending only on the degree n, we can benefit from the fact that the computation of the scaling and wavelet functions is drastically simplified, cf. the definitions (3.57) to (3.61). This does not only follow from the fact that the values of $\Phi_j(\boldsymbol{x}, \boldsymbol{x}_q)$ and $\Psi_j(\boldsymbol{x}, \boldsymbol{x}_q)$ depend only on $\boldsymbol{\xi}^T \boldsymbol{\xi}_q \in [-1, +1]$ rather than on the tuple $(\boldsymbol{x}, \boldsymbol{x}_q)$, but also relies on the observation that now only the Legendre polynomials P_n instead of all associated Legendre polynomials $P_{n,m}$ enter the computation of Φ_j and Ψ_j. When one is only interested in a multiresolution representation of the Earth's gravity field without downward or upward continuation of gravity data, more generally, solving geodetic boundary value problems, it follows that one should use the special spherical theory with its order-independent coefficients for better computational efficiency.

Besides that we emphasize in advance that we cannot get around order-dependent coefficients in the next section when we describe regularization. Thus, we want to finish this section by illustrating how the general ellipsoidal wavelet theory allows us to use a multiresolution analysis, which is better suited to the special geometry of the ellipsoid. More precisely, we want to outline the construction of scaling and wavelet functions $\Phi_j(\boldsymbol{x}, \boldsymbol{x}_q)$ and $\Psi_j(\boldsymbol{x}, \boldsymbol{x}_q)$ for a fixed reference ellipsoid $\mathbb{E}^2_{a_0,b_0}$ with the fixed absolute eccentricity $\epsilon_0 = \sqrt{a_0^2 - b_0^2}$ according to Eq. (2.1), which are not fully isotropic, but depend only up to a minimal error on the geometric distance of $\boldsymbol{\xi}$ and $\boldsymbol{\xi}_q$ with respect to the standard metric on $\mathbb{E}^2_{a_0,b_0}$.

For this purpose let us introduce beside the *fixed* reference ellipsoid $\mathbb{E}^2_{a_0,b_0}$ a second (auxiliary) ellipsoid $\mathbb{E}^2_{a,b}$, which is *variable* in the sense that the eccentricity $\epsilon = \sqrt{a^2 - b^2}$ is allowed to vary. We identify both ellipsoids $\mathbb{E}^2_{a_0,b_0}$ and $\mathbb{E}^2_{a,b}$ via the standard ellipsoidal coordinates (λ, ϕ), which we have on both of them, cf. Eq. (2.3). Choosing a countable (for practical purposes still finite) sequence of half axes $u_1 > \ldots > u_j > \ldots > u_\infty = b$, note that we get a countable family of ellipsoidal Abel-Poisson kernels $K^e_{AP,j}$, defined as

$$\begin{aligned} K^e_{AP}(\boldsymbol{x}, \boldsymbol{x}_q) &= \sum_{n=0}^{\infty} \sum_{m=-n}^{n} \frac{Q^*_{nm}(\frac{u_j}{\epsilon})}{Q^*_{nm}(\frac{b}{\epsilon})}\, e_{nm}(\boldsymbol{\xi})\, e_{nm}(\boldsymbol{\xi}_q) \\ &= K^e_{AP,j}(\boldsymbol{\xi}, \boldsymbol{\xi}_q) \end{aligned} \tag{3.65}$$

according to Eq. (2.24) with $j = 1, \ldots, \infty$. Now observe that the ellipsoidal kernels (3.65) naturally can serve as scaling functions Φ^ϵ_j of an ellipsoidal multiresolution representation on the fixed reference ellipsoid $\mathbb{E}^2_{a_0,b_0}$ by identifying $\mathbb{E}^2_{a_0,b_0}$ and $\mathbb{E}^2_{a,b}$ via setting

$$\Phi^\epsilon_j(\boldsymbol{x}, \boldsymbol{x}_q) \;:=\; K^e_{AP,j}(\boldsymbol{\xi}, \boldsymbol{\xi}_q) \tag{3.66}$$

with $\boldsymbol{x}, \boldsymbol{x}_q \in \mathbb{E}^2_{a_0,b_0}$. While the sequence of half axis $u_1, \ldots, u_j, \ldots, u_\infty$ describes the different levels of resolution, observe that the variable eccentricity ϵ of the auxiliary ellipsoid $\mathbb{E}^2_{a,b}$ plays the role of a shape parameter for the scaling functions Φ^ϵ_j. Choosing this shape parameter in an optimal way one can achieve that the scaling functions ϕ^ϵ_j depend only up to a minimal error on the geometric distance of $\boldsymbol{\xi}$ and $\boldsymbol{\xi}_q$ with respect to the standard metric on $\mathbb{E}^2_{a_0,b_0}$.

Chapter 4

Regularization

As mentioned before one of the main applications of the spherical wavelet theory lies in the *regularization* of inverse problems related to the sphere. In Earth's gravity field studies regularization usually concerns the downward-continuation of the gravity data, e.g., from a satellite orbit to the Earth's surface. Since the upward-continuation can be performed by convolving the gravity function with a rotational symmetric kernel, namely the (spherical) Abel-Poisson kernel (2.48), and therefore represents a compact operator, the inverse operator is not everywhere defined and unbounded. Given a spherical wavelet transform one can construct out of the rotational symmetric wavelet functions and the rotational symmetric Abel-Poisson kernel a family of rotational symmetric regularization wavelets to solve the inverse problem, see e.g., Freeden (1999). In the ellipsoidal case the upward-continuation of a gravity potential from the reference ellipsoid $\mathbb{E}^2_{a,b}$ to an ellipsoid $\mathbb{E}^2_{\sqrt{u^2+\epsilon^2},u}$, (Eq. 2.8), with $u > b$ again leads to an integral operator. However, in this case the ellipsoidal Abel-Poisson kernel (2.24) is not rotational symmetric anymore, which is expressed by the quotient

$$\frac{Q^\star_{nm}(\frac{u}{\epsilon})}{Q^\star_{nm}(\frac{b}{\epsilon})} \; ;$$

according to Eq. (2.34) the quotient $(R/r)^{n+1}$ within the spherical Abel-Poisson kernel (2.48) depends only on the degree value n and not on the order values m.

4.1 Sobolev Spaces

With Eq. (2.58) we introduced an integral operator $\mathcal{K}^s$ with kernel (2.57) applied to a function $f(\boldsymbol{x})$ on the sphere $\mathbb{S}^2_R$. The corresponding Fourier coefficients were defined with Eq. (2.60). When moving from operators on the sphere to their ellipsoidal analogues, the essential difference is that the coefficients for the ellipsoidal operators do no longer only depend on the degree value n, but they explicitly become functions of both degree n and order n. Thus, an ellipsoidal integral operator $\mathcal{K}^e$,

with kernel

$$K^e(\boldsymbol{x}, \boldsymbol{x}_q) = \sum_{n=0}^{\infty} \sum_{m=-n}^{n} k_{nm}\, h^b_{nm}(\boldsymbol{x})\, h^b_{nm}(\boldsymbol{x}_q)$$

$$= \sum_{n=0}^{\infty} \sum_{m=-n}^{n} \frac{Q^\star_{nm}(\frac{u}{\epsilon})}{Q^\star_{nm}(\frac{b}{\epsilon})}\, k_{nm}\, e_{nm}(\boldsymbol{\xi})\, e_{nm}(\boldsymbol{\xi}_q) \tag{4.1}$$

according to Eq. (3.1) with $\boldsymbol{x}_q \in \mathbb{E}^2_{a,b}$, is defined by the set of coefficients

$$k_{nm} \quad \text{with} \quad n \in \mathbb{N}_0 \quad \text{and} \quad -n \leq m \leq n\ . \tag{4.2}$$

The Fourier coefficients of the ellipsoidal convolution $\mathcal{K}^e f(\boldsymbol{x})$ were defined in Eq. (3.8), i.e.,

$$(\mathcal{K}^e f)_{nm} = k_{nm}\ f_{nm}\ . \tag{4.3}$$

Solving the equation

$$(\mathcal{K}^e f)(\boldsymbol{x}) = g(\boldsymbol{x})\ , \tag{4.4}$$

wherein $g(\boldsymbol{x})$ is given and $f(\boldsymbol{x})$ the unknown target function with $f \in L_2(\mathbb{E}^2_{a,b})$, is called a *well-posed* problem, whenever $\mathcal{K}^e$ is bijective and the inverse operator is bounded (*reference*). However, it is a well-known fact from functional analysis, that operators of the above form are *compact*, i.e., the image of the unit ball in $L^2(\mathbb{E}^2_{a,b})$ under $\mathcal{K}^e$ is a compact subset of $L_2(\mathbb{E}^2_{a,b})$. As an important consequence, $\mathcal{K}^e$ cannot possess a bounded inverse: Provided there exists a bounded operator $(\mathcal{K}^e)^{-1}$, the unit ball in $L_2(\mathbb{E}^2_{a,b})$ must be compact, which would prove that $L_2(\mathbb{E}^2_{a,b})$ has a finite basis. Although $\mathcal{K}^e$ is injective in many cases, it follows from the non-existence of the bounded inverse $(\mathcal{K}^e)^{-1}$, that $\mathcal{K}^e$ is not surjective, more precisely, the image

$$\operatorname{Im} \mathcal{K}^e = \{\, \mathcal{K}^e f \mid f \in L_2(\mathbb{E}^2_{a,b})\}\tag{4.5}$$

is not a proper subspace of $L_2(\mathbb{E}^2_{a,b})$. In order to proof this statement we introduce the space of functions $f \in L_2(\mathbb{E}^2_{a,b})$, Eq. (3.9), with

$$\sum_{n=0}^{\infty} \sum_{m=-n}^{n} (k_{nm})^{-2}\ (f_{nm})^2 < \infty \tag{4.6}$$

and denote it by $H(\mathcal{K}^e; \mathbb{E}^2_{a,b})$. From Eq. (3.12) we know that $f \in L_2(\mathbb{E}^2_{a,b})$ is equivalent to the condition

$$\sum_{n=0}^{\infty} \sum_{m=-n}^{n} (f_{nm})^2 < \infty\ . \tag{4.7}$$

Since the coefficients k_{nm} converge to zero for growing degree value n, it follows that the coefficients f_{nm} of the functions $f \in H(\mathcal{K}^e; \mathbb{E}^2_{a,b})$ must converge very fast to zero in order to keep the left-hand side of Eq. (4.6), i.e., the norm

$$\|f\|_{H(\mathcal{K}^e;\mathbb{E}^2_{a,b})} = \sqrt{\sum_{n=0}^{\infty} \sum_{m=-n}^{n} (k_{nm})^{-2} \, (f_{nm})^2} \tag{4.8}$$

finite. If we introduce a function

$$\kappa(\boldsymbol{x}) = \sum_{n=0}^{\infty} \sum_{m=-n}^{n} k_{nm} \, e_{nm}(\boldsymbol{\xi}) \tag{4.9}$$

according to Eq. (3.9), we notice that the condition (4.7) is fulfilled, i.e., $\kappa \in L_2(\mathbb{E}^2_{a,b})$, but $\kappa \notin H(\mathcal{K}^e; \mathbb{E}^2_{a,b})$, since the condition (4.6) fails. Consequently, $H(\mathcal{K}^e; \mathbb{E}^2_{a,b})$ is a proper subspace of $L_2(\mathbb{E}^2_{a,b})$. Since the norm (4.8) is defined as weighted sum of Fourier coefficients, spaces of the above form are called *Sobolev spaces*. Furthermore, $H(\mathcal{K}^e; \mathbb{E}^2_{a,b})$ is naturally equipped with the inner product

$$\left\langle \, f(\boldsymbol{x}) \,|\, g(\boldsymbol{x}) \, \right\rangle_{H(\mathcal{K}^e;\mathbb{E}^2_{a,b})} = \sum_{n=0}^{\infty} \sum_{m=-n}^{n} (k_{nm})^{-2} \, f_{nm} \, g_{nm} \tag{4.10}$$

for functions $f, g \in H(\mathcal{K}^e; \mathbb{E}^2_{a,b})$.

After this short excursion into functional analysis, we return to the study of ellipsoidal operators. As we have seen above, solving the equation (4.4) is not a well-posed problem, i.e., it is *ill-posed*. It is well-known that solving ill-posed problems requires regularization. Here, a *regularization* of the ill-posed problem $(\mathcal{K}^e)^{-1}$ is defined as a countable family of linear operators $\mathcal{A}_j$ such that $\mathcal{A}_j$ is bounded for all $j \in \mathbb{N}_0$ and that it converges pointwise to $(\mathcal{K}^e)^{-1}$ on $\operatorname{Im} \mathcal{K}^e$, i.e.,

$$\lim_{j \to \infty} \mathcal{A}_j g(\boldsymbol{x}) = (\mathcal{K}^e)^{-1} g(\boldsymbol{x}) \tag{4.11}$$

for all $g \in \operatorname{Im} \mathcal{K}^e$ in the L_2-sense.

For a particular choice of j, it can be seen that we are now confronted with two types of errors, namely a *regularization error* and a *data error* from the measurement. In general, an increase of j leads to a decrease of the regularization error whereas the data error increases. The optimal level value j if obtained by minimizing the sum of data and regularization error.

4.2 Ellipsoidal Wavelet Regularization

As mentioned before, the multi-resolution representation provides a way to regularize ill-posed problems. In order to make this clear, fix an integral operator $\mathcal{K}^e$ and a multi-resolution representation of

$L^2(\mathbb{E}^2_{a,b})$ with ellipsoidal scaling functions $\Phi_j(\boldsymbol{x}, \boldsymbol{x}_q)$ and ellipsoidal wavelet functions $\Psi_j(\boldsymbol{x}, \boldsymbol{x}_q)$ according to the Eqs. (3.16) and (3.27) for $j \in \mathbb{N}_0$. In the sequel we directly assume that all scaling and wavelet functions are *rotational symmetric* as defined with the Eqs. (3.52) and (3.54), which makes the computations much more efficient, because only Legendre polynomials have to be evaluated.

In analogy to the definition of Sobolev spaces $H(\mathcal{K}^e; \mathbb{E}^2_{a,b})$, we introduce the subspace $H(\mathcal{K}^e; [-1,1]) \subset L^2([-1,1])$ of functions

$$\kappa(\boldsymbol{x}, \boldsymbol{x}_q) = \sum_{n=0}^{\infty} \sum_{m=-n}^{n} (2n+1)\ \kappa_n\ P_n(\boldsymbol{\xi}^T \boldsymbol{\xi}_q) \tag{4.12}$$

fulfilling the condition

$$\sum_{n=0}^{\infty} \sum_{m=-n}^{n} (k_{nm})^{-2}\ \kappa_n^2 < \infty\ . \tag{4.13}$$

Note, that we write $L^2([-1,1])$ in order to indicate, that the argument t of the Legendre polynomials $P_n(t)$ is restricted to the interval $[-1,1]$, cf. Eq. (2.62). Under these assumptions we define *regularized scaling functions* and *regularized wavelet functions* $\widetilde{\Phi}_j(\boldsymbol{x}, \boldsymbol{x}_q)$, and $\widetilde{\Psi}_j(\boldsymbol{x}, \boldsymbol{x}_q)$, respectively, via the series expansions

$$\widetilde{\Phi}_j(\boldsymbol{x}, \boldsymbol{x}_q) = \sum_{n=0}^{\infty} \sum_{m=-n}^{n} (k_{nm})^{-1}\ \phi_{j;n}\ e_{nm}(\boldsymbol{\xi})\ e_{nm}(\boldsymbol{\xi}_q)\ , \tag{4.14}$$

$$\widetilde{\Psi}_j(\boldsymbol{x}, \boldsymbol{x}_q) = \sum_{n=0}^{\infty} \sum_{m=-n}^{n} (k_{nm})^{-1}\ \psi_{j;n}\ e_{nm}(\boldsymbol{\xi})\ e_{nm}(\boldsymbol{\xi}_q)\ . \tag{4.15}$$

It is important to observe, that both regularization functions are no longer rotational symmetric, since their coefficients

$$\widetilde{\phi}_{j;nm} := (k_{nm})^{-1}\ \phi_{j;n}\ , \tag{4.16}$$

$$\widetilde{\psi}_{j;nm} := (k_{nm})^{-1}\ \psi_{j;n} \tag{4.17}$$

now explicitely depend on the order m.

Analogous to the Eqs. (3.24) and (3.25) we define the level$-j$ *regularized smoothed signal*

$$f_j(\boldsymbol{x}) = \left(\ \widetilde{\Phi}_j\ \star\ \Phi_j\ \star\ f\ \right)_w(\boldsymbol{x}) =: \widetilde{\mathcal{P}}_j f(\boldsymbol{x}) \tag{4.18}$$

as well as the level$-j$ *regularized detail signal*

$$g_j(\boldsymbol{x}) = \left(\ \widetilde{\Psi}_j\ \star\ \Psi_j\ \star\ f\ \right)_w(\boldsymbol{x}) =: \widetilde{\mathcal{R}}_j f(\boldsymbol{x}) \tag{4.19}$$

of the signal $f(\boldsymbol{x})$ with $\boldsymbol{x} \in \overline{\mathbb{E}}^{2,\mathrm{ext}}_{a,b}$. An easy calculation shows

$$\mathcal{P}_j f(\boldsymbol{x}) = \mathcal{K}^e \, \widetilde{\mathcal{P}}_j f(\boldsymbol{x}) = \widetilde{\mathcal{P}}_j \, \mathcal{K}^e f(\boldsymbol{x}) \; , \tag{4.20}$$

$$\mathcal{R}_j f(\boldsymbol{x}) = \mathcal{K}^e \, \widetilde{\mathcal{R}}_j f(\boldsymbol{x}) = \widetilde{\mathcal{R}}_j \, \mathcal{K}^e f(\boldsymbol{x}) \; . \tag{4.21}$$

Let $\mathcal{A}_j$ be recursively defined as

$$\mathcal{A}_{j'} f(\boldsymbol{x}) = \widetilde{\mathcal{P}}_{j'} f(\boldsymbol{x}) \; , \tag{4.22}$$

$$\mathcal{A}_{j+1} f(\boldsymbol{x}) = \mathcal{A}_j f(\boldsymbol{x}) + \widetilde{\mathcal{R}}_j f(\boldsymbol{x}) \; . \tag{4.23}$$

Then we have under the consideration of the Eqs. (3.40) and (4.4)

$$\begin{aligned}
\lim_{J\to\infty} \mathcal{A}_{J+1} \mathcal{K}^e f(\boldsymbol{x}) = \lim_{J\to\infty} \mathcal{A}_{J+1} g(\boldsymbol{x}) &= \lim_{J\to\infty} (\widetilde{\mathcal{P}}_{j'} \mathcal{K}^e f(\boldsymbol{x}) + \sum_{j=j'}^{J} \widetilde{\mathcal{R}}_j \mathcal{K}^e f(\boldsymbol{x}) \\
&= \lim_{J\to\infty} \left(\mathcal{P}_{j'} f(\boldsymbol{x}) + \sum_{j=j'}^{J} \mathcal{R}_j f(\boldsymbol{x}) \right) \\
&= \lim_{J\to\infty} \left(f_{j'}(\boldsymbol{x}) + \sum_{j=j'}^{J} g_j(\boldsymbol{x}) \right) \\
&= f(\boldsymbol{x}) \; .
\end{aligned} \tag{4.24}$$

Comparing this result with Eq. (4.11) yields

$$f(\boldsymbol{x}) = (\mathcal{K}^e)^{-1} g(\boldsymbol{x}) = \lim_{J\to\infty} \mathcal{A}_{J+1} g(\boldsymbol{x}) \; . \tag{4.25}$$

Hence, the family $\mathcal{A}_j$ with $j = j', \ldots, J$ is a regularization of $(\mathcal{K}^e)^{-1}$.

Chapter 5

Multi-Resolution Representation of Bandlimited Signals

So far we studied non-bandlimited functions or signals $f(\boldsymbol{x})$, i.e., their representation (3.9) in ellipsoidal harmonics (2.11) means an infinite series expansion. In the sequel, however, we deal with *bandlimited* signals.

5.1 Basic Settings

Let $f(\boldsymbol{x})$ be a *bandlimited* signal $f(\boldsymbol{x})$ defined as the finite sum

$$f(\boldsymbol{x}) = \sum_{n=0}^{n'} \sum_{m=-n}^{n} f_{nm}\, h_{nm}^{b}(\boldsymbol{x}) \tag{5.1}$$

with $\boldsymbol{x} \in \overline{\mathbb{E}}_{a,b}^{2,\mathrm{ext}}$ and highest degree value $n' < \infty$. According to Eq. (2.17) the $2n+1$ ellipsoidal harmonics $e_{nm}(\boldsymbol{\xi})$ of a specific degree value n and order $m = -n, \ldots, n$ constitute an orthonormal basis of the finite dimensional *Hilbert space* $\mathrm{Harm}_n(\mathbb{E}_{a,b}^2)$. Consequently, all ellipsoidal harmonics $e_{nm}(\boldsymbol{\xi})$ of degree values $n = 0, \ldots, n'$ and order $m = -n, \ldots, n$ establish an orthonormal basis of the Hilbert space

$$\mathrm{Harm}_{0,\ldots,n'}(\mathbb{E}_{a,b}^2) = \bigoplus_{n=0}^{n'} \mathrm{Harm}_n(\mathbb{E}_{a,b}^2) \tag{5.2}$$

with dimension

$$\dim(\mathrm{Harm}_{0,\ldots,n'}(\mathbb{E}_{a,b}^2)) = (n'+1)^2 =: \overline{n}\,. \tag{5.3}$$

In addition, we define the space $\mathrm{Harm}_n(\overline{\mathbb{E}}^{2,\mathrm{ext}}_{a,b})$ spanned by the $2n+1$ outer ellipsoidal harmonics $h^b_{nm}(\boldsymbol{x})$ of the specific degree value n and order $m = -n, \ldots, n$ as well as the space

$$\mathrm{Harm}_{0,\ldots,n'}(\overline{\mathbb{E}}^{2,\mathrm{ext}}_{a,b}) = \bigoplus_{n=0}^{n'} \mathrm{Harm}_n(\overline{\mathbb{E}}^{2,\mathrm{ext}}_{a,b}) \tag{5.4}$$

of all outer ellipsoidal harmonics $h^b_{nm}(\boldsymbol{x})$ of the degree values $n = 0, \ldots, n'$ and order $m = -n, \ldots, n$. If we assume, that the potential $U(\boldsymbol{x})$ is *bandlimited*, i.e. $U \in \mathrm{Harm}_{0,\ldots,n'}(\overline{\mathbb{E}}^{2,\mathrm{ext}}_{a,b})$, we can rewrite Eq. (2.10) as

$$\begin{aligned} U(\boldsymbol{x}) &= \sum_{n=0}^{n'} \sum_{m=-n}^{n} u_{nm}\, h^b_{nm}(\boldsymbol{x}) \\ &= \boldsymbol{h}(\boldsymbol{x})^T \boldsymbol{u} \end{aligned} \tag{5.5}$$

with $\boldsymbol{x} \in \overline{\mathbb{E}}^{2,\mathrm{ext}}_{a,b}$. Herein $\boldsymbol{u}$ and $\boldsymbol{h}(\boldsymbol{x})$ denote $\overline{n} \times 1$ vectors given by

$$\boldsymbol{u} = \left[\, u_{00},\ u_{1,-1},\ \ldots,\ u_{n',n'} \,\right]^T, \tag{5.6}$$

$$\boldsymbol{h}(\boldsymbol{x}) = \left[\, h^b_{00}(\boldsymbol{x}),\ h^b_{1,-1}(\boldsymbol{x}),\ \ldots,\ h^b_{n',n'}(\boldsymbol{x}) \,\right]^T; \tag{5.7}$$

the vector $\boldsymbol{h}(\boldsymbol{x})$ was already defined in Eq. (3.19).

The *reproducing kernel*

$$K^e_{\mathrm{rep}}(\boldsymbol{x}, \boldsymbol{x}_q) = \sum_{n=0}^{n'} \sum_{m=-n}^{n} \frac{Q^\star_{nm}(\frac{u}{\epsilon})}{Q^\star_{nm}(\frac{b}{\epsilon})} \frac{Q^\star_{nm}(\frac{u_q}{\epsilon})}{Q^\star_{nm}(\frac{b}{\epsilon})}\, e_{nm}(\boldsymbol{\xi})\, e_{nm}(\boldsymbol{\xi}_q) \tag{5.8}$$

of the Hilbert space $\mathrm{Harm}_{0,\ldots,n'}(\overline{\mathbb{E}}^{2,\mathrm{ext}}_{a,b})$ has to fulfill the conditions $K^e_{\mathrm{rep}} \in \mathrm{Harm}_{0,\ldots,n'}(\overline{\mathbb{E}}^{2,\mathrm{ext}}_{a,b})$ and

$$f(\boldsymbol{x}) = \left(\, K^e_{\mathrm{rep}} \star f \,\right)_w(\boldsymbol{x}); \tag{5.9}$$

see e.g. Moritz (1980). Recall, that for $n' \to \infty$ the reproducing kernel K^e_{rep} equals the *Abel-Poisson kernel* K^e_{AP} as defined in Eq. (2.24) for $\boldsymbol{x} \in \overline{\mathbb{E}}^{2,\mathrm{ext}}_{a,b}$ and $\boldsymbol{x}_q \in \mathbb{E}^2_{a,b}$.

As mentioned before the ellipsoidal harmonics are a very suitable system of base functions for modeling the geopotential globally. However, for regional or local representations we would prefer a system of base functions which allows the computation of $U(\boldsymbol{x})$ mainly from signal values given in the vicinity of $P(\boldsymbol{x})$, i.e. which is characterized by the ability to localize. As shown in the Figures 4.1 and 4.2 ellipsoidal scaling functions are examples for such kind of localizing functions.

In the following we study Eq. (3.23) for $j = J+1$ and $f_{J+1} =: U_{J+1}$ in more detail. From Eq. (3.7) we obtain analogously to Eq. (3.30)

$$U_{J+1}(\boldsymbol{x}) = \left(\, \Phi_{J+1} \star \Phi_{J+1} \star U \,\right)_w(\boldsymbol{x}) = \sum_{n=0}^{\infty} \sum_{m=-n}^{n} (\phi_{J+1;nm})^2\, u_{nm}\, h^b_{nm}(\boldsymbol{x}) \tag{5.10}$$

for $\boldsymbol{x} \in \overline{\mathbb{E}}^{2,\mathrm{ext}}_{a,b}$. As mentioned before we want to restrict our investigations to bandlimited rotational symmetric scaling functions according to (3.58) and (3.61); thus, Eq. (5.10) reduces to

$$U_{J+1}(\boldsymbol{x}) = \big(\ \Phi_{J+1} \star \Phi_{J+1} \star U\ \big)_w(\boldsymbol{x}) = \sum_{n=0}^{n'_{J+1}} \sum_{m=-n}^{n} (\phi_{J+1;n})^2\ u_{nm}\ h^b_{nm}(\boldsymbol{x})\ , \tag{5.11}$$

wherein $n'_{J+1} = 2^{J+1} - 1$. Next we define the bandlimited kernel

$$\begin{aligned}\Theta_{J+1}(\boldsymbol{x}, \boldsymbol{x}_q) &= \big(\ \Phi_{J+1} \star \Phi_{J+1}\ \big)_w(\boldsymbol{x}, \boldsymbol{x}_q) \\ &= \sum_{n=0}^{n'_{J+1}} \sum_{m=-n}^{n} \theta_{J+1;n}\ h^b_{nm}(\boldsymbol{x})\ h^b_{nm}(\boldsymbol{x}_q)\end{aligned} \tag{5.12}$$

with Legendre coefficients

$$\theta_{J+1;n} = (\phi_{J+1;n})^2 \tag{5.13}$$

and rewrite Eq. (5.11) as

$$U_{J+1}(\boldsymbol{x}) = \big(\ \Theta_{J+1} \star U\ \big)_w(\boldsymbol{x}) = \sum_{n=0}^{n'_{J+1}} \sum_{m=-n}^{n} \theta_{J+1;n}\ u_{nm}\ h^b_{nm}(\boldsymbol{x})\ . \tag{5.14}$$

Defining with $\overline{n}_{J+1} = (n'_{J+1} + 1)^2 = 2^{2J+2}$ the $\overline{n}_{J+1} \times 1$ vectors

$$\boldsymbol{u} = \big[\ u_{00},\ u_{1,-1},\ \ldots,\ u_{n'_{J+1},n'_{J+1}}\ \big]^T\ , \tag{5.15}$$

$$\boldsymbol{h}(\boldsymbol{x}) = \big[\ h^b_{00}(\boldsymbol{x}),\ h^b_{1,-1}(\boldsymbol{x}),\ \ldots,\ h^b_{n'_{J+1},n'_{J+1}}(\boldsymbol{x})\ \big]^T \tag{5.16}$$

as well as the $\overline{n}_{J+1} \times \overline{n}_{J+1}$ positive definite diagonal matrix

$$\boldsymbol{B}_{J+1} = \mathrm{diag}(\theta_{J+1;0}, \theta_{J+1;1}, \theta_{J+1;1}, \theta_{J+1;1}, \theta_{J+1;2}, \ldots, \theta_{J+1;n'_{J+1}}) \tag{5.17}$$

we rewrite Eq. (5.14) as

$$U_{J+1}(\boldsymbol{x}) = \big(\ \Theta_{J+1} \star U\ \big)_w(\boldsymbol{x}) = \boldsymbol{h}(\boldsymbol{x})^T \boldsymbol{B}_{J+1}\ \boldsymbol{u}\ . \tag{5.18}$$

In the context of Eq. (3.15) we argued that the infinite set of base functions $K^e(\boldsymbol{x}, \boldsymbol{x}_q)$ with $\boldsymbol{x}, \boldsymbol{x}_q \in \mathbb{E}^2_{a,b}$ spans the space $L_2(\mathbb{E}^2_{a,b})$. Consequently, the finite set $K^e(\boldsymbol{x}, \boldsymbol{x}_k)$ with $\boldsymbol{x} \in \overline{\mathbb{E}}^{2,\mathrm{ext}}_{a,b}$ and $\boldsymbol{x}_k \in \mathbb{E}^2_{a,b}$ spans the space $\mathrm{Harm}_{0,\ldots,n'}(\overline{\mathbb{E}}^{2,\mathrm{ext}}_{a,b})$, i.e.,

$$\mathrm{Harm}_{0,\ldots,n'}(\overline{\mathbb{E}}^{2,\mathrm{ext}}_{a,b}) = \mathrm{span}\{K^e(\boldsymbol{x}, \boldsymbol{x}_k)\,|\,\boldsymbol{x} \in \overline{\mathbb{E}}^{2,\mathrm{ext}}_{a,b}\ ,\ \boldsymbol{x}_k \in \mathbb{E}^2_{a,b}\ ,\ k = 1, \ldots, N\} \tag{5.19}$$

with $N \geq \overline{n}$. Based on this insight we conclude, that the convolution $\big(\ \Theta_{J+1} \star U\ \big)_w(\boldsymbol{x})$ is a member of the space $\mathrm{Harm}_{0,\ldots,n'_{J+1}}(\overline{\mathbb{E}}^{2,\mathrm{ext}}_{a,b})$ and can be modeled as a series expansion

$$U_{J+1}(\boldsymbol{x}) = \big(\ \Theta_{J+1} \star U\ \big)_w(\boldsymbol{x}) = \sum_{k=1}^{N_J} d_{J,k}\ \Theta_{J+1}(\boldsymbol{x}, \boldsymbol{x}^J_k) \tag{5.20}$$

in terms of ellipsoidal base functions $\Theta_{J+1}(\boldsymbol{x}, \boldsymbol{x}_k^J)$; the level$-J$ scaling cofficients $d_{J,k}$ are linked to the N_J computation points $P(\boldsymbol{x}_k^J)$ with $k = 1, \ldots, N_J$ on the reference ellipsoid $\mathbb{E}_{a,b}^2$. Note that the right-hand side of Eq. (5.20) also can be seen as a discretization of the convolution $\left(\Theta_{J+1} \star U \right)_w(\boldsymbol{x})$ as defined in Eq. (3.3). Analogously to Eq. (5.5) we rewrite Eq. (5.20) as the scalar product

$$U_{J+1}(\boldsymbol{x}) = \boldsymbol{\theta}_{J+1}(\boldsymbol{x})^T \, \boldsymbol{d}_J \tag{5.21}$$

with $\boldsymbol{x} \in \overline{\mathbb{E}}_{a,b}^{2,\mathrm{ext}}$ of the two $N_J \times 1$ vectors

$$\boldsymbol{d}_J = \left[\, d_{J,1}, \; d_{J,2}, \; \ldots, \; d_{J,N_J} \, \right]^T , \tag{5.22}$$

$$\boldsymbol{\theta}_{J+1}(\boldsymbol{x}) = \left[\, \Theta_{J+1}(\boldsymbol{x}, \boldsymbol{x}_1^J), \; \Theta_{J+1}(\boldsymbol{x}, \boldsymbol{x}_2^J), \; \ldots, \; \Theta_{J+1}(\boldsymbol{x}, \boldsymbol{x}_{N_J}^J) \, \right]^T . \tag{5.23}$$

According to Eq. (3.17) the expression

$$\Theta_{J+1}(\boldsymbol{x}, \boldsymbol{x}_k^J) = \boldsymbol{h}(\boldsymbol{x}_k^J)^T \, \boldsymbol{B}_{J+1} \, \boldsymbol{h}(\boldsymbol{x}) \tag{5.24}$$

holds for each component of the vector $\boldsymbol{\theta}_{J+1}(\boldsymbol{x})$. Hence, we obtain from the Eqs. (5.23) and (5.24)

$$\boldsymbol{\theta}_{J+1}(\boldsymbol{x}) = \boldsymbol{H} \, \boldsymbol{B}_{J+1} \, \boldsymbol{h}(\boldsymbol{x}) \; , \tag{5.25}$$

wherein

$$\boldsymbol{H} = \left[\, \boldsymbol{h}(\boldsymbol{x}_1^J), \; \boldsymbol{h}(\boldsymbol{x}_2^J), \; \ldots, \; \boldsymbol{h}(\boldsymbol{x}_{N_J}^J) \, \right]^T \tag{5.26}$$

means an $N_J \times \overline{n}_{J+1}$ matrix. As mentioned before the $\overline{n}_{J+1}$ components of the vector $\boldsymbol{h}(\boldsymbol{x})$, Eq. (5.16), establish a complete basis of the space $\mathrm{Harm}_{0,\ldots,n'_{J+1}}(\overline{\mathbb{E}}_{a,b}^{2,\mathrm{ext}})$. If for $N_J \geq \overline{n}_{J+1}$ the matrix $\boldsymbol{H}$ is of full column rank, i.e. $\mathrm{rank}\, \boldsymbol{H} = \mathrm{rank}\, (\boldsymbol{H} \, \boldsymbol{B}_{J+1}) = \overline{n}_{J+1}$, the altogether N_J components $\Theta_{J+1}(\boldsymbol{x}, \boldsymbol{x}_k^J)$ with $k = 1, \ldots, N_J$ of the vector $\boldsymbol{\theta}_{J+1}(\boldsymbol{x})$ span the space $\mathrm{Harm}_{0,\ldots,n'_{J+1}}(\overline{\mathbb{E}}_{a,b}^{2,\mathrm{ext}})$, too, as required in Eq. (5.19). In this case the system

$$S_{N_J}(\mathbb{E}_{a,b}^2) = \{ \boldsymbol{x}_k^J \in \mathbb{E}_{a,b}^2 \,|\, k = 1, \ldots, N_J \} \tag{5.27}$$

of points $P(\boldsymbol{x}_k^J)$ on the reference ellipsoid $\mathbb{E}_{a,b}^2$ is called *admissible*. If even the equality $N_J = \overline{n}_{J+1}$ holds, the matrix $\boldsymbol{H}$ is regular and $S_{N_J}(\mathbb{E}_{a,b}^2)$ is called *fundamental*; see Freeden et al. (1998). In the following we always assume that point systems $S_{N_j}(\mathbb{E}_{a,b}^2)$ such as $S_{N_J}(\mathbb{E}_{a,b}^2)$ are at least admissible.

Note, that the series expansion (5.20) means the desired counterpart to the representation (5.5) in terms of ellipsoidal harmonics; the level$-J$ *scaling coefficients* $d_{J,k}$ with $k = 1, \ldots, N_J$ play the role of the ellipsoidal harmonic coefficients u_{nm} for $n = 0, \ldots, n'_{J+1}$ and $m = -n, \ldots, n$ collected in the $\overline{n}_{J+1} \times 1$ vector $\boldsymbol{u}$, Eq. (5.15). In order to find a relation between the two sets of coefficients we insert Eq. (5.25) into Eq. (5.21) and obtain for $U = U_{J+1}$

$$U(\boldsymbol{x}) = \boldsymbol{h}(\boldsymbol{x})^T \, \boldsymbol{B}_{J+1} \, \boldsymbol{H}^T \, \boldsymbol{d}_J \; . \tag{5.28}$$

Comparing the right-hand sides of the Eqs. (5.18) and (5.28) the desired relation

$$\boldsymbol{u} = \boldsymbol{H}^T \, \boldsymbol{d}_J \tag{5.29}$$

follows. Note, that from this result the $\overline{n}_{J+1}$ ellipsoidal harmonic coefficients u_{nm} with $n = 0, \ldots, n'_{J+1}$ and $m = -n, \ldots, n$ are uniquely computable from the N_J level$-J$ scaling coefficients $d_{J,k}$ with $k = 1, \ldots, N_J$. However, only in case of a fundamental point system, i.e, for $N_J = \overline{n}_{J+1}$ the reverse does also hold. Before we procede with the computation of the detail signals, we want to emphasize the main difference between the representation of a signal in terms of ellipsoidal harmonics and its decomposition into detail signals by means of ellipsoidal wavelets:

– The ellipsoidal harmonic coefficients u_{nm}, are *global parameters*, because they do not depend on a spatial position. On the other hand these coefficients are characterized by an *optimal frequency localization*, because u_{nm} is directly related to the frequency value n.

– The scaling coefficients $d_{J,k}$, however, are *point parameters*, because they are a function of the position vector $\boldsymbol{x}_k^J$ with $\boldsymbol{x}_k^J \in \mathbb{E}^2_{a,b}$. The frequency localization is worse than in the ellipsoidal harmonic case, because each coefficient is related to a frequency band B_j, defined in Eq. (3.62).

The items listed before are the consequences of the so-called *uncertainty principle* (Mertins 1999), originally introduced in the context of quantum mechanics. The necessity of the gravity field representation in point parameters was already identified and discussed more than 30 years ago (Heitz 1975).

Next, we introduce the wavelet function $\Psi_J(\boldsymbol{x}, \boldsymbol{x}_k^J)$ represented analogously to Eq. (5.24) as

$$\Psi_J(\boldsymbol{x}, \boldsymbol{x}_k^J) = \boldsymbol{h}(\boldsymbol{x}_k^J)^T \, \boldsymbol{C}_J \, \boldsymbol{h}(\boldsymbol{x}) \; . \tag{5.30}$$

In opposite to the matrix $\boldsymbol{B}_{J+1}$ we assume now that the $\overline{n}_{J+1} \times \overline{n}_{J+1}$ diagonal matrix

$$\boldsymbol{C}_J = \text{diag}(\psi_{J;0}, \psi_{J;1}, \psi_{J;1}, \psi_{J;1}, \psi_{J;2}, \ldots, \psi_{J;n'_{J+1}}) \tag{5.31}$$

might be just positive semidefinite since the Legendre coefficients $\psi_{J;n}$ fulfill the condition

$$\begin{aligned} \psi_{J;n} \, \widetilde{\psi}_{J;n} &= \sqrt{(\phi_{J+1;n})^2 - (\phi_{J;n})^2} \\ &= \sqrt{\theta_{J+1;n} - \theta_{J;n}} \qquad \forall \qquad n = 0, \ldots, n'_{J+1} \end{aligned} \tag{5.32}$$

according to the Eqs. (3.32) and (5.13). It follows from Eq. (3.39) that the convolution $\left(\, \Psi_J \star f \, \right)_w(\boldsymbol{x})$ has to be evaluated to calculate the level$-J$ wavelet coefficients $c_J(\boldsymbol{x})$. Thus, it follows analogously to Eq. (5.18)

$$c_J(\boldsymbol{x}) = \left(\, \Psi_J \star U \, \right)_w(\boldsymbol{x}) = \boldsymbol{h}(\boldsymbol{x})^T \boldsymbol{C}_J \, \boldsymbol{u} \; . \tag{5.33}$$

Substituting the result (5.29) for $\boldsymbol{u}$ yields

$$c_J(\boldsymbol{x}) = \left(\Psi_J \star U \right)_w(\boldsymbol{x}) = \boldsymbol{h}(\boldsymbol{x})^T \boldsymbol{C}_J \boldsymbol{H}^T \boldsymbol{d}_J$$
$$= \boldsymbol{\psi}_J(\boldsymbol{x})^T \boldsymbol{d}_J \tag{5.34}$$

wherein

$$\boldsymbol{\psi}_J(\boldsymbol{x}) = \left[\Psi_J(\boldsymbol{x}, \boldsymbol{x}_1^J),\ \Psi_J(\boldsymbol{x}, \boldsymbol{x}_2^J),\ \ldots,\ \Psi_J(\boldsymbol{x}, \boldsymbol{x}_{N_J}^J) \right]^T . \tag{5.35}$$

means an $N_J \times 1$ vector collecting the wavelet functions $\Psi_J(\boldsymbol{x}, \boldsymbol{x}_k^J)$ as defined in Eq. (5.30). Thus, if the coefficient vector $\boldsymbol{d}_J$ is known once, it can be used to calculate both, the ellipsoidal harmonic coefficients u_{nm} according to Eq. (5.29) and any convolution of the function $U(\boldsymbol{x})$ with kernel functions

$$K^e(\boldsymbol{x}, \boldsymbol{x}_k) = \sum_{n=0}^{n'_{J+1}} \sum_{m=-n}^{n} k_n\ h_{nm}^b(\boldsymbol{x})\ h_{nm}^b(\boldsymbol{x}_k) \tag{5.36}$$

with $\boldsymbol{x} \in \overline{\mathbb{E}}_{a,b}^{2,\mathrm{ext}}$ and $\boldsymbol{x}_k \in S_{N_J}(\mathbb{E}_{a,b}^2)$ fulfilling the condition

$$k_n \geq 0 \qquad \forall \qquad n = 0, \ldots, n'_{J+1} \tag{5.37}$$

for the Legendre coefficients k_n. As seen before the ellipsoidal wavelet function Ψ_J means an example for such a kernel K^e. All ellipsoidal scaling functions Φ_j with $j \leq J$ and all ellipsoidal wavelet functions Ψ_j with $j < J$ as well as their duals $\widetilde{\Psi}_j$ are further examples.

5.2 Decomposition and Reconstruction

Based on the definition (5.32) of an ellipsoidal wavelet function the two main steps to create a multiresolution representation of a given band-limited input signal $f(\boldsymbol{x})$ can be outlined as follows:

1. *Analysis*: The (primal) ellipsoidal wavelet function $\Psi_j(\boldsymbol{x}, \boldsymbol{x}_k)$ with $j \in \{j', \ldots, J\}$ decomposes the input signal $f(\boldsymbol{x})$ into its *wavelet coefficients*

   $$c_j(\boldsymbol{x}) = \left(\Psi_j \star f \right)_w(\boldsymbol{x}) = \boldsymbol{\psi}_j(\boldsymbol{x})^T \boldsymbol{d}_j \tag{5.38}$$

   with the $N_j \times 1$ vector

   $$\boldsymbol{\psi}_j(\boldsymbol{x}) = \left[\Psi_j(\boldsymbol{x}, \boldsymbol{x}_1^j),\ \Psi_j(\boldsymbol{x}, \boldsymbol{x}_2^j),\ \ldots,\ \Psi_j(\boldsymbol{x}, \boldsymbol{x}_{N_j}^j) \right]^T \tag{5.39}$$

   of wavelet functions $\Psi_j(\boldsymbol{x}, \boldsymbol{x}_k^j)$ and the $N_j \times 1$ vector

   $$\boldsymbol{d}_j = \left[d_{j,1},\ d_{j,2},\ \ldots,\ d_{j,N_j} \right]^T \tag{5.40}$$

of the level$-j$ scaling coefficients $d_{j,k}$ with $k = 1, \ldots, N_j$ and $N_j \geq \overline{n}_{j+1} = (n'_{j+1} + 1)^2$. As mentioned before we assume that the position vectors $\boldsymbol{x}_k^j$ are related to the N_j points of the admissible system $S_{N_J}(\mathbb{E}^2_{a,b})$. The decomposition of the input signal into wavelet coefficients via Eq. (5.38) is also known as *multi-resolution analysis* (MRA).

2. *Synthesis*: The dual ellipsoidal wavelet function $\widetilde{\Psi}_j(\boldsymbol{x}, \boldsymbol{x}_k)$ performs the reconstruction

$$f(\boldsymbol{x}) = f_{j'}(\boldsymbol{x}) + \sum_{j=j'}^{J} g_j(\boldsymbol{x}) \tag{5.41}$$

by means of the *level$-j'$ approximation*

$$f_{j'}(\boldsymbol{x}) = \left(\Theta_{j'} \star f \right)_w(\boldsymbol{x}) \tag{5.42}$$

and the *level$-j$ detail signals*

$$g_j(\boldsymbol{x}) = \left(\widetilde{\Psi}_j \star c_j \right)_w(\boldsymbol{x}) \tag{5.43}$$

with $j = j', \ldots, J < \infty$. The ellipsoidal kernel function $\Theta_{j'}(\boldsymbol{x}, \boldsymbol{x}_k)$ is given as

$$\Theta_{j'}(\boldsymbol{x}, \boldsymbol{x}_k) = \sum_{n=0}^{n'_{j'}} \sum_{m=-n}^{n} \theta_{j';n} \, h^b_{nm}(\boldsymbol{x}) \, h^b_{nm}(\boldsymbol{x}_q) \tag{5.44}$$

according to Eq. (5.12).

In the sequel we describe at first the decomposition process (analysis) in more detail by identifying the input signal $f(\boldsymbol{x})$ with the gravitational potential $U(\boldsymbol{x})$ or the disturbing potential $T(\boldsymbol{x})$.

Today geopotential models are either *satellite-only models* mostly based on measurements from the modern gravity space missions, namely the CHAllenging Minisatellite Payload (CHAMP), the Gravity Recovery And Climate Experiment (GRACE) as well as the Gravity field and steady-state Ocean Circulation Explorer (GOCE) or so-called *combined models*; for more details concerning these gravity missions see, e.g. Reigber et al. (2000, 2005). The new high-resolution Earth Gravity Model 2007 (EGM07), for instance, is computed until degree $n = 2160$ from a combination of satellite and surface data; see e.g., Pavlis et al. (2005). Nowadays, besides the classical procedures, alternative methods such as the *energy balance approach* or the *Fredholm integral approach* (see e.g., Mayer-Gürr et al. 2005, 2006) are used to derive global and regional geopotential models.

The energy balance approach and its application to Low-Earth-Orbiting (LEO) satellites goes back to the 60's (Bjerhammer 1967) and was rediscovered by Jekeli (1999), van Loon and Kusche (2005), Ilk and Löcher (2005) and others. An extensive overview about this topic is presented by Han (2003) and Han et al. (2006).

5.2.1 Initial Step

As the result of the energy balance approach we assume in the initial step of the decomposition process that geopotential measurements $U(\boldsymbol{x}_p) \equiv U_{J+1}(\boldsymbol{x}_p)$ are given along the orbit of a LEO satellite.

According to Eq. (5.21) the observation equation reads

$$U(\boldsymbol{x}_p) = \boldsymbol{\theta}_{J+1}(\boldsymbol{x}_p)^T \, \boldsymbol{d}_J \ . \tag{5.45}$$

The numerical value for the highest resolution level, i.e. $J+1$ depends on the maximum degree $n_{\max}$ we want to solve for. Thus, it follows $J+1 \geq \log_2(n_{\max}+1)$. For the CHAMP case, e.g., we may choose $n_{\max} = 120$. Consequently, the value $J+1 = 7$ follows.

Furthermore, as mentioned in the context of Eq. (5.26) the number N_J of points $P(\boldsymbol{x}_k^J)$ with $k = 1, \ldots, N_J$ of the level$-J$ admissible system $S_{N_J}(\mathbb{E}_{a,b}^2)$, Eq. (5.27), is restricted to $N_J \geq 2^{2J+2} = \overline{n}_{J+1}$. In order to estimate the unknown $N_J \times 1$ vector $\mathbf{d}_J$ of *scaling coefficients* $d_{J,k}$ with $k = 1, \ldots, N_J$ from Eq. (5.45), we need altogether P discrete observation points $P(\boldsymbol{x}_p)$ with $p = 1, \ldots, P$ and $P \geq N_J$. However, *geodetic measurements* $y(\boldsymbol{x}_p) =: y_p$ are always erroneous, i.e. $U(\boldsymbol{x}_p) = y(\boldsymbol{x}_p) + e(\boldsymbol{x}_p)$ or $U_p = y_p + e_p$. Herein $e_p := e(\boldsymbol{x}_p)$ denotes the measurement error. Under these assumptions Eq. (5.45) can be rewritten as the *observation equation*

$$y_p + e_p = \boldsymbol{\theta}_{J+1;\,p}^T \, \mathbf{d}_J \tag{5.46}$$

for a single observation y_p; herein we set $\boldsymbol{\theta}_{J+1}(\boldsymbol{x}_p) =: \boldsymbol{\theta}_{J+1;\,p}$. Note, that usually the observations are reduced by so-called background models, i.e., all the informations which are a priori known are subtracted from the original observations. This way, the observations y_p have to be interpreted as *residual observations*; see e.g. Schmidt et al. (2006, 2007a).

The procedure described here allows the combination of different kinds of measurements, e.g., geopotential values and gravity anomalies. In such a combination case additional operators, like the Stokes operator, have probably to be considered in the vector $\boldsymbol{\theta}_{J+1;\,p}$. Introducing the $P \times 1$ vectors

$$\boldsymbol{y} = \left[\, y_1, \ y_2, \ \ldots, \ y_P \, \right]^T \ , \tag{5.47}$$

$$\boldsymbol{e} = \left[\, e_1, \ e_2, \ \ldots, \ e_P \, \right]^T \tag{5.48}$$

of the observations and the measurement errors, respectively, the $P \times N_J$ coefficient matrix

$$\mathbf{A}_J = \left[\, \boldsymbol{\theta}_{J+1;\,1}, \ \boldsymbol{\theta}_{J+1;\,2}, \ \ldots, \ \boldsymbol{\theta}_{J+1;\,P} \, \right]^T \tag{5.49}$$

and the $P \times P$ covariance matrix $D(\boldsymbol{y}) = \boldsymbol{\Sigma}_y$ of the observations, the linear model

$$\boldsymbol{y} + \mathbf{e} = \boldsymbol{A}_J \, \boldsymbol{d}_J \quad \text{with} \quad D(\boldsymbol{y}) = \boldsymbol{\Sigma}_y = \sigma_y^2 \, \boldsymbol{V}_y^{-1} \tag{5.50}$$

is established; see e.g. Koch (1999). Herein σ_y^2 and $\boldsymbol{V}_y$ are denoted as the variance factor and the weight matrix, which is assumed to be positive definite. Analog to the matrix $\boldsymbol{H}$, Eq. (5.26), and

depending on the distribution of the observation sites the matrix $\boldsymbol{A}_J$ is of rank $\boldsymbol{A}_J \leq \overline{n}_{J+1}$, i.e. a rank deficiency of at least $N_J - \overline{n}_{J+1}$ exists. Besides the rank deficiency problem the resulting normal equation system might be *ill-conditioned*. If we, for instance, want to compute the gravity field at the Earth's surface just from satellite data, *regularization procedures* have generally to be applied. Solution strategies for these problems have been already discussed in section 4.2. However, in the following we want to pursue a different way.

Let us assume that according to Eq. (5.5) a geopotential model

$$U_0(\boldsymbol{x}) = \sum_{n=0}^{n'} \sum_{m=-n}^{n} u_{nm;0}\, h_{nm}^b(\boldsymbol{x}) = \boldsymbol{h}(\boldsymbol{x})^T \boldsymbol{u}_0 \tag{5.51}$$

with $\boldsymbol{x} \in \overline{\mathbb{E}}_{a,b}^{2,\mathrm{ext}}$ in terms of outer harmonics exists. The given series coefficients $u_{nm;0}$ are collected in the $\overline{n} \times 1$ vector

$$\boldsymbol{u}_0 = \left[\, u_{00;0},\ u_{1,-1;0},\ \ldots,\ u_{n',n';0} \,\right]^T \tag{5.52}$$

with $\overline{n} = (n'+1)^2$. Now we interprete $\boldsymbol{u}_0$ and the associated covariance matrix $D(\boldsymbol{u}_0)$ as prior information for the expectation vector $E(\boldsymbol{u}) = \boldsymbol{\mu}_u$ and the covariance matrix $D(\boldsymbol{u}) = \boldsymbol{\Sigma}_u$ of the vector $\boldsymbol{u}$ collecting the ellipsoidal series coefficients u_{nm} for $n = 0, \ldots, n'$ and $m = -n, \ldots, n$ and introduce the additional linear model

$$\boldsymbol{\mu}_u + \boldsymbol{e}_u = \boldsymbol{A}\ \boldsymbol{d}_J \quad \text{with} \quad D(\boldsymbol{\mu}_u) = \sigma_u^2\ \boldsymbol{\Sigma}_u \tag{5.53}$$

following Eq. (5.29) with $\boldsymbol{H}^T =: \boldsymbol{A}$. In Eq. (5.53) $\boldsymbol{e}_u$ is defined as the error vector of the prior information and σ_u^2 the corresponding unknown variance factor. The combination of the two models (5.50) and (5.53) gives an extended linear model with unknown variance components σ_y^2 and σ_u^2, namely

$$\begin{bmatrix} \boldsymbol{y} \\ \boldsymbol{\mu}_u \end{bmatrix} + \begin{bmatrix} \boldsymbol{e} \\ \boldsymbol{e}_u \end{bmatrix} = \begin{bmatrix} \boldsymbol{A}_J \\ \boldsymbol{A} \end{bmatrix} \boldsymbol{d}_J \quad \text{with} \quad D\Big(\begin{bmatrix} \boldsymbol{y} \\ \boldsymbol{\mu}_u \end{bmatrix} \Big) \ = \sigma_y^2 \begin{bmatrix} \boldsymbol{V}_y^{-1} & \boldsymbol{0} \\ \boldsymbol{0} & \boldsymbol{0} \end{bmatrix} + \sigma_u^2 \begin{bmatrix} \boldsymbol{0} & \boldsymbol{0} \\ \boldsymbol{0} & \boldsymbol{\Sigma}_u \end{bmatrix} . \tag{5.54}$$

The method of estimating variance components (e.g. Koch, 1999) yields the solution

$$\widehat{\boldsymbol{d}}_J = (\boldsymbol{A}_J^T \boldsymbol{V}_y\, \boldsymbol{A}_J + \lambda\, \boldsymbol{A}^T \boldsymbol{\Sigma}_u^{-1} \boldsymbol{A})_{rs}^{-}\ (\boldsymbol{A}_J^T\ \boldsymbol{V}_y\, \boldsymbol{y} + \lambda\, \boldsymbol{A}^T \boldsymbol{\Sigma}_u^{-1} \boldsymbol{\mu}_u) \tag{5.55}$$

with the covariance matrix

$$D(\widehat{\boldsymbol{d}}_J) = \sigma_y^2\ (\boldsymbol{A}_J^T \boldsymbol{V}_y\, \boldsymbol{A}_J + \lambda\, \boldsymbol{A}^T \boldsymbol{\Sigma}_u^{-1} \boldsymbol{A})_{rs}^{-}\ ; \tag{5.56}$$

$\lambda := \sigma_y^2 / \sigma_u^2$ might be interpreted as a regularization parameter. Note, that $(\,\cdot\,)_{rs}^{-}$ means a symmetrical reflexive generalized inverse.

Other solution strategies can be found in the literature; see e.g. Freeden and Michel (2004) or Schmidt et al. (2007a). In the following we assume that the vector $\boldsymbol{d}_J$ and its covariance matrix $D(\boldsymbol{d}_J)$ are given and mean the starting point of the multi-resolution representation.

5.2.2 Pyramid Step

In the so-called pyramid step we compute the level$-j$ results from the level$-(j+1)$ results for $j = j', \ldots, J-1$. To be more specific, the $(J-j)^{th}$ pyramid step consists mainly of the linear equations

$$\boldsymbol{d}_j = \boldsymbol{P}_j \, \boldsymbol{d}_{j+1} = \boldsymbol{P}_j \, \boldsymbol{P}_{j+1} \, \ldots \, \boldsymbol{P}_{J-1} \, \boldsymbol{d}_J =: \boldsymbol{P}_{j,J} \, \boldsymbol{d}_J \; , \tag{5.57}$$

$$\boldsymbol{c}_j = \boldsymbol{Q}_j \, \boldsymbol{d}_j = \boldsymbol{Q}_j \, \boldsymbol{P}_{j,J} \, \boldsymbol{d}_J \; , \tag{5.58}$$

wherein $\boldsymbol{P}_j$, $\boldsymbol{P}_{j+1}$, $\ldots$, $\boldsymbol{P}_{J-1}$ are *low-pass filter matrices*. In particular $\boldsymbol{P}_j$ is an $N_j \times N_{j+1}$ matrix, which transforms the $N_{j+1} \times 1$ scaling coefficient vector $\boldsymbol{d}_{j+1}$ of level $j+1$ into the $N_j \times 1$ scaling coefficient vector $\boldsymbol{d}_j$ of level j. Next, the vector $\boldsymbol{d}_j$ is used to calculate the $N_j \times 1$ level$-j$ wavelet coefficient vector $\boldsymbol{c}_j = (c_{j,k})$ of wavelet coefficients $c_{j,k}$, $k = 1, \ldots, N_j$ according to Eq. (5.58) using the $N_j \times N_j$ *band-pass filter matrix* $\boldsymbol{Q}_j$. As mentioned in the context of Eq. (5.36) the convolution $\left(\Psi_j \star U \right)_w(\boldsymbol{x})$ can be evaluated also by means of the scaling vector $\boldsymbol{d}_J$ calculated (estimated) within the initial step. This procedure would have the drawback that in each pyramid step the same admissible system $S_{N_J}(\mathbb{E}^2_{a,b})$ would be used. But as a matter of fact coarser structures are modelable by less terms than finer structures. Since usually the inequality $N_j < N_{j+1}$ holds, the $N_j \times N_{j+1}$ transformation matrix $\boldsymbol{P}_j$ in Eq. (5.57) effects a downsampling process as the key point of the *pyramid algorithm* visualized in Fig. 5.1 by means of a filter bank scheme.

a) Filter bank of the decomposition process

$$\begin{array}{ccccccccccccc}
\boldsymbol{y} & \rightarrow & \boldsymbol{d}_J & \stackrel{\downarrow}{\rightarrow} & \boldsymbol{d}_{J-1} & \stackrel{\downarrow}{\rightarrow} & \cdots & \stackrel{\downarrow}{\rightarrow} & \boldsymbol{d}_{j+1} & \stackrel{\downarrow}{\rightarrow} & \boldsymbol{d}_j & \stackrel{\downarrow}{\rightarrow} \cdots \stackrel{\downarrow}{\rightarrow} & \boldsymbol{d}_{j'} \\
 & & \downarrow & & \downarrow & & & & \downarrow & & \downarrow & & & \downarrow \\
 & & \boldsymbol{c}_J & & \boldsymbol{c}_{J-1} & & & & \boldsymbol{c}_{j+1} & & \boldsymbol{c}_j & & & \boldsymbol{c}_{j'}
\end{array}$$

b) Filter bank of the reconstruction process

$$\begin{array}{ccccccccccccc}
\boldsymbol{c}_J & & \boldsymbol{c}_{J-1} & & & & & & \boldsymbol{c}_{j+1} & & \boldsymbol{c}_j & & & & \boldsymbol{c}_{j'} \\
\downarrow & & \downarrow & & & & & & \downarrow & & \downarrow & & & & \downarrow \\
\boldsymbol{g}_J & + & \boldsymbol{g}_{J-1} & + & \cdots & + & & + & \boldsymbol{g}_{j+1} & + & \boldsymbol{g}_j & + & \cdots & + & \boldsymbol{g}_{j'}
\end{array}$$

Figure 5.1: Filter banks of the multi-resolution representation using wavelets. '$\stackrel{\downarrow}{\rightarrow}$' means a symbol for downsampling, e.g., from level $j+1$ to level j by a factor N_{j+1}/N_j.

For the derivation of the matrix $\boldsymbol{P}_j$ we start from the Eqs. (5.20) and (5.21), set $J =: j$ and obtain

$$\begin{aligned}\big(\, \Theta_{j+1} \star U \,\big)_w(\boldsymbol{x}_p) &= \boldsymbol{\theta}_{j+1}(\boldsymbol{x}_p)^T\, \boldsymbol{d}_j \\ &=: \boldsymbol{\theta}^T_{j+1;\,p;N_j}\, \boldsymbol{d}_j \ . \end{aligned} \tag{5.59}$$

Recall, that the $N_j \times 1$ scaling vector $\boldsymbol{\theta}_{j+1}(\boldsymbol{x}_p) =: \boldsymbol{\theta}_{j+1;\,p;N_j}$ is computed by the level$-(j+1)$ kernel function Θ_{j+1} and related to the admissible point system $S_{N_j}(\mathbb{E}^2_{a,b})$ defined in Eq. (5.27). Due to the condition (5.37) it follows in addition

$$\begin{aligned}\big(\, \Theta_{j+1} \star U \,\big)_w(\boldsymbol{x}_p) &= \boldsymbol{\theta}_{j+1}(\boldsymbol{x}_p)^T\, \boldsymbol{d}_{j+1} \\ &=: \boldsymbol{\theta}^T_{j+1;\,p;N_{j+1}}\, \boldsymbol{d}_{j+1} \ . \end{aligned} \tag{5.60}$$

The $N_{j+1} \times 1$ vector $\boldsymbol{\theta}_{j+1}(\boldsymbol{x}_p) =: \boldsymbol{\theta}_{j+1;\,p;N_{j+1}}$ is in fact also computed by the level$-(j+1)$ kernel function Θ_{j+1}, but in opposite to Eq. (5.59) related to the admissible point system $S_{N_{j+1}}(\mathbb{E}^2_{a,b})$. Equating the right-hand sides of the Eqs. (5.59) and (5.60) therefore yields

$$\boldsymbol{\theta}^T_{j+1;\,p;N_j}\, \boldsymbol{d}_j = \boldsymbol{\theta}^T_{j+1;\,p;N_{j+1}}\, \boldsymbol{d}_{j+1} \ . \tag{5.61}$$

Note, that due to condition (5.37) the level$-(j+1)$ kernel function Θ_{j+1} can be replaced by the reproducing kernel K^e_{rep} of the space $\mathrm{Harm}_{0,\ldots,n'_{j+1}}(\overline{\mathbb{E}}^{2,\mathrm{ext}}_{a,b})$ as defined in Eq. (5.8).

Next, we identify the vector $\boldsymbol{x}_p$ with $\boldsymbol{x}_p \in \overline{\mathbb{E}}^{2,\mathrm{ext}}_{a,b}$ one after another with the elements of the admissible point system $S_{N_j}(\mathbb{E}^2_{a,b})$. Hence, we obtain the linear equation system

$$\begin{aligned}&\big[\, \boldsymbol{\theta}_{j+1;1;N_j},\, \boldsymbol{\theta}_{j+1;2;N_j},\, \ldots,\, \boldsymbol{\theta}_{j+1;N_j;N_j} \,\big]^T\, \boldsymbol{d}_j \\ &\qquad = \big[\, \boldsymbol{\theta}_{j+1;1;N_{j+1}},\, \boldsymbol{\theta}_{j+1;2;N_{j+1}},\, \ldots,\, \boldsymbol{\theta}_{j+1;N_j;N_{j+1}} \,\big]^T\, \boldsymbol{d}_{j+1} \ , \end{aligned} \tag{5.62}$$

which can be rewritten as

$$\boldsymbol{A}_j\, \boldsymbol{d}_j = \boldsymbol{B}_{j+1}\, \boldsymbol{d}_{j+1} \tag{5.63}$$

by introducing the $N_j \times N_j$ matrix

$$\boldsymbol{A}_j = \big[\, \boldsymbol{\theta}_{j+1;1;N_j},\, \boldsymbol{\theta}_{j+1;2;N_j},\, \ldots,\, \boldsymbol{\theta}_{j+1;N_j;N_j} \,\big]^T \tag{5.64}$$

with rank $\boldsymbol{A}_j = \overline{n}_{j+1} = 2^{2j+2}$ and the $N_j \times N_{j+1}$ matrix

$$\boldsymbol{B}_{j+1} = \big[\, \boldsymbol{\theta}_{j+1;1;N_{j+1}},\, \boldsymbol{\theta}_{j+1;2;N_{j+1}},\, \ldots,\, \boldsymbol{\theta}_{j+1;N_j;N_{j+1}} \,\big]^T \ . \tag{5.65}$$

Hence, the left-hand side multiplication of Eq. (5.63) with the matrix $\boldsymbol{A}^T_j$, i.e.

$$\boldsymbol{A}^T_j\, \boldsymbol{A}_j\, \boldsymbol{d}_j = \boldsymbol{A}^T_j\, \boldsymbol{B}_{j+1}\, \boldsymbol{d}_{j+1} \ , \tag{5.66}$$

yields a solution

$$\boldsymbol{d}_j = (\boldsymbol{A}_j^T \boldsymbol{A}_j)_{\mathrm{rs}}^{-} \, \boldsymbol{A}_j^T \boldsymbol{B}_{j+1} \, \boldsymbol{d}_{j+1} \; , \tag{5.67}$$

wherein $(\boldsymbol{A}_j^T \boldsymbol{A}_j)_{\mathrm{rs}}^{-}$ means a symmetrical reflexive generalized inverse of the matrix $\boldsymbol{A}_j^T \boldsymbol{A}_j$. The comparison of the result (5.67) with Eq. (5.57) defines the low-pass filter matrix $\boldsymbol{P}_j$ as

$$\boldsymbol{P}_j := (\boldsymbol{A}_j^T \boldsymbol{A}_j)_{\mathrm{rs}}^{-} \, \boldsymbol{A}_j^T \boldsymbol{B}_{j+1} \; . \tag{5.68}$$

Note, that this result is not unique, because any generalized inverse $(\boldsymbol{A}_j^T \boldsymbol{A}_j)^{-}$ would solve the linear system (5.66) for the coefficient vector $\boldsymbol{d}_j$ (Koch 1999). For numerical investigations we may use the pseudoinverse $(\boldsymbol{A}_j^T \boldsymbol{A}_j)^{+}$, which is unique. In order to avoid the matrix calculations derived before other strategies can be applied to compute the transformation (5.57) of the scaling coefficients; see e.g. Freeden (1999) and Schmidt et al. (2007a).

Due to the condition (5.37) Eq. (5.59) can be rewritten as $\left(\, \Theta_{j+1} \star U \, \right)_w (\boldsymbol{x}_p) =: \boldsymbol{\theta}_{j+1;\,p;N_J}^T \, \boldsymbol{d}_J$, i.e. the convolution is computed by the scaling coefficient vector $\boldsymbol{d}_J$ of highest resolution level J. Thus, the low-pass filter matrix $\boldsymbol{P}_{j;J}$, introduced in Eq. (5.57), can be computed directly by solving the linear equation system $\boldsymbol{A}_j \, \boldsymbol{d}_j = \boldsymbol{B}_J \, \boldsymbol{d}_J$ with the $N_j \times N_J$ matrix

$$\boldsymbol{B}_J = \left[\, \boldsymbol{\theta}_{J;1;N_J}, \; \boldsymbol{\theta}_{J;2;N_J}, \; \ldots, \; \boldsymbol{\theta}_{J;N_J;N_{J+1}} \, \right]^T \; . \tag{5.69}$$

analog to the procedure described before. Instead of the solution (5.68) we obtain $\boldsymbol{P}_{j,J} := (\boldsymbol{A}_j^T \boldsymbol{A}_j)_{\mathrm{rs}}^{-} \, \boldsymbol{A}_j^T \boldsymbol{B}_J$. A construction of $\boldsymbol{P}_{j;J}$ by evaluating the matrix products $\boldsymbol{P}_j \, \boldsymbol{P}_{j+1} \, \ldots \, \boldsymbol{P}_{J-1}$ according to Eq. (5.57) is therefore not necessary.

The $N_j \times N_j$ band-pass filter matrix $\boldsymbol{Q}_j$, defined in Eq. (5.58), follows from Eq. (5.38) and reads

$$\boldsymbol{Q}_j = \left[\, \boldsymbol{\psi}_{j;1}, \; \boldsymbol{\psi}_{j;2}, \; \ldots, \; \boldsymbol{\psi}_{j;N_j} \, \right]^T \tag{5.70}$$

with $\boldsymbol{\psi}_j(\boldsymbol{x}_p) =: \boldsymbol{\psi}_{j;\,p}$ and $p = 1, \ldots, N_j$.

The different steps of the decomposition process are illustrated in the top part of the filter bank scheme shown in Fig. 5.1. Since all computations are performed by linear equation systems the *law of error propagation* can be applied easily in order to calculate the corresponding covariance matrices; e.g. the covariance matrix $D(\boldsymbol{c}_j)$ of the level$-j$ wavelet coefficient vector $\boldsymbol{c}_j$ reads under the consideration of the right-hand side of Eq. (5.57)

$$\begin{aligned} D(\boldsymbol{c}_j) &= \boldsymbol{Q}_j \, D(\boldsymbol{d}_j) \, \boldsymbol{Q}_j^T \\ &= \boldsymbol{Q}_j \, \boldsymbol{P}_{j,J} \, D(\boldsymbol{d}_J) \, \boldsymbol{P}_{j,J}^T \, \boldsymbol{Q}_j^T \; . \end{aligned} \tag{5.71}$$

That way, tests of hypothesis can be applied in order to check the wavelet coefficients for significance. This procedure means a kind of *data compression* based on statistics.

5.2.3 Reconstruction Step

In the reconstruction step we start from the wavelet coefficient vector $\boldsymbol{c}_j$ of level $j \in \{j', \ldots, J\}$ and compute in accordance with Eq. (5.43) the $M \times 1$ *level-j detail signal vector* $\boldsymbol{g}_j$ from the matrix equation

$$\boldsymbol{g}_j = \boldsymbol{K}_j \, \boldsymbol{c}_j \; . \tag{5.72}$$

Herein the $M \times N_j$ matrix $\boldsymbol{K}_j$ works as a *band-pass filter* and has to be computed from the dual ellipsoidal wavelet function $\widetilde{\Psi}_j$ as will be demonstrated in the following. The elements $g_j(\boldsymbol{x}_q)$ of the vector $\boldsymbol{g}_j$ are related to the points $P(\boldsymbol{x}_q)$ with $\boldsymbol{x}_q \in \overline{\mathbb{E}}_{a,b}^{2,\mathrm{ext}}$ and $q = 1, \ldots, M$. According to Eq. (5.41) the multi-resolution representation reads

$$\boldsymbol{f} = \boldsymbol{f}_{j'} + \sum_{j=j'}^{J} \boldsymbol{g}_j \; , \tag{5.73}$$

wherein $\boldsymbol{f}$ means the $M \times 1$ vector of *filtered* or *predicted* signal values $f(\boldsymbol{x}_q)$ not necessarily being the geopotential values $U(\boldsymbol{x}_q)$. Since these values might also be functionals of U we keep in the following the letter f. Thus, the components of the vector $\boldsymbol{f}_{j'} = (f_{j'}(\boldsymbol{x}_q))$ are calculated from

$$f_{j'}(\boldsymbol{x}_q) = \boldsymbol{\theta}_{j'}(\boldsymbol{x}_q)^T \, \boldsymbol{d}_{j'} \tag{5.74}$$

according to Eq. (5.59) and mean the level$-j'$ approximation of the signal values $f(\boldsymbol{x}_q)$. The $N_{j'} \times 1$ vector $\boldsymbol{\theta}_{j'}(\boldsymbol{x}_q)$ is given by Eq. (5.23) replacing $J+1$ by j'.

In order to compute the $M \times N_i$ matrix $\boldsymbol{K}_j$, defined in Eq. (5.72), we subsitute the $N_j \times 1$ wavelet coefficient vector $\boldsymbol{c}_j$ for the $N \times 1$ observation vector $\mathbf{y}$ on the left-hand side of the linear model (5.50). Thus, it follows with $\boldsymbol{d}_j =: \boldsymbol{t}_j$ and $\boldsymbol{e} = \mathbf{0}$

$$\boldsymbol{c}_j = \boldsymbol{A}_j \, \boldsymbol{t}_j \; , \tag{5.75}$$

wherein the $N_j \times N_j$ matrix

$$\boldsymbol{A}_j = \left[\, \boldsymbol{\theta}_{j+1;\,1}, \; \boldsymbol{\theta}_{j+1;\,2}, \; \ldots, \; \boldsymbol{\theta}_{j+1;\,N_j} \, \right]^T \tag{5.76}$$

with $\operatorname{rank} \boldsymbol{A}_j = \overline{n}_{j+1}$ is defined analogously to Eq. (5.49). Recall that $\overline{n}_{j+1} = (n'_{j+1}+1)^2 = 2^{2j+2}$ holds. Equation (5.75) can be solved by

$$\boldsymbol{t}_j = (\boldsymbol{A}_j^T \boldsymbol{A}_j)_{\mathrm{rs}}^{-} \, \boldsymbol{A}_j^T \, \boldsymbol{c}_j \; , \tag{5.77}$$

wherein $(\boldsymbol{A}_j^T \boldsymbol{A}_j)_{\mathrm{rs}}^{-}$ means a symmetrical reflexive generalized inverse of the matrix $\boldsymbol{A}_j^T \boldsymbol{A}_j$.

Analog to the matrix $\boldsymbol{Q}_j$, defined in Eq. (5.70), we introduce the $M \times N_i$ matrix

$$\widetilde{\boldsymbol{Q}}_j = \left[\, \widetilde{\boldsymbol{\psi}}_{j;1}, \; \widetilde{\boldsymbol{\psi}}_{j;2}, \; \ldots, \; \widetilde{\boldsymbol{\psi}}_{j;M} \, \right]^T \; . \tag{5.78}$$

The M vectors $\widetilde{\boldsymbol{\psi}}_j(\boldsymbol{x}_q) =: \widetilde{\boldsymbol{\psi}}_{j;\,q}$ with $q = 1, \ldots, M$ are assembled by the dual ellipsoidal wavelet function values $\widetilde{\psi}_j(\boldsymbol{x}_q, \boldsymbol{x}_k^j)$ with $\boldsymbol{x}_k^j \in S_{N_j}(\mathbb{E}_{a,b}^2)$. Due to the condition (5.37) we substitute $\widetilde{\boldsymbol{Q}}_j$ for $\boldsymbol{A}_j$ in Eq. (5.75) and obtain with the result (5.77)

$$\boldsymbol{g}_j = \widetilde{\boldsymbol{Q}}_j\, \boldsymbol{t}_j = \widetilde{\boldsymbol{Q}}_j\, (\boldsymbol{A}_j^T \boldsymbol{A}_j)_{\mathrm{rs}}^{-}\, \boldsymbol{A}_j^T\, \boldsymbol{c}_j\ . \tag{5.79}$$

The comparison of the Eqs. (5.72) and (5.79) defines the matrix $\boldsymbol{K}_j$ as

$$\boldsymbol{K}_j := \widetilde{\boldsymbol{Q}}_j\, (\boldsymbol{A}_j^T \boldsymbol{A}_j)_{\mathrm{rs}}^{-}\, \boldsymbol{A}_j^T\ . \tag{5.80}$$

As in Eq. (5.68) we may substitute the pseudoinverse $(\boldsymbol{A}_j^T \boldsymbol{A}_j)^+$ in Eq. (5.80) for the symmetrical reflexive generalized inverse $(\boldsymbol{A}_j^T \boldsymbol{A}_j)_{\mathrm{rs}}^{-}$ for numerical computations.

The covariance matrix $D(\boldsymbol{g}_j)$ of the detail signal vector $\boldsymbol{g}_j$ follows from Eq. (5.72) under the consideration of Eq. (5.71) by applying the law of error propagation, i.e.

$$\begin{aligned} D(\boldsymbol{g}_j) &= \boldsymbol{K}_j\, D(\boldsymbol{c}_j)\, \boldsymbol{K}_j^T \\ &= \boldsymbol{K}_j\, \boldsymbol{Q}_j\, \boldsymbol{P}_{j,J}\, D(\boldsymbol{d}_J)\, \boldsymbol{P}_{j,J}^T\, \boldsymbol{Q}_j^T\, \boldsymbol{K}_j^T\ . \end{aligned} \tag{5.81}$$

The generalization of this result gives the covariance matrix

$$C(\boldsymbol{g}_j, \boldsymbol{g}_k) = \boldsymbol{K}_j\, \boldsymbol{Q}_j\, \boldsymbol{P}_{j,J}\, D(\boldsymbol{d}_J)\, \boldsymbol{P}_{k,J}^T\, \boldsymbol{Q}_k^T\, \boldsymbol{K}_k^T \tag{5.82}$$

between two detail signal vectors $\boldsymbol{g}_j$ and $\boldsymbol{g}_k$ with $j, k = j', \ldots, J$.

As in the decomposition case the different steps of the reconstruction process (Eqs. (5.72) and (5.73)) can be illustrated by a *synthesis filter bank* as shown in Fig. 4-3b.

In the decomposition process, Eq. (5.57), $\boldsymbol{P}_{J-1}$ is the low-pass filter matrix of largest size, namely $N_{J-1} \times N_J$. According to Eq. (5.68) the application of $\boldsymbol{P}_{J-1}$ requires the computation of the symmetrical reflexive generalized inverse $(\boldsymbol{A}_{J-1}^T \boldsymbol{A}_{J-1})_{\mathrm{rs}}^{-}$ or any other generalized inverse. In the reconstruction process, however, the matrix $\boldsymbol{K}_J$ of highest level J is of size $M \times N_J$ with $N_J > N_{J-1}$. As can be seen from Eq. (5.80) we have to compute the symmetrical reflexive generalized inverse $(\boldsymbol{A}_J^T \boldsymbol{A}_J)_{\mathrm{rs}}^{-}$ or any other generalized inverse of size $N_J \times N_J$. Thus, the reconstruction needs more computational efforts and storage space than the decomposition. In order to avoid the calculation of $(\boldsymbol{A}_J^T \mathbf{A}_J)_{\mathrm{rs}}^{-}$, but to perform the multi-resolution representation (5.73) we may prefer the ellipsoidal multi-resolution representation of the first kind as explained in subsection 3.2.2.

In the latter case we replace Eq. (5.72) by

$$\boldsymbol{g}_j = \boldsymbol{L}_j\, \boldsymbol{d}_j \tag{5.83}$$

with $j = j', \ldots, J$. The $M \times N_j$ matrix $\boldsymbol{L}_j$ works as a *band-pass filter* and is computed according to Eq. (3.44) by the ellipsoidal wavelet function $\Psi_j(\boldsymbol{x}_q, \boldsymbol{x}_k^j)$ with $\boldsymbol{x}_k^j \in S_{N_j}(\mathbb{E}_{a,b}^2)$ and $q = 1, \ldots, M$. To be more specific we obtain analogously to Eq. (5.70)

$$\boldsymbol{L}_j = \left[\ \boldsymbol{\psi}_{j;1},\ \boldsymbol{\psi}_{j;2},\ \ldots,\ \boldsymbol{\psi}_{j;M}\ \right]^T \tag{5.84}$$

with $\boldsymbol{\psi}_j(\boldsymbol{x}_q) =: \boldsymbol{\psi}_{j;\,q}$ and $q = 1, \ldots, M$. The covariance matrix (5.82) reads now

$$C(\boldsymbol{g}_j, \boldsymbol{g}_k) = \boldsymbol{L}_j \; \boldsymbol{P}_{j,J} \; D(\boldsymbol{d}_J) \; \boldsymbol{P}_{k,J}^T \; \boldsymbol{L}_k^T \; . \tag{5.85}$$

The main advantage of this second approach is the efficient computation of the detail signal vectors. On the other hand the analysis step is reduced to the computation of the vectors $\boldsymbol{d}_j$ of scaling coefficients according to the Eq. (5.57). *Data compression techniques* are usually applied to wavelet coefficients, because these quantities express the band-pass behavior of the data with respect to the spatial position. Since the scaling coefficients reflect the corresponding low-pass behavior, data compression techniques applied to these values will not be as effective than in the case of wavelet coefficients.

5.3 Numerical Example

The concept presented in the last subsection shall now be applied to a simulated global data set based on the EGM 96 gravity model. We choose a reference ellipsoid $\mathbb{E}^2_{a_0,b_0}$ with a semi-minor axis $b_0 = 6356.75192$ km and an absolute eccentricity $\epsilon = 521.85358$ km. Hence, the semi-major axis is given as $a_0 = 6378.13657$ km. We first compute disturbing potential values $f(\boldsymbol{x}) =: T(\boldsymbol{x})$ up to degree $n = 63$ from EGM 96 on a standard spherical longitude-latitude grid at satellite altitudes randomly distributed between 450 km and 500 km, i.e. the vector $\boldsymbol{x}$ is defined by Eq. (2.36). Furthermore, we consider additional noise for the disturbing potential values with a prior standard deviation of 0.8 m^2/s^2. Next, we transform the data to a Jacobian ellipsoidal coordinate system, i.e. we solve the components of the vector $\boldsymbol{x}$ as defined in Eq. (2.1) for the spheriodal coordinates λ, ϕ and u; cf. Grafarend et al. (1999). The altogether $P = 12960$ observations $T(\boldsymbol{x}_p)$ with $p = 1, \ldots, P$, shown in Fig. 5.2 neglecting the altitude variations, are collected in the $P \times 1$ observation vector $\boldsymbol{y}$ of the linear model (5.50) and mean the global input signal of the multi-resolution representation. A diagonal weight matrix $\boldsymbol{V}_y = (v_{y;p})$ with purely latitude-dependent elements $v_{y;p} = \cos\phi_p$ was chosen, wherein ϕ_p is the spheroidal latitude of the observation point $P(\boldsymbol{x}_p)$.

In order to construct a multi-resolution representation of the given disturbing potential data based on the Blackman scaling and wavelet functions (cf. Eqs. (3.59) to (3.61)) we set $J = 5$ (see Fig. 3.2) and estimate the vector $\boldsymbol{d}_5 = (d_{5,k})$ from the model (5.50). To be more specific, the coefficients $d_{5,k}$ with $k = 1, \ldots, N_5$ are in this example related to a level-5 *Reuter grid* consisting of $N_5 = 5180$ points $P(\boldsymbol{x}_k^5)$ on the reference ellipsoid $\mathbb{E}^2_{a_0,b_0}$. Figure 5.3 shows, for instance, a level-3 Reuter grid with altogether $N_3 = 317$ points. Note, that Reuter grids are non-hierarchical but equidistributed point systems, i.e. the corresponding integration weights are independent on the position. The $P \times N_5$ coefficient matrix $\boldsymbol{A}_5$, defined in Eq. (5.49) is of rank $\overline{n}_6 = 4096$, i.e. a rank deficiency of $r = N_5 - \overline{n}_6 = 184$ exists.

Figure 5.4 displays exemplarily the estimated level-5 wavelet coefficients $\widehat{c}_{5,k}$ collected in the $N_5 \times 1$ vector $\widehat{\boldsymbol{c}}_5$ computed by Eq. (5.58). The related estimated covariance matrix is calculated from Eq.

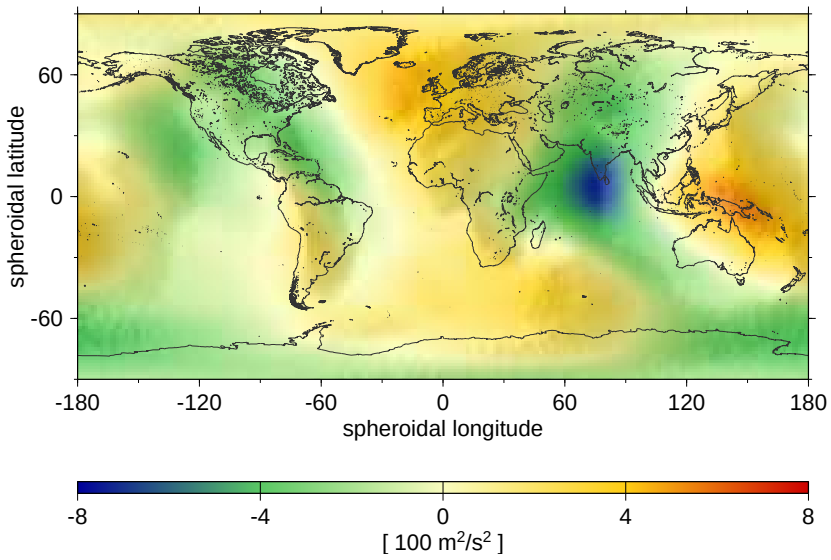

Figure 5.2: Observed disturbing potential data in $P = 12960$ grid points $P(\boldsymbol{x}_p)$ with $p = 1, \ldots, P$ at satellite altitude. Note, that due to the reason of visualization the altitude variations are neglected in this figure.

(5.71) after replacing the variance factor σ_y^2 by its estimation

$$\widehat{\sigma}_y^2 = \frac{\widehat{\boldsymbol{e}}^T \, \boldsymbol{P}_y \, \widehat{\boldsymbol{e}}}{P - \overline{n}_6} \,, \tag{5.86}$$

wherein

$$\widehat{\boldsymbol{e}} = \boldsymbol{A}_5 \, \widehat{\boldsymbol{d}}_5 - \boldsymbol{y} \tag{5.87}$$

means the $P \times 1$ vector of the residuals.

The histogram in Fig. 5.5 depicts clearly that a large number of level-5 wavelet coefficients is numerically close to zero. A test of significance proved that $n_5 = 3001$ coefficients are statistically negligible. The data compression rate

$$\kappa_j = n_j / N_j \tag{5.88}$$

of level j amounts for $j = 5$ therefore $\kappa_5 = 58\,\%$. These results and the corresponding values for the other levels j are listed in Table 5.1. Various data compression or wavelet thresholding techniques are treated in detail, e.g., by Ogden (1997).

Fig. 5.6 shows the altogether six detail signals $\widehat{g}_j(\boldsymbol{x})$ according to Eq. (5.72) with $j' = 0$ on the reference ellipsoid $\mathbb{E}^2_{a0,b0}$ as the building blocks of the multi-resolution representation of the input signal shown in Fig. 5.2. Note, that in this example the points $P(\boldsymbol{x}_q)$, introduced in the context of

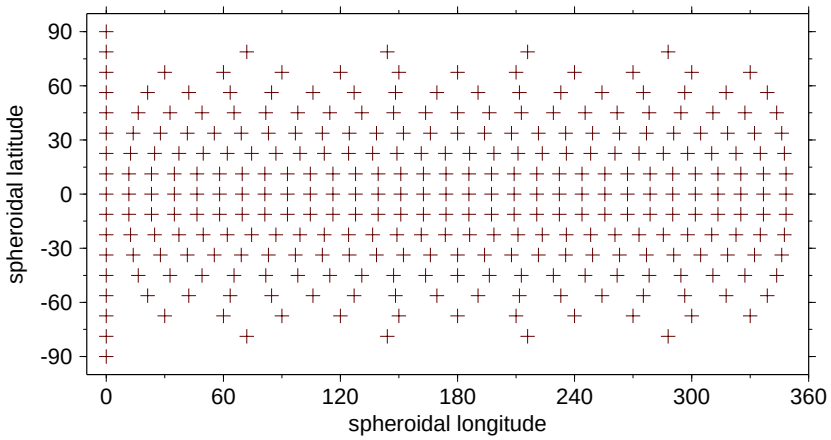

Figure 5.3: Level-3 Reuter grid with $N_3 = 317$ points $P(\boldsymbol{x}_k^3)$ and $k = 1, \ldots, N_3$.

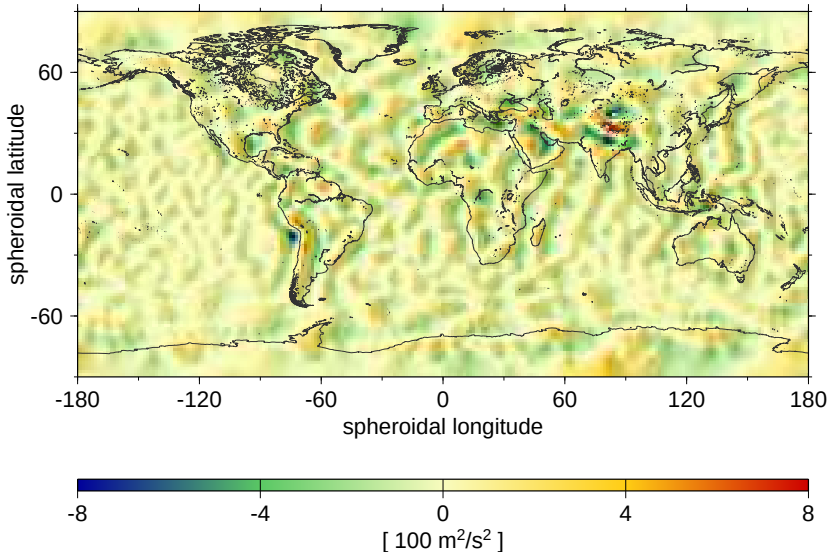

Figure 5.4: Estimated level-5 wavelet coefficients $\widehat{c}_{5,k}$ defined on a level-5 Reuter grid with $k = 1, \ldots, N_5 = 5180$. Note, that these discrete values were interpolated for visualization.

Eq. (5.72), are identified with the observation sites $P(\boldsymbol{x}_p)$, i.e. $M = N = 12960$. Whereas Table 5.1 shows some statistics for the wavelet coefficients Table 5.2 presents the corresponding values for the detail signals. The estimated standard deviations $\widehat{\sigma}(\widehat{g}_{j,k})$ are computed from the diagonal elements of the covariance matrix (5.81) substituting again the estimation $\widehat{\sigma}_y^2$ for the variance factor σ_y^2.

As can be seen from Eq. (5.73) the sum of the six detail signal vectors $\boldsymbol{g}_j$ of the levels $j = 0, \ldots, 5$ yields an approximation of the disturbing potential on the reference ellipsoid $\mathbb{E}_{a_0,b_0}^2$, since the vector

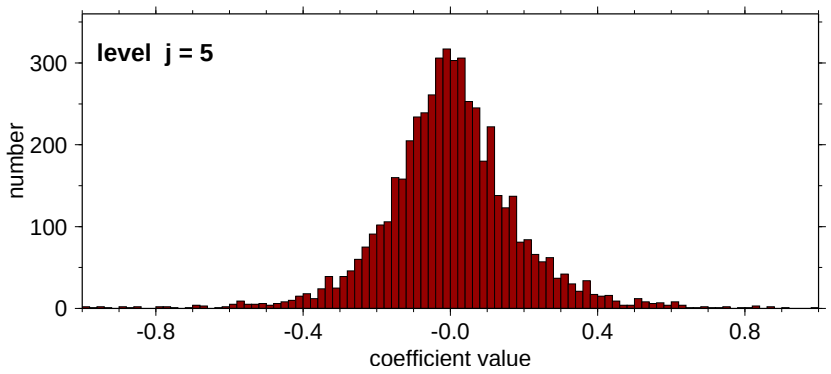

Figure 5.5: Histogram of the estimated level-5 wavelet coefficients $\widehat{c}_{5,k}$. Almost $60\,\%$ of them are statistically non-significant.

level j	N_j	$\widehat{\sigma}(\widehat{c}_{j,k})$	n_j	κ_j [%]
5	5180	0.035 – 0.043	3001	58
4	1290	$\approx$ 0.0049	45	4
3	317	$\approx$ 0.0013	0	0
2	77	$\approx$ 0.0005	0	0
1	20	$\approx$ 0.0002	0	0
0	6	$\approx$ 0.0002	6	100

Table 5.1: Numbers N_j of wavelet coefficients $c_{j,k}$ of the levels $j = 0, \ldots, 5$, estimated standard deviations $\widehat{\sigma}(\widehat{c}_{j,k})$ and results for the test of significance; $n_j =$ number of non-significant coefficients, $\kappa_j =$ data compression rate.

$\widehat{\boldsymbol{f}}_0$ reduces to

$$\widehat{\boldsymbol{f}}_0 = \widehat{\mu}_y \, \mathbf{1} \ , \tag{5.89}$$

wherein $\widehat{\mu}_y$ means the estimator of the mean value of the observations over the ellipsoid and $\mathbf{1} = [\,1,\,1,\,\ldots,\,1\,]^T$ denotes an $M \times 1$ vector. Figure 5.7 shows the elements of the $M \times 1$ vector $\widehat{\mathbf{f}}$ as the output signal of the multi-resolution representation. Note, that these results consider all coefficients, even those which were downgraded as non-significant by the statistical test mentioned before.

level j	M	$\widehat{\sigma}(\widehat{g}_{j,k})$	n_j	κ_j [%]
5	12960	2.61 – 3.00	6306	49
4	12960	$\approx$ 0.39	421	4
3	12960	$\approx$ 0.11	41	0.4
2	12960	$\approx$ 0.04	4	0.03
1	12960	$\approx$ 0.02	5	0.04
0	12960	$\approx$ 0.02	12960	100

Table 5.2: Numbers of detail signal values $g_{j,q}$ of the levels $j = 0, \ldots, 5$, estimated standard deviations $\widehat{\sigma}(\widehat{g}_{j,q})$ in $[m^2/s^2]$ and results for the test of significance; n_j = number of non-significant values, κ_j = data compression rate.

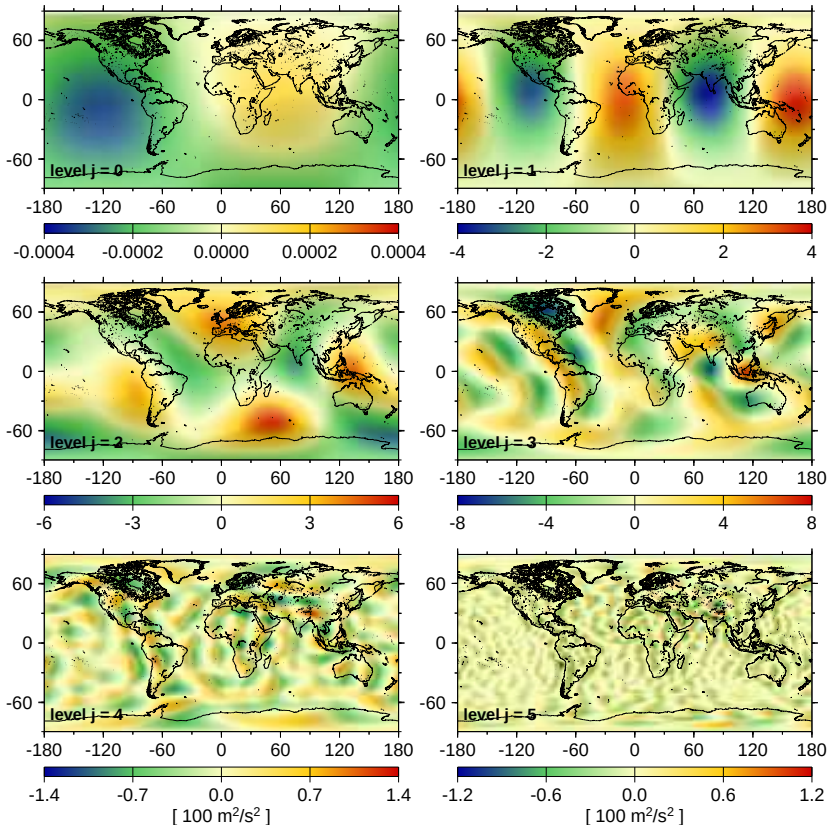

Figure 5.6: Detail signals $\mathbf{g}_j$ of levels $j = 0, \ldots, 5$ at the Earth's surface. The higher the level value the finer the structures of the details. Each detail signal means a band-pass filtered version of the input signal shown in Fig. 5.2.

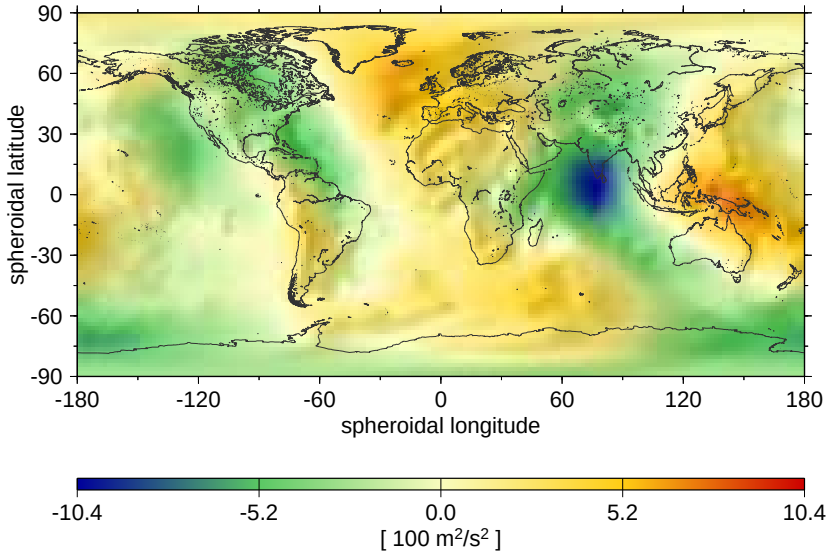

Figure 5.7: Disturbing potential values $\widehat{\boldsymbol{f}}(\boldsymbol{x}_q)$ at the Earth's surface in points $P(\boldsymbol{x}_q)$ with $q = 1, \ldots, M = N$, collected in the $M \times 1$ output signal vector $\widehat{\boldsymbol{f}}$.

Chapter 6

Multi-Resolution Representation of Spatio-Temporal Signals

Mass redistributions within and between various components of the Earth system cause temporal variations of the Earth's gravity field which have been continuously observed by the GRACE satellite mission since April 2002. As mentioned before in satellite gravity recovery problems the global gravity field of the Earth is traditionally modeled as a spherical harmonic expansion. Furthermore, spatio-temporal gravity fields from GRACE are usually computed for fixed time intervals, like one month or one week; see e.g. Tapley et al. (2004).

6.1 Tensor Product Approach

As described in the previous sections the multi-resolution representation based on ellipsoidal scaling and wavelet functions means an appropriate method for modeling the spatial structures of the Earth's gravity field. For considering the temporal variations of the gravity field within the multi-resolution representation we rewrite Eq. (5.41) as

$$f(\boldsymbol{x},t) = f_{j'}(\boldsymbol{x},t) + \sum_{j=j'}^{J} g_j(\boldsymbol{x},t) \qquad \text{with} \qquad j' \in \mathbb{N}_0 \tag{6.1}$$

wherein t means the time. According to Eq. (3.25) each level$-j$ detail signal is computable from

$$g_j(\boldsymbol{x},t) = \left(\widetilde{\Psi}_j \star c_j(\,\cdot\,,t) \right)_w(\boldsymbol{x}) \tag{6.2}$$

by means of the level$-j$ wavelet coefficients

$$c_j(\boldsymbol{x},t) = \left(\Psi_j \star f(\,\cdot\,,t) \right)_w(\boldsymbol{x}) \tag{6.3}$$

From the Eqs. (6.2) and (6.3) in combination with the Figures 3.1 and 3.2 we expect that different detail signals would be more sensitive to particular input signals $f(\boldsymbol{x}, t)$ in dependence on their spectral behavior and noise characteristics. Schmidt et al. (2006) constructed a procedure to establish a spatio-temporal multi-resolution representation based on this expectation; see also Prijatna and Haagmans (2001) and Haagmans et al. (2002). To be more specific, we rewrite Eq. (5.38) as

$$c_j(\boldsymbol{x}, t) = \boldsymbol{\psi}_j(\boldsymbol{x})^T \, \boldsymbol{d}_j(t) \tag{6.4}$$

and model each component $d_{j,k}(t)$ of the $N_j \times 1$ vector $\boldsymbol{d}_j(t)$ as an expansion

$$d_{j,k}(t) = \sum_{l=0}^{K_j-1} d_{j,k;l} \; \phi_{j,l}(t) \tag{6.5}$$

in terms of time-dependent base functions $\phi_{j,l}(t)$ with unknown spatio-temporal (4-D) scaling coefficients $d_{j,k;l}$; $k = 1, \ldots, N_j$; $l = 0, \ldots, K_j - 1$. Introducing the $K_j \times 1$ vector

$$\boldsymbol{\phi}_j(t) = \left[\; \phi_{j,0}(t), \; \phi_{j,1}(t), \; \ldots, \; \phi_{j,K_j-1}(t) \; \right]^T \tag{6.6}$$

and the $N_j \times K_j$ matrix

$$\boldsymbol{D}_j = \begin{bmatrix} d_{j,1;0} & d_{j,1;1} & \ldots & d_{j,1;K_j-1} \\ d_{j,2;0} & d_{j,2;1} & \ldots & d_{j,2;K_j-1} \\ \ldots\ldots\ldots\ldots\ldots\ldots\ldots\ldots \\ d_{j,N_j;0} & d_{j,N_j;1} & \ldots & d_{j,N_j;K_j-1} \end{bmatrix} \tag{6.7}$$

of the spatio-temporal coefficients $d_{j,k;l}$ we obtain

$$\boldsymbol{d}_j(t) = \boldsymbol{D}_j \, \boldsymbol{\phi}_j(t) \tag{6.8}$$

from Eq. (6.5). Inserting Eq. (6.8) into Eq. (6.4) yields the *tensor product approach*

$$\begin{aligned} c_j(\boldsymbol{x}, t) &= \boldsymbol{\psi}_j^T(\boldsymbol{x}) \; \boldsymbol{D}_j \; \boldsymbol{\phi}_j(t) \\ &= (\boldsymbol{\phi}_j^T(t) \otimes \boldsymbol{\psi}_j^T(\boldsymbol{x})) \; \mathrm{vec}\boldsymbol{D}_j \; ; \end{aligned} \tag{6.9}$$

a short introduction into tensor products of Hilbert spaces is given by Weidmann (1976). In Eq. (6.9) we applied computation rules for the Kronecker product symbolized by '$\otimes$' (Koch, 1999); in addition the vec$-$operator orders the columns of a matrix one below the other as a vector. The matrix $\boldsymbol{D}_j$ is estimated by means of the observation equation

$$\begin{aligned} y(\boldsymbol{x}, t) + e(\boldsymbol{x}, t) &= \boldsymbol{\theta}_{j+1}^T(\boldsymbol{x}) \, \boldsymbol{d}_j(t) \\ &= (\boldsymbol{\phi}_j^T(t) \otimes \boldsymbol{\theta}_{j+1}^T(\boldsymbol{x})) \; \mathrm{vec}\boldsymbol{D}_j \end{aligned} \tag{6.10}$$

following from Eq. (5.46) for $\boldsymbol{x}_p = \boldsymbol{x}$.

Schmidt et al. (2006) use (resolution) level-dependent piecewise constant functions, i.e., the spatio-temporal coefficients are estimated for specific level$-j$-dependent time intervals such as one month (for the finer structures) or ten days (for the coarser structures). To be more specific, the total observation interval ΔT is divided into K_j non-overlapping level-dependent observation sub-intervals

$$\Delta T_{j,k_j} = [t_{j,k_j}, t_{j,k_j+1}) \tag{6.11}$$

of constant length, i.e. $t_{j,k_j+1} - t_{j,k_j} = \Delta T_j$ for $k_j = 0, \ldots, K_j - 1$. Thus, it follows

$$\Delta T = K_j \, \Delta T_j \ . \tag{6.12}$$

The motivation for this partitioning scheme is that the determination of finer structures of the gravity field requires a denser distribution of satellite observations than the computation of coarser structures. By introducing the stepwise functions $\phi_{j,k_j}(t) = \chi_{j,k_j}(t)$ defined as

$$\chi_{j,k_j}(t) = \left\{ \begin{array}{ll} 1 & \text{if} \quad t \in \Delta T_{j,k_j} \\ 0 & \text{otherwise} \end{array} \right\} \tag{6.13}$$

Eq. (6.5) reads

$$d_{j,k}(t) = \sum_{k_j=0}^{K_j-1} d_{j,k;k_j} \ \chi_{j,k_j}(t) \ . \tag{6.14}$$

Under this assumption for a specific observation time $t = t_n$ the $K_j \times 1$ vector $\boldsymbol{\phi}_j(t)$ as defined in Eq. (6.6) reduces to the unit vector $\boldsymbol{\phi}_j(t_n) = \boldsymbol{e}_n$ with the value '1' at the nth position. Choosing an appropriate ellipsoidal scaling function the spatio-temporal scaling coefficients $d_{j,k;k_j}$ can be estimated from the observations $y(\boldsymbol{x}, t)$ by means of the observation equation (6.10).

In opposite to that approach sketched before Schmidt et al. (2007b) model the time-dependency of each scaling coefficient $d_{J,k}(t)$ of the highest level J by a Fourier series. As disadvantages of this approach the authors mention that a multi-resolution representation with respect to time cannot be considered and the detail signals of different levels are characterized by the same temporal behavior. In order to consider a different temporal behavior for each spatial level j, we now introduce a level-dependent 1-D multi-resolution representation with respect to time for each scaling coefficient $d_{j,k}(t)$ analogously to the approach (6.9). To be more specific, in this 4-D multi-resolution representation approach we distinguish between the spatial level $j \in \{j', \ldots, J\}$ and the temporal level $i_j \in \{i'_j, \ldots, I_j\}$ depending on j. Thus, we expand each time-dependent scaling coefficient $d_{j,k}(t)$ by a series

$$d_{j,k}(t) = \sum_{l=0}^{m_{I_j}-1} d_{j,k;I_j,l} \ \phi_{I_j,l}(t) \tag{6.15}$$

in terms of (temporal) level$-I_j$ scaling functions $\phi_{I_j,l}(t)$ with unknown spatio-temporal (4-D) scaling coefficients $d_{j,k;I_j,l}$; $k = 1, \ldots, N_j$; $l = 0, \ldots, m_{I_j} - 1$.

6.2 B-Spline Modeling

For modeling the temporal behavior of the geopotential we apply *normalized quadratic B-splines* $N^2(\tau)$ as 1-D base functions depending on the real-valued variable τ. Let m_i be a positive integer number, $i \in \{0, \ldots, I\}$ the temporal level and assume further that a sequence of non-decreasing knots $\tau_0^i, \tau_1^i, \ldots, \tau_{m_i+2}^i$ is given, the normalized quadratic B-spline functions are defined recursively with $l = 0, \ldots, m_i - 1$ and $m = 1, 2$ as

$$N_{i,l}^m(\tau) = \frac{\tau - \tau_l^i}{\tau_{l+m}^i - \tau_l^i}\, N_{i,l}^{m-1}(\tau) + \frac{\tau_{l+m+1}^i - \tau}{\tau_{l+m+1}^i - \tau_{l+1}^i}\, N_{i,l+1}^{m-1}(\tau) \tag{6.16}$$

with the initial values

$$N_{i,l}^0(\tau) = \left\{ \begin{array}{ll} 1 & \text{if} \quad \tau_l^i \leq \tau < \tau_{l+1}^i \quad \text{and} \quad \tau_l^i < \tau_{l+1}^i \\ 0 & \text{otherwise} \end{array} \right\}; \tag{6.17}$$

e.g., Stollnitz et al. (1995) or Schmidt (2006). A B-spline is compactly supported, i.e. its values are different from zero only in a finite range on the real axis. Since $N_{i,l}^2(\tau) \neq 0$ for $\tau_l^i \leq \tau < \tau_{l+3}^i$ and $N_{i,l}^2(\tau) = 0$ otherwise, this finite range is defined by the interval $[\tau_l^i, \tau_{l+3}^i)$, mathematically abbreviated as supp$N_{i,l}^2 = [\tau_l^i, \tau_{l+3}^i)$. Since we want to use this approach for the finite time interval ΔT as defined in Eq. (6.12) we introduce the *endpoint-interpolating quadratic B-splines* defined on the unit interval $\mathbb{I} = [0, 1]$; e.g., Lyche and Schumaker (2001), Stollnitz et al. (1995), Schmidt (2006) and Schmidt et al. (2007c). To be more specific, we set the first three knots to zero and the last three knots to one. Hence, the level$-i$ knot sequence for endpoint-interpolating quadratic B-splines reads

$$0 = \tau_0^i = \tau_1^i = \tau_2^i < \tau_3^i < \ldots < \tau_{m_i-1}^i < \tau_{m_i}^i = \tau_{m_i+1}^i = \tau_{m_i+2}^i = 1 \tag{6.18}$$

with $\tau_{l+1}^i - \tau_l^i = 2^{-i}$ for $l = 2, \ldots, m_i - 1$ and $m_i = 2^i + 2$. Note, that in Eq. (6.16) under the assumption (6.18) the factors are taken as zero if their denominators are zero. Since we apply normalized quadratic endpoint-interpolating B-splines (6.16) as scaling functions $\phi_{I_j,l}$, i.e.,

$$\phi_{I_j,l}(\tau) := N_{I_j,l}^2(\tau) \tag{6.19}$$

with $l = 0, \ldots, m_{I_j} - 1$, we actually have to replace the time variable t in Eq. (6.15) by the normalized time variable $\tau = (t - t_0)/\Delta T$; $t_0 =$ initial time epoch. But in order to avoid too much confusion we do not distinguish between the two variables t and τ in the sequel and use always the letter t. Figure 6.1 depicts the $m_{I_j} = 2^{I_j} + 2$ B-spline scaling functions for level $I_j = 3$ with $\tau =: x$.

6.3 4-D Multi-Resolution Representation

Introducing the $m_{I_j} \times 1$ vector

$$\boldsymbol{\phi}_{I_j}(t) = \left[\, \phi_{I_j,0}(t),\ \phi_{I_j,1}(t),\ \ldots,\ \phi_{I_j,m_{I_j}-1}(t) \,\right]^T \tag{6.20}$$

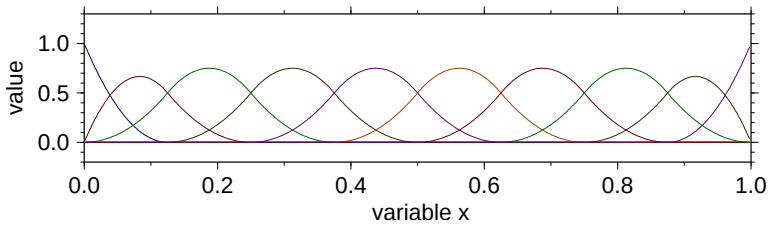

Figure 6.1: B-spline functions $\phi_{I_j,l}$ of resolution level $I_j = 3$ with $l = 0, \ldots, m_3 - 1$ and $m_3 = 2^3 + 2 = 10$. Only the B-spline functions $\phi_{3,l}$ for $l = 2, \ldots, 7$ are not affected by the endpoint interpolating procedure. The other four functions with $l = 0, 1, 8, 9$ are modified by the endpoint-interpolationg procedure. The larger the level value I_j is chosen the more narrow are the B-spline functions; for details see e.g. Schmidt (2006).

and the $N_j \times m_{I_j}$ matrix

$$\boldsymbol{D}_{j;I_j} = \begin{bmatrix} d_{j,1;I_j,0} & d_{j,1;I_j,1} & \ldots & d_{j,1;I_j,m_{I_j}-1} \\ d_{j,2;I_j,0} & d_{j,2;I_j,1} & \ldots & d_{j,2;I_j,m_{I_j}-1} \\ \ldots & \ldots & \ldots & \ldots \\ d_{j,N_j;I_j,0} & d_{j,N_j;I_j,1} & \ldots & d_{j,N_j;I_j,m_{I_j}-1} \end{bmatrix} \tag{6.21}$$

of the spatio-temporal coefficients $d_{j,k;I_j,l}$ we obtain

$$\boldsymbol{d}_j(t) = \boldsymbol{D}_{j;I_j}\, \boldsymbol{\phi}_{I_j}(t) \tag{6.22}$$

from Eq. (6.15). Inserting Eq. (6.22) into Eq. (6.4) yields

$$\begin{aligned} c_j(\boldsymbol{x}, t) &= \boldsymbol{\psi}_j^T(\boldsymbol{x})\, \boldsymbol{D}_{j;I_j}\, \boldsymbol{\phi}_{I_j}(t) \\ &= (\boldsymbol{\phi}_{I_j}^T(t) \otimes \boldsymbol{\psi}_j^T(\boldsymbol{x}))\, \mathrm{vec}\boldsymbol{D}_{j;I_j} \\ &= c_{j;I_j}(\boldsymbol{x}, t)\ . \end{aligned} \tag{6.23}$$

Note, that the quantity $c_{j;I_j}(\boldsymbol{x}, t)$ means the wavelet coefficient on the spatial level j and the temporal level I_j; it will be denoted in the following as level$-(j; I_j)$ wavelet coefficient of the input signal. According to Eq. (6.2) the detail signal $g_j(\boldsymbol{x}, t)$ is computed as

$$\begin{aligned} g_j(\boldsymbol{x}, t) &= \left(\widetilde{\Psi}_j \star c_{j;I_j}(\,\cdot\,, t) \right)_w(\boldsymbol{x}) \\ &= g_{j;I_j}(\boldsymbol{x}, t)\ . \end{aligned} \tag{6.24}$$

With Eq. (3.32) we introduced the decomposition equation with respect to space. The corresponding equation with respect to the time domain reads

$$\boldsymbol{\phi}_{i_j}(t) = \overline{\boldsymbol{P}}_{i_j}^T\, \boldsymbol{\phi}_{i_j-1}(t) + \overline{\boldsymbol{Q}}_{i_j}^T\, \boldsymbol{\psi}_{i_j-1}(t)\ , \tag{6.25}$$

wherein

$$\boldsymbol{\phi}_{i_j-1}(t) = \left[\, \phi_{i_j-1,0}(t),\ \phi_{i_j-1,1}(t),\ \ldots,\ \phi_{i_j-1,m_{i_j-1}-1}(t) \,\right]^T \tag{6.26}$$

is the $m_{i_j-1} \times 1$ vector of level$-(i_j-1)$ scaling functions $\phi_{i_j-1,l}(t)$ with $l = 0, \ldots, m_{i_j-1} - 1$. The $n_{i_j-1} \times 1$ vector

$$\boldsymbol{\psi}_{i_j-1}(t) = \left[\, \psi_{i_j-1,0}(t),\ \psi_{i_j-1,1}(t),\ \ldots,\ \psi_{i_j-1,n_{i_j-1}-1}(t) \,\right]^T \tag{6.27}$$

contains the level$-(i_j-1)$ B-spline wavelet functions $\psi_{i_j-1,l}(t)$ with $l = 0, \ldots, n_{i_j-1} - 1$ and $n_{i_j-1} = m_{i_j} - m_{i_j-1}$. The $m_{i_j-1} \times m_{i_j}$ matrix $\overline{\boldsymbol{P}}_{i_j}$ and the $n_{i_j-1} \times m_{i_j}$ matrix $\overline{\boldsymbol{Q}}_{i_j}$ are computable from

$$\begin{bmatrix} \overline{\boldsymbol{P}}_{i_j} \\ \overline{\boldsymbol{Q}}_{i_j} \end{bmatrix} = \left[\, \boldsymbol{P}_{i_j}\ \boldsymbol{Q}_{i_j} \,\right]^{-1} ; \tag{6.28}$$

the entries of the $m_{i_j} \times m_{i_j-1}$ matrix $\boldsymbol{P}_{i_j}$ and the $m_{i_j} \times n_{i_j-1}$ matrix $\boldsymbol{Q}_{i_j}$ can be taken from Stollnitz et al. (1995). Figure 6.2 shows two selected level-3 B-spline wavelets of the family $\psi_{3,l}$ with $l = 0, \ldots, n_3 - 1$, which are compactly supported, too.

Inserting the two-scale relation (6.25) for $i_j = I_j$ into Eq. (6.23) we obtain the decomposition

$$\begin{aligned} c_{j;I_j}(\boldsymbol{x}, t) &= \boldsymbol{\psi}_j^T(\boldsymbol{x})\ \boldsymbol{D}_{j;I_j-1}\ \boldsymbol{\phi}_{I_j-1}(t) + \boldsymbol{\psi}_j^T(\boldsymbol{x})\ \boldsymbol{W}_{j;I_j-1}\ \boldsymbol{\psi}_{I_j-1}(t) \\ &= c_{j;I_j-1}(\boldsymbol{x}, t) + \overline{c}_{j;I_j-1}(\boldsymbol{x}, t)\ , \end{aligned} \tag{6.29}$$

wherein

$$\boldsymbol{D}_{j;I_j-1} = \boldsymbol{D}_{j;I_j}\ \overline{\boldsymbol{P}}_{I_j}^T \tag{6.30}$$

is the $N_j \times m_{I_j-1}$ matrix of the spatio-temporal scaling coefficients $d_{j,k;I_j-1,l}$ needed to compute the level$-(j; I_j-1)$ approximation $c_{j;I_j-1}(\boldsymbol{x}, t)$ of the level$-(j; I_j)$ wavelet coefficients $c_{j;I_j}(\boldsymbol{x}, t)$; the $N_j \times n_{I_j-1}$ matrix

$$\boldsymbol{W}_{j;I_j-1} = \boldsymbol{D}_{j;I_j}\ \overline{\boldsymbol{Q}}_{I_j}^T \tag{6.31}$$

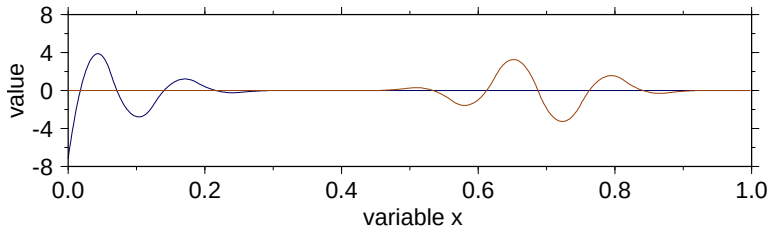

Figure 6.2: Selected wavelets $\psi_{i_j,l}$ of resolution level $i_j = 3$ for $l = 0$ (blue) and $l = 5$ (red) of altogether $n_3 = m_4 - m_3 = 8$ wavelets $\psi_{3,l}(x)$ with $l = 0, \ldots, n_3 - 1$. The wavelet $\psi_{3,0}(x)$ is affected by the endpoint interpolating procedure.

contains the spatio-temporal sub-wavelet coefficients $w_{j,k;I_j-1,l}$ of the level$-(j;I_j-1)$ detail-wavelet coefficients $\overline{c}_{j;I_j-1}(\boldsymbol{x},t)$. The recursive application of this procedure gives finally the temporal (1-D) multi-resolution representation

$$c_{j;I_j}(\boldsymbol{x},t) = c_{j;i'_j}(\boldsymbol{x},t) + \sum_{i_j=i'_j}^{I_j-1} \overline{c}_{j;i_j}(\boldsymbol{x},t) \ . \tag{6.32}$$

of the level$-(j;I_j)$ wavelet coefficients $c_{j;I_j}(\boldsymbol{x},t)$. According to Eq. (6.29) the level$-(j;i_j)$ approximation $c_{j;i_j}(\boldsymbol{x},t)$ and the level$-(j;i_j)$ detail-wavelet coefficients $\overline{c}_{j;i_j}(\boldsymbol{x},t)$ are defined as

$$c_{j;i_j}(\boldsymbol{x},t) = \boldsymbol{\psi}_j^T(\boldsymbol{x}) \ \boldsymbol{D}_{j;i_j} \ \boldsymbol{\phi}_{i_j}(t) \ , \tag{6.33}$$

$$\overline{c}_{j;i_j}(\boldsymbol{x},t) = \boldsymbol{\psi}_j^T(\boldsymbol{x}) \ \boldsymbol{W}_{j;i_j} \ \boldsymbol{\psi}_{i_j}(t) \ . \tag{6.34}$$

and computable via the pyramid algorithm. To be more specific, starting with the initial matrix $\boldsymbol{D}_{j;I_j}$ the $N_j \times m_{i_j}$ matrix $\boldsymbol{D}_{j;i_j}$ of level$-(j;i_j)$ scaling coefficients $d_{j,k;i_j,l}$ and the $N_j \times n_{i_j}$ matrix of level$-(j;i_j)$ sub-wavelet coefficients $w_{j,k;i_j,l}$ are computed recursively as

$$\boldsymbol{D}_{j;i_j} = \boldsymbol{D}_{j;i_j+1} \ \overline{\boldsymbol{P}}_{i_j+1}^T \ , \tag{6.35}$$

$$\boldsymbol{W}_{j;i_j} = \boldsymbol{D}_{j;i_j+1} \ \overline{\boldsymbol{Q}}_{i_j+1}^T \tag{6.36}$$

for $i_j = j_{i'}, \ldots, I_j - 1$.

Inserting Eq. (6.32) into Eq. (6.24) yields

$$\begin{aligned} g_{j;I_j}(\boldsymbol{x},t) &= \left(\ \widetilde{\Psi}_j \star c_{j;i'_j}(\,\cdot\,,t) \ \right)_w(\boldsymbol{x}) + \sum_{i_j=i'_j}^{I_j-1} \left(\ \widetilde{\Psi}_j \star \overline{c}_{j;i_j}(\,\cdot\,,t) \ \right)_w(\boldsymbol{x}) \\ &= g_{j;i'_j}(\boldsymbol{x},t) + \sum_{i_j=i'_j}^{I_j-1} \overline{g}_{j;i_j}(\boldsymbol{x},t) \ . \end{aligned} \tag{6.37}$$

Herein

$$g_{j;i'_j}(\boldsymbol{x},t) = \left(\ \widetilde{\Psi}_j \star c_{j;i'_j}(\,\cdot\,,t) \ \right)_w(\boldsymbol{x}) \tag{6.38}$$

means the level$-(j;i'_j)$ approximation of the level$-(j;I_j)$ detail signal $g_{j;I_j}(\boldsymbol{x},t)$. The functions

$$\overline{g}_{j;i_j}(\boldsymbol{x},t) = \left(\ \widetilde{\Psi}_j \star \overline{c}_{j;i_j}(\,\cdot\,,t) \ \right)_w(\boldsymbol{x}) \tag{6.39}$$

we will call sub-detail signal of level $(j;i_j)$.

Next we consider Eq. (6.37) in Eq. (6.1) and obtain the spatio-temporal (4-D) multi-resolution representation

$$f(\boldsymbol{x},t) = f_{j'}(\boldsymbol{x},t) + \sum_{j=j'}^{J} g_{j;i'_j}(\boldsymbol{x},t) + \sum_{j=j'}^{J} \sum_{i_j=i'_j}^{I_j-1} \overline{g}_{i;i_j}(\boldsymbol{x},t) \tag{6.40}$$

with given values $j' \in \{0,\ldots,J\}$ and $i'_j \in \{0,\ldots,I_j-1\}$.

If we identify the function $f(\boldsymbol{x},t)$ with the gravitational potential, i.e. $f(\boldsymbol{x},t) =: U(\boldsymbol{x},t)$, we may subtract a reference potential $U_{\mathrm{ref}}(\boldsymbol{x},t)$ and rewrite Eq. (6.40) as

$$\begin{aligned}\delta U(\boldsymbol{x},t) &= U(\boldsymbol{x},t) - U_{\mathrm{ref}}(\boldsymbol{x},t) \\ &= \delta U_{j'}(\boldsymbol{x},t) + \sum_{j=j'}^{J} g_{j;i'_j}(\boldsymbol{x},t) + \sum_{j=j'}^{J} \sum_{i_j=i'_j}^{I_j-1} \overline{g}_{j;i_j}(\boldsymbol{x},t) + \Delta U(\boldsymbol{x},t)\ .\end{aligned} \tag{6.41}$$

Herein, the signal $\Delta U(\boldsymbol{x},t)$ stands for all the parts of the gravitational potential difference $\delta U(\boldsymbol{x},t)$ not considered in the series expansion until highest spatial level J. Furthermore, in Eq. (6.41) $\delta U_{j'}(\boldsymbol{x},t)$ means the level$-j'$ approximation of the residual gravitational potential $\delta U(\boldsymbol{x},t)$, the signals $g_{j;i'_j}(\boldsymbol{x},t)$ and $\overline{g}_{j;i_j}(\boldsymbol{x},t)$ are the corresponding level$-(j;i'_j)$ detail signal approximation and the level$-(j;i_j)$ sub-detail signals, respectively. If the summation limits in Eq. (6.41) are chosen appropriately, the subsignals $\delta U_{j'}(\boldsymbol{x},t)$ and $\Delta U(\boldsymbol{x},t)$ can be omitted, i.e. we define $\delta U_{J+1;I_J}(\boldsymbol{x},t) =: U_{J+1;I_J}(\boldsymbol{x},t) - U_{\mathrm{ref}}(\boldsymbol{x},t)$ and obtain

$$\delta U_{J+1;I_J}(\boldsymbol{x},t) = \sum_{j=j'}^{J} g_{j;i'_j}(\boldsymbol{x},t) + \sum_{j=j'}^{J} \sum_{i_j=i'_j}^{I_j-1} \overline{g}_{j;i_j}(\boldsymbol{x},t)\ . \tag{6.42}$$

Note, that due to the ansatz (6.15) with (spatial) level-dependent numbers I_j the pyramid algorithm - explained before in subsection 5.2.2 in detail - cannot be applied anymore.

In the following we outline the different steps of the spatio-temporal procedure:

1. In the initial step we estimate the unknown parameter matrix $\boldsymbol{D}_{J;I_J}$ as defined in Eq. (6.21) for $j = J$. For that purpose we recall Eq. (6.10) for $j = J$ set $y(\boldsymbol{x},t) = \delta U_{J+1;I_J}(\boldsymbol{x},t) + e(\boldsymbol{x},t)$ and obtain the level$-(J+1;I_J)$ observation equation

$$\delta U_{J+1;I_J}(\boldsymbol{x},t) = (\boldsymbol{\phi}^T_{I_J}(t) \otimes \theta^T_{J+1}(\boldsymbol{x}))\ \mathrm{vec}\boldsymbol{D}_{J;I_J}\ . \tag{6.43}$$

2. In the second step the estimator $\widehat{\boldsymbol{D}}_{J;I_J}$ of the matrix $\boldsymbol{D}_{J;I_J}$ is used to calculate the estimations $\widehat{\boldsymbol{D}}_{J;i_J}$ and $\widehat{\boldsymbol{W}}_{J;i_J}$ for $i_J = i'_J,\ldots,I_J-1$ according to the Eqs. (6.35) and (6.36). Based on

these results the estimators $\widehat{c}_{J;i_J}$ and $\widehat{\overline{c}}_{J;i_J}$ of the the level$-(J;i_J)$ approximations $c_{J;i_J}$ and the level$-(J;i_J)$ detail-wavelet coefficients $\overline{c}_{J;i_J}$ are computed via the Eqs. (6.33) and (6.34), i.e.,

$$\widehat{c}_{J;i_J}(\boldsymbol{x},t) = \boldsymbol{\psi}_J^T(\boldsymbol{x})\ \widehat{\boldsymbol{D}}_{J;i_J}\ \boldsymbol{\phi}_{i_J}(t)\ , \tag{6.44}$$

$$\widehat{\overline{c}}_{J;i_J}(\boldsymbol{x},t) = \boldsymbol{\psi}_J^T(\boldsymbol{x})\ \widehat{\boldsymbol{W}}_{J;i_J}\ \boldsymbol{\psi}_{i_J}(t)\ . \tag{6.45}$$

These results are then used to calculate the estimated level$-(J;i'_J)$ approximation

$$\widehat{g}_{J;i'_J}(\boldsymbol{x},t) = \big(\ \widetilde{\Psi}_J \star \widehat{c}_{J;i'_J}(\,\cdot\,,t)\ \big)_w(\boldsymbol{x}) \tag{6.46}$$

of the level$-(J;I_J)$ detail signal $g_{J;I_J}(\boldsymbol{x},t)$ and the estimated level$-(J;i_J)$ sub-detail signals

$$\widehat{\overline{g}}_{J;i_J}(\boldsymbol{x},t) = \big(\ \widetilde{\Psi}_J \star \widehat{\overline{c}}_{J;i_J}(\,\cdot\,,t)\ \big)_w(\boldsymbol{x}) \tag{6.47}$$

following the Eqs. (6.38) and (6.39). Consequently, at the end of the second step the estimation

$$\widehat{g}_{J;I_J}(\boldsymbol{x},t) = \widehat{g}_{J;i'_J}(\boldsymbol{x},t) + \sum_{i_J=i'_J}^{I_J-1} \widehat{\overline{g}}_{J;i_J}(\boldsymbol{x},t) \tag{6.48}$$

of the level$-(J;I_J)$ detail signal is given.

3. In the next intermediate step we subtract the estimated signal (6.43) from $\delta U_{J+1;I_J}(\boldsymbol{x},t) = \delta U_{J;I_{J-1}}(\boldsymbol{x},t) - \widehat{g}_{J;I_J}(\boldsymbol{x},t)$, define the reduced level$-(J;I_{J-1})$ observation equation

$$\delta U_{J;I_{J-1}}(\boldsymbol{x},t) = (\boldsymbol{\phi}_{I_{J-1}}^T(t) \otimes \boldsymbol{\phi}_J^T(\boldsymbol{x}))\ \mathrm{vec}\boldsymbol{D}_{J-1;I_{J-1}} \tag{6.49}$$

analogously to Eq. (6.40).

4. In the fourth step we perform the same estimation process as explained in the second step. To be more specific, with the estimator $\widehat{\boldsymbol{D}}_{J-1;I_{J-1}}$ of the matrix $\boldsymbol{D}_{J-1;I_{J-1}}$ we calculate the estimations $\widehat{\boldsymbol{D}}_{J-1;i_{J-1}}$ and $\widehat{\boldsymbol{W}}_{J-1;i_{J-1}}$ for $i_{J-1} = i'_{J-1},\ldots,I_{J-1}-1$ according to the Eqs. (6.35) and (6.36). Based on these results the estimators $\widehat{c}_{J-1;i_{J-1}}$ and $\widehat{\overline{c}}_{J;i_{J-1}}$ of the the level$-(J;i_{J-1})$ approximations $c_{J;i_{J-1}}$ and the level$-(J;i_{J-1})$ detail-wavelet coefficients $\overline{c}_{J;i_{J-1}}$ are computed via the Eqs. (6.33) and (6.34), i.e.,

$$\widehat{c}_{J-1;i_{J-1}}(\boldsymbol{x},t) = \boldsymbol{\psi}_{J-1}^T(\boldsymbol{x})\ \widehat{\boldsymbol{D}}_{J-1;i_{J-1}}\ \boldsymbol{\phi}_{i_{J-1}}(t)\ , \tag{6.50}$$

$$\widehat{\overline{c}}_{J-1;i_{J-1}}(\boldsymbol{x},t) = \boldsymbol{\psi}_{J-1}^T(\boldsymbol{x})\ \widehat{\boldsymbol{W}}_{J-1;i_{J-1}}\ \boldsymbol{\psi}_{i_{J-1}}(t)\ . \tag{6.51}$$

These results are then used to calculate the estimated level$-(J-1;i'_{J-1})$ approximation

$$\widehat{g}_{J-1;i'_{J-1}}(\boldsymbol{x},t) = \big(\ \widetilde{\Psi}_{J-1} \star \widehat{c}_{J-1;i'_{J-1}}(\,\cdot\,,t)\ \big)_w(\boldsymbol{x}) \tag{6.52}$$

of the level$-(J-1;I_{J-1})$ detail signal $g_{J-1;I_{J-1}}(\boldsymbol{x},t)$ and the estimated level$-(J-1;i_{J-1})$ sub-detail signals

$$\widehat{\overline{g}}_{J-1;i_{J-1}}(\boldsymbol{x},t) = \big(\ \widetilde{\Psi}_{J-1} \star \widehat{\overline{c}}_{J-1;i_{J-1}}(\,\cdot\,,t)\ \big)_w(\boldsymbol{x}) \tag{6.53}$$

following the Eqs. (6.38) and (6.39). Consequently, at the end of the fourth step the estimation

$$\widehat{g}_{J-1;I_{J-1}}(\boldsymbol{x},t) = \widehat{g}_{J-1;i'_{J-1}}(\boldsymbol{x},t) + \sum_{i_{J-1}=i'_{J-1}}^{I_{J-1}-1} \widehat{\overline{g}}_{J-1;i_{J-1}}(\boldsymbol{x},t) \tag{6.54}$$

of the level$-(J-1;I_{J-1})$ detail signal is given.

5. In the next intermediate step we subtract the estimated signal (6.54) from $\delta U_{J;I_{J-1}}(\boldsymbol{x},t) = \delta U_{J-1;I_{J-2}}(\boldsymbol{x},t) - \widehat{g}_{J-1;I_{J-1}}(\boldsymbol{x},t)$, define the reduced level$-(J-1;I_{J-2})$ observation equation

$$\delta U_{J-1;I_{J-2}}(\boldsymbol{x},t) = (\boldsymbol{\phi}^T_{I_{J-2}}(t) \otimes \boldsymbol{\phi}^T_{J-1}(\boldsymbol{x}))\ \mathrm{vec}\boldsymbol{D}_{J-2;I_{J-2}} \tag{6.55}$$

analogously to Eq. (6.49).

6. If we proceed in the same manner as explained for the second and the fourth step until spatial level $j = j'$, we end up with estimations of all signals introduced on the right-hand side of Eq. (6.42).

Following this procedure, our final result for the geopotential $U(\boldsymbol{x},t)$ reads

$$\widehat{U}(\boldsymbol{x},t) = U_{\mathrm{ref}}(\boldsymbol{x},t) + \sum_{j=j'}^{J} \widehat{g}_{j;i'_j}(\boldsymbol{x},t) + \sum_{j=j'}^{J} \sum_{i_j=i'_j}^{I_j-1} \widehat{\overline{g}}_{j;i_j}(\boldsymbol{x},t)\ . \tag{6.56}$$

For monitoring the climate change as mentioned in the introduction mass variations estimated from GRACE observations can be transferred to equivalent water heights or to height deformations following Farrell's (1972) theory. To be more specific, the geopotential U or the residual geopotential δU as estimated by Eq. (6.56) can be transformed into height deformations

$$\delta h(\boldsymbol{x},t) = \sum_{j=j'}^{J} h_j(\boldsymbol{x},t) \tag{6.57}$$

at the Earth's surface with respect to the reference model $U_{\mathrm{ref}}(\boldsymbol{x},t)$ by evaluating the ellipsoidal convolutions

$$h_j(\boldsymbol{x},t) = \left(K^e \star g_{j;I_j}(\,\cdot\,,t) \right)_w(\boldsymbol{x}) \tag{6.58}$$

with respect to the detail signals $g_{j;I_j}$ as introduced in Eq. (6.37). In Eq. (6.58) the kernel $K^e(\boldsymbol{x},\boldsymbol{x}_q)$ is defined as

$$K^e(\boldsymbol{x},\boldsymbol{x}_q) = \sum_{n=0}^{\infty}(2n+1)\,\frac{h'_n}{g\,(1+k'_n)}\,P_n(\boldsymbol{\xi}^T\boldsymbol{\xi}_q) \tag{6.59}$$

with k'_n and h'_n being the static gravitational and vertical load Love numbers of degree n, respectively; $g =$ (mean) absolute value of the gravity acceleration; for more details see Schmidt et al. (2006).

References

Ardalan A, Grafarend EW (2001) Somigliana-Pizetti gravity: the international gravity formula accurate to the sub-nanoGal level. J Geod, 75, 424-437

Bjerhammer A (1967) On the energy integral for satellites. Rep. of the R. Inst. of Techn. Sweden, Stockholm

Farrell WE (1972) Deformation of the Earth by surface loads. Rev. Geophys. Space Phys., 10, 761-797

Freeden W (1999) Multiscale Modelling of Spaceborne Geodata. Teubner, Stuttgart

Freeden W, Michel V (2004) Multiscale Potential Theory (With Applications to Earth's Sciences). Birkhäuser Verlag, Boston

Freeden W, Gervens T, Schreiner M (1998) Constructive Approximation on the Sphere (With Applications to Geomathematics). Clarendon Press, Oxford

Grafarend EW, Ardalan A, Sideris M (1999) The ellipsoidal fixed-free two-boundary value problem for geoid determination (the ellipsoidal Bruns transform). J Geod, 73, 513-533

Grafarend EW, Finn G, Ardalan A (2006) Ellipsoidal vertical deflections and ellipsoidal gravity disturbances: case studies. Studia geophysica and geodaetica, 50, 1-57

Haagmans R, Prijatna K, Omang OD (2002) An Alternative Concept for Validation of GOCE Gradiometry Results Based on Regional Gravity. Proceedings of the 3rd meeting the International Gravity and Geoid Commission. Thessaloniki, Greece

Han SC (2003) Efficient global gravity determination from satellite-to-satellite tracking (SST). PhD-thesis, Geodetic and Geoinformation Science, Department of Civil and Environmental Engineering and Geodetic Science, The Ohio State University, Columbus

Han SC, Shum CK, Jekeli C (2006) Precise estimation of in situ geopotential differences from GRACE low-low satellite-to-satellite tracking and accelerometry data. J. Geophy. Res., 111, B4411, doi:10.1029/2005JB003719

Heiskanen W, Moritz H (1967) Physical Geodesy. Freeman, San Francisco

Heitz S (1975): Zur interpolatorischen Darstellung von Funktionen. Publications of Bayerischen Kommission für die internationale Erdmessung, 33, 109-116

Jekeli C (1999) The determination of gravitational potential differences from satellite-to-satellite tracking. Cel Mech Dyn Astr, 75, 85-100

Ilk KH, Löcher A (2005) The use of the energy balance relations for validation of gravity field models and orbit determination. In: Sansò F (ed.) A Window on the Future of Geodesy. Springer, Berlin, 494-499

Koch KR (1999) Parameter Estimation and Hypothesis Testing in Linear Models. Springer, Berlin

Kusche J (2002) Inverse Probleme bei der Gravitationsfeldbestimmung mittels SST- und SGG-Satellitenmissionen. German Geodetic Commission, Series C, 548, Munich.

Lyche T, Schumaker LL (2001) A Multiresolution Tensor Spline Method for Fitting Functions on the Sphere. SIAM Journal of Scientific Computing, 22(2), 724-746

Martinez Z, Grafarend EW (1997) Solution to the Stokes boundary-value problem on the ellipsoid of revolution. Studia Geoph. et Geod. 41, 103-129

Mayer-Gürr T, Ilk KH, Eicker A, Feuchtinger M (2005) ITG-CHAMP01: A CHAMP Gravity Field Model from Short Kinematical Arcs of a One-Year Observation Period. J Geod, 78, 462-480

Mayer-Gürr T, Eicker A, Ilk KH (2006) Gravity Field Recovery from GRACE-SST Data of Short Arcs. In: Flury J, Rummel R, Reigber C, Rothacher M, Boedecker G, Schreiber U (eds.) Observation of the Earth system from Space. Springer, Berlin, 131-148

Mertins A (1999) Signal Analysis: Wavelets, Filter banks, Time-frequency Transforms and Applications. Wiley, Chichester

Moritz H (1980) Advanced Physical Geodesy. Wichmann, Karlsruhe

Ogden RT (1997) Essential Wavelets for Statistical Applications and Data Analysis. Birkhäuser, Boston

Panet I, Jamet O, Diament M, Chambodut A (2005) Modelling the Earth's gravity field using wavelet frames. In: Jekeli C, Bastos L, Fernandes J (eds.) Gravity, Geoid and Space Missions. Springer, Berlin, 48-53

Pavlis NK, Holmes SA, Kenyon SC, Schmidt D, Trimmer R (2005) A Preliminary Gravitational Model to Degree 2160. In: Jekeli C, Bastos L, Fernandes J (eds.) Gravity, Geoid and Space Missions. Springer, Berlin, 18-23

Prijatna K, Haagmans R (2001) Combination of a Global Geopotential Model, GOCE Gradiometry and Gravity Data in Regional Geoid Determination. JoG.

Reigber C, Lühr H, Schwintzer P (2000). CHAMP mission status and perspectives. Suppl. to EOS, Transactions, AGU, 81, 48, F307.

Reigber C, Schmidt R, Flechtner F, König R, Meyer U, Neumayer KH, Schwintzer P, Zhu SY (2005) An Earth gravity field model complete to degree and order 150 from GRACE: EIGEN-GRACE02S. Journal of Geodynamics, 39, 1-10

Schmidt, M (2006). Wavelet modeling in support of IRI. J. Adv. in Space Res., doi:10.1016/j.asr.2006.09.030

Schmidt M, Han SC, Kusche J, Sánchez L, Shum CK (2006) Regional high-resolution spatiotemporal gravity modeling from GRACE data using spherical wavelets. Geophys. Res. Lett., 33, L08403, doi:10.1029/2005GL025509

Schmidt M, Fengler M, Mayer-Gürr T, Eicker A, Kusche J, Sánchez L, Han SC (2007a), Regional Gravity Modelling in Terms of Spherical Base Functions, J Geod, 81, pp 17-38, doi: 10.1007/s00190-006-0101-5

Schmidt M, Kusche J, Han SC, Shum CK, Karslioglu MO (2007b). Multi-resolution representation of the gravity field from satellite data based on wavelet expansions with time-dependent coefficients. in press

Schmidt M, Seitz F, Shum CK (2007c), Modeling and validation of GRACE 4-D hydrology. Submitted to J. Geophy. Res..

Stollnitz EJ, DeRose TD, Salesin DH (1995) Wavelets for Computer Graphics: A Primer, Part I, IEEE Computer Graphics and Applications, 15(3), 76-84; Part II, IEEE Computer Graphics and Applications, 15(4), 75-85

Tapley BD, Bettadpur S, Ries J, Thopmson P, Watkins M (2004) GRACE measurements of mass variability in the Earth system, Science, 305, 503-505

Torge W (2001) Geodesy. de Gruyter, Berlin

van Loon J, Kusche J (2005) Stochastic model validation of satellite gravity data: A test with CHAMP pseudo-observations. In: Jekeli C, Bastos L, Fernandes J (eds.) Gravity, Geoid and Space Missions. Springer, Berlin, 24-29

Weidmann J (1976) Lineare Operatoren in Hilberträumen. Teubner, Stuttgart